Diversity of *Cryptosporidium* PKS gene and using metabolomics to identify a polyketide product

Mukan Ji

School of Biotechnology and Biomolecular Sciences,
University of New South Wales

A thesis submitted in fulfilment of the requirements for the degree of Master of Philosophy
Supervisor: Dr. Belinda Ferrari
Co Supervisor: Prof. Brett Neilan

THE UNIVERSITY OF NEW SOUTH WALES

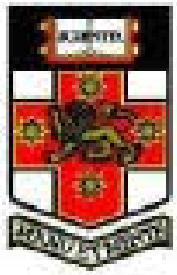

PLEASE TYPE

THE UNIVERSITY OF NEW SOUTH WALES
Thesis/Dissertation Sheet

Surname or Family name: Ji

First name: Mukan Other name/s:

Abbreviation for degree as given in the University calendar: M.phil

School: BABS Faculty: Science

Title: Diversity of Cryptosporidium PKS gene and using metabolomics to identify a polyketide product

Abstract 350 words maximum: (PLEASE TYPE)

The protozoan parasite Cryptosporidium causes cryptosporidiosis and it is a major cause of non-viral diarrhoeal illness. Currently, five Cryptosporidium species are considered as human infectious and over 90% of infections are caused by C. parvum and C. hominis. A polyketide synthase (PKS) gene identified in C. parvum has been speculated to be involved in toxin production. The PKS gene has been identified in the C. parvum, C. hominis, and C. muris but the PKS protein has only been identified in the human infectious intestinal species: C. parvum and C. hominis. In this study, the PKS gene was identified in C. cuniculus, C. fayeri, C. andersoni and C. bovis. The identification was based on degenerate primer sets targeting various domains within the PKS gene. The results revealed that significant variability exists between the PKS gene in intestinal and gastric species of Cryptosporidium.

The PKS gene sequence of 30 Cryptosporidium isolates from 21 subtypes within the three most common and waterborne outbreak causing Cryptosporidium species: C. parvum, C. hominis, and C. cuniculus were characterised. The resulting PKS gene sequences were divided into two distinct groups where C. parvum isolates formed one cluster (II) and C. hominis and C. cuniculus isolates formed another cluster (I). The CpPKS1 in C. parvum was highly conserved, by comparison, there was much more variation observed at the species level in C. hominis and C. cuniculus.

The feasibility of using mass spectroscopy (MS) for a metabolomics investigation into Cryptosporidium with an aim of identifying a potential polyketide was conducted. The results demonstrated the possibility of constructing a metabolomics profile of Cryptosporidium. While a polyketide was not identified, an unusual sphingoid base related molecule: 2-amino,3,4-dihydroxyl heptadecane was found. This molecule is potentially cell toxic and may be related to host cell apoptosis attributed to Cryptosporidium infections.

Further works are required on sequencing more subtypes of C. parvum and C. hominis isolates to increase the confidence on the polymorphism identified between species. In the future, HPLC based separation should allow purification of the 2-amino, 3,4-dihydroxyl heptadecane from a crude extract, then the stereochemistry of the molecule can be determined by NMR and cell-based cell toxicity assays can be performed.

FOR OFFICE USE ONLY Date of completion of requirements for Award:

THIS SHEET IS TO BE GLUED TO THE INSIDE FRONT COVER OF THE THESIS

ORIGINALITY STATEMENT

„I hereby declare that this submission is my own work and to the best of my knowledge it contains no materials previously published or written by another person, or substantial proportions of material which have been accepted for the award of any other degree or diploma at UNSW or any other educational institution, except where due acknowledgement is made in the thesis. Any contribution made to the research by others, with whom I have worked at UNSW or elsewhere, is explicitly acknowledged in the thesis. I also declare that the intellectual content of this thesis is the product of my own work, except to the extent that assistance from others in the project's design and conception or in style, presentation and linguistic expression is acknowledged.'

Signed …….....

Date …….....

Table of Contents

Abstract……..…1-2

Chapter 1 Introduction……..3-29

1.1 *Cryptosporidium* and cryptosporidiosis.....3

1.2 Lifecycle of *Cryptosporidium*.....4

1.3 Cultivation of *Cryptosporidium*.....7

1.4 Clinical diagnosis, species identification and subtyping 8

1.4.1 Diagnostics and Detection 8

1.4.1.1 Microscopic methods.....8

1.4.1.2 Molecular detection methods.....9

1.4.2 Taxonomy.....9

1.4.3 Intraspecies subtyping.....10

1.5 Epidemiology.....15

1.5.1 Clinical manifestations.....15

1.5.2 Transmission and sources of *Cryptosporidium*.....16

1.5.3 Pathogenesis.....17

1.8 *Cryptosporidium* Polyketide Synthase and its Polyketide Product.....18

1.8.1 Polyketide synthase and polyketides 18

1.8.2 Classification of PKS.....19

1.9 PKS in *Cryptosporidium*.....20

1.9.1 Structure of PKS and CpPKS1 21

1.10 Function and localisation of CpPKS1 23

1.11 Mass Spectroscopy (MS) and its application in *Cryptosporidium* polyketide identification 25

1.11.1 Theory of Mass Spectroscopy 25

1.11.1 The Application of MS in metabolomics studies 28

1.12 Aims and implications of this study 29

Chapter 2 Material and methods…….30-44

2.1 Source of oocysts and DNA for molecular characterisation 30

2.2 Molecular characterisation of *Cryptosporidium* PKS gene 30

2.2.1 DNA extraction 30

2.2.2 60 kDa glycoprotein gene sequence based genotyping 31

2.2.3 CpPKS1gene characterisation 32

2.2.3.1 Primers used in CpPKS1 characterisation and novel primers design 32

2.2.3.2 Primers used in PKS gene characterisation in human infectious *Cryptosporidium* species at subtype level 33

2.2.3.3 Optimisation of *Cryptosporidium*-specific PKS PCRs using in-house designed primer sets 36

2.2.4 Visualisation of PCR products 36

2.2.5 PCR amplicon purification 36

2.2.6 Sequencing of purified PCR amplicons 37

2.2.7 DNA Sequence analysis and phylogenetic tree construction.....37

2.3 Polyketide identification 38

2.3.1 Oocyst purification.....38

2.3.1.1 Initial screening for *Cryptosporidium* oocysts in faeces.....38

2.3.1.2 Purification of *Cryptosporidium* oocysts from calf faeces 39

2.3.2 Determining total oocyst counts and purity by Flow Cytometry (FCM)....40

2.3.2.1 Oocyst fluorescent staining.....40

2.3.2.2 FCM setup.....40

2.3.2.3 Data acquisition and analysis.....40

2.3.3 Oocyst excystation 42

2.3.4 Polyketide extraction 43

2.3.5 Nanospray and tandem MS.....43

Chapter 3 Results on PKS gene diversity in *Cryptosporidium* species……..46-70

3.1 Background and aims.....45

3.2 Design and optimisation of degenerate primer sets for PKS gene identification using PCR 47

3.3 Identification of PKS gene in *Cryptosporidium* species.....51

3.4 PKS gene diversity in human infectious *Cryptosporidium* species.....54

3.4.1 Summary of human infectious *Cryptosporidium* isolates used 54

3.4.2 Genetic diversity of the PKS gene across human infectious *Cryptosporidium* species.....56

3.4.2.1 Gene and protein sequence polymorphism within the KS domain of

module 5.....57

3.4.2.2 Gene and protein sequence polymorphism within the ER domain of module 1.....60

3.4.2.3 Gene and protein sequence polymorphism within the ACP and KS domains of module 3.....63

3.5 Conclusion 67

Chapter 4 Results on metabolomics and polyketide identification in *C. parvum*……71-90

4.1 Introduction and aims 69

4.2 Quantification of purified oocysts and purity estimation 71

4.3 Oocyst disruption by sonication for Mass Spectroscopy (MS) analysis.....71

4.4 Detection of potential metabolites of *Cryptosporidium* by MS.....73

4.4.1 Detection of potential metabolites and their location during the excystation process.....73

4.4.2 Identification of potential metabolites from intact oocyst 77

4.4.2.1 Number of potential metabolites identified in the intact oocysts 77

4.4.3 Structure elucidation of 288.28 Da metabolite 82

4.5 Conclusion 88

Chapter 5 Discussion……....91-100

5.1. The diversity of PKS gene in *Cryptosporidium* spp. 90

5.2 A novel identification tool for human infectious *Cryptosporidium*.....91

5.3 Metabolomics profiling of *Cryptosporidium* and polyketide identification.....93

5.4 The potential application of 2-amino-3,4-dihydroxy heptadecane 95

5.5 Future direction 98

5.5.1 PKS gene diversity in *Cryptosporidium* and towards a novel identification tool for human infectious *Cryptosporidium* 98

5.5.2 Metabolomics profiling and polyketide identification 99

5.6 Conclusion 100

References……..102-111

Appendices…….112-131

Abstract

The protozoan parasite *Cryptosporidium* causes cryptosporidiosis and it is a major cause of non-viral diarrhoeal illness. Currently, five *Cryptosporidium* species are considered as human infectious and over 90% of infections are caused by *C. parvum* and *C. hominis*. A polyketide synthase (PKS) gene identified in *C. parvum* has been speculated to be involved in toxin production. The PKS gene has been identified in the *C. parvum*, *C. hominis,* and *C. muris* but the PKS protein has only been identified in the human infectious intestinal species: *C. parvum* and *C. hominis*.

In this study, the PKS gene was identified in *C. cuniculus, C. fayeri, C. andersoni* and *C. bovis*. The identification was based on degenerate primer sets targeting various domains within the PKS gene. The results revealed that significant variability exists between the PKS gene in intestinal and gastric species of *Cryptosporidium*.

The PKS gene sequence of 30 *Cryptosporidium* isolates from 21 subtypes within the three most common and waterborne outbreak causing *Cryptosporidium* species: *C. parvum*, *C. hominis*, and *C. cuniculus* were characterised. The resulting PKS gene sequences were divided into two distinct groups where *C. parvum* isolates formed one cluster (II) and *C. hominis* and *C. cuniculus* isolates formed another cluster (I). The CpPKS1 in *C. parvum* was highly conserved, by comparison, there was much more

variation observed at the species level in *C. hominis* and *C. cuniculus*.

The feasibility of using mass spectroscopy (MS) for a metabolomics investigation into *Cryptosporidium* with an aim of identifying a potential polyketide was conducted. The results demonstrated the possibility of constructing a metabolomics profile of *Cryptosporidium*. While a polyketide was not identified, an unusual sphingoid base related molecule: 2-amino,3,4-dihydroxyl heptadecane was found. This molecule is potentially cell toxic and may be related to host cell apoptosis attributed to *Cryptosporidium* infections.

Further works are required on sequencing more subtypes of *C. parvum* and *C. hominis* isolates to increase the confidence on the polymorphism identified between species. In the future, HPLC based separation should allow purification of the 2-amino, 3,4-dihydroxyl heptadecane from a crude extract, then the stereochemistry of the molecule can be determined by NMR and cell-based cell toxicity assays can be performed.

Chapter 1. Introduction

1.1 *Cryptosporidium* and cryptosporidiosis

Cryptosporidium is a waterborne protozoan parasite that is a major cause of diarrhoeal disease in humans[1,2], livestock[3] and other animals[4]. The disease cryptosporidiosis caused by *Cryptosporidium* infection is a major non-viral causes of diarrhoeal disease in children, and HIV infected humans[5-8].

While *Cryptosporidium* was first described in 1907[9], it only began to receive considerable attention when reports of *Cryptosporidium* infection in humans increased significantly after the 1980s[10,11]. *Cryptosporidium* is now considered as one of the major concerns to the water industry[12]. In a review of more than 131,000 patients exhibiting diarrhoeal symptoms, up to 6.1% cases were caused by *Cryptosporidium* in immunocompetent patients, while this increased to 24% in HIV-infected patients[13]. The ID_{50} of one particular *Cryptosporidium* isolate, *Cryptosporidium parvum* Iowa strain, has been observed to be around 132 oocysts[14]. By comparison there have been reports in extreme cases where one oocyst was sufficient to cause infection[13]. In 1995, the most notable waterborne outbreak due to *Cryptosporidium* contaminated water occured in Milwaukee, Wisconsin, with estimated of more than 403,000 people being infected, demonstrating the efficacy of

oocyst transmission[15].

1.2 Lifecycle of *Cryptosporidium*

Cryptosporidium primarily infects the epithelial cells of the gastrointestinal or respiratory tracts. It positions itself in a unique intracellular but extracytoplasmic location, and attaches to the host cell via a specialised feeder organelle to facilitate nutrition uptake[16]. *Cryptosporidium* can complete its entire lifecycle in a single host and like most of other members of Apicomplexa, *Cryptosporidium* has a complex lifecycle including both sexual and asexual stages (**Figure 1.1**).

For *C. parvum*, after sporulation thick-walled oocysts are ingested or inhaled from the environment by a suitable host, excystation takes place in the intestinal lumen and releases four sporozoites from each oocyst (**Figure 1.1**)[17]. Sporozoites penetrate the host cell and develop into trophozoites located in the microvilous region of the mucosal epithelium (**Figure 1.2**). Trophozoites undergo asexual merogony division to form merozoites. The released merozoites enter adjacent host cells and multiply to form either additional type I or type II meronts. Type I meronts repeat this cycle, where type II meronts do not recycle but form microgamonts and macrogamonts commencing the sexual phase of the lifecycle. The majority (80%) of zygotes formed after fertilisation develop into environmentally resistant, thick walled oocysts that passed into the environment in faeces. The rest of the zygotes (20%) form thin-walled

oocysts which are involved in autoinfection by recycling of sporozoites from thin-walled oocysts[18]. As most of the lifecycle is intracellular, the majority of studies have concentrated on the sporozoite stage from the intact oocysts[19] .

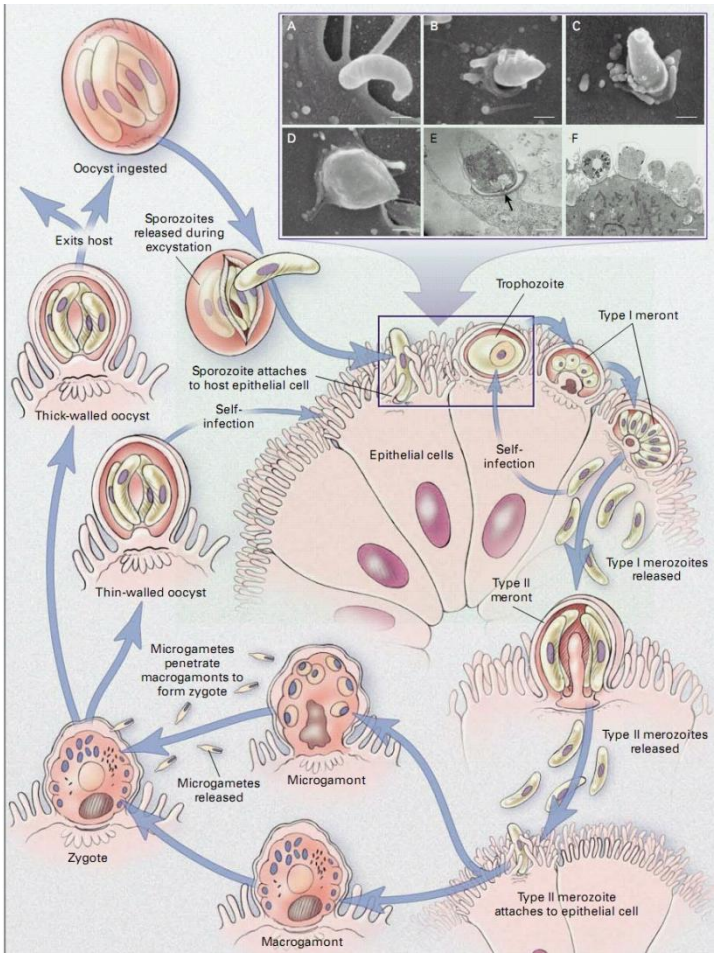

Figure 1.1. Lifecycle of *Cryptosporidium* and infection of host epithelial cells (reproduced from Chen[17])

A figure represents the lifecycle of *Cryptosporidium* infection. Panel A, B, C and D are scanning electron micrographs, and Panels E and F are transmission electron micrographs. Panel A, a sporozoite attaching to the apical membrane surface of a biliary epithelial cell; Panels B and C, a sporozoite invading a host cell; Panels D and E, a zoite being enveloped by the host- cell membrane and formation of a vacuole, the anterior end of the zoite was inserted into the host-cell membrane (arrow); Panel F, the intestinal biopsy specimen of HIV patient with intestinal cryptosporidiosis.

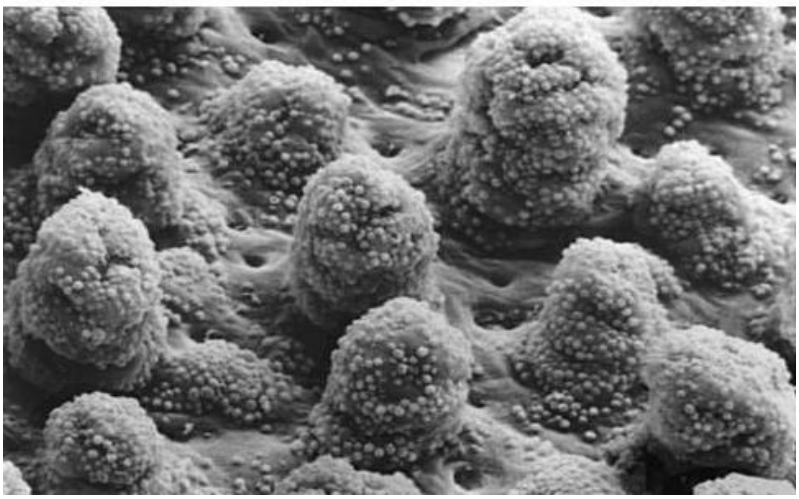

Figure 1.2 Scanning electron microscope image of Villar and intervillar surface of small intestine of an experimentally infected mouse with *Cryptosporidium* (Reproduced from Fayer[20]).

1.3 Cultivation of *Cryptosporidium*

Oocysts have a limited lifespan, after 6 to 8 weeks storage at 25 ℃ , infectivity has been markedly diminished in both *in vivo* and *in vitro* infectivity studies[21]. Since long-term storage is not possible, maintenance of *Cryptosporidium* isolates require that they have to be continuously passaged through animals. *In vitro* culture of *Cryptosporidium* in mammalian cell lines can allow the completion of sexual and asexual stages of development[22,23]. However, successful propagation in host cell free culture still remains controversial and is the main obstacle to progress in *Cryptosporidium* studies[24-26].

Since *Cryptosporidium* cannot be effectively cultured in high numbers *in vitro*,

acquiring high quantities in all development stages is the main limitation of this field[25]. *Cryptosporidium* is mostly extensively studied at the oocyst stage that is the transmissive stage; and predominately through purification from the stools of naturally or experimentally infected hosts or through animal passaging[27,28].

1.4 Clinical diagnosis, species identification and subtyping

1.4.1 Diagnostics and Detection

1.4.1.1 Microscopic methods

Histologically, *Cryptosporidium* infection was diagnosed by examining the microvillus region of the intestinal samples obtained by biopsy or at necropsy[29]. As sample preparation was invasive, it has been replaced with alternative techniques for clinical diagnostics[30]. Both chemical and antibody staining methods have been developed. Among these, Auramine phenol, Ziehl-Neelsen stain and fluorescently labeled antibodies are most commonly used[29]. However, they suffer from poor detection limits in concentrated faeces with high background fluorescence[30,31], and are ineffective when oocyst numbers are low as observed in asymptomatic infections or immunosuppressed individuals[32]. In addition, these staining based methods do not provide information on the species and subtype of the parasite that causes the

infection[30], .

1.4.1.2 Molecular detection methods

Polymerase Chain Reaction (PCR)-based methods provide a significantly higher detection efficiency and accuracy, as it has been reported to be able to detect a single purified oocyst[33,34]. Several commonly used loci include: 18S rRNA[35,36], heat shock protein 70 (Hsp70)[37], *Cryptosporidium* oocyst wall protein (COWP)[38], and Glycoprotein 60 (GP60)[19]. By combining PCR with the restriction fragment length polymorphism (RFLP)[35,38] and DNA sequencing techniques[39], they can provide valuable information on the species and subtypes of the *Cryptosporidium* that are responsible for an infection. It can be used in tracking the source of the contamination and in studying epidemiology of *Cryptosporidium* infection[40].

1.4.2 Taxonomy

Cryptosporidium is currently assigned to the class of Coccidia. However, phylogenetic analysis of the 18S small subunit ribosomal DNA sequence and a gregarines-similar trophozoite/gamont stage in *Cryptosporidium* lifecycle has suggested a closer relationship with gregarines[41,42]. At least 21 valid named species of *Cryptosporidium* (**Table 1.1**) and nearly 61 *Cryptosporidium* genotypes have now been described[43,44]. The phylogenetic relationship of major *Cryptosporidium* species is shown in **Figure 1.3**. The majority of *Cryptosporidium* species are host-specific in

that they only infect one type or group of host organism. While *C. parvum* is capable of zoonotic transmission, meaning it is capable infects humans and animals and thus is a substantial source of human disease[45,46]. However, cross-transmission is possible, and infections of different hosts occasionally occur[47]. For example, *C. muris* infects predominantly rodents, yet human infections have been reported[48,49].

1.4.3 Intraspecies subtyping

There is a lack of a broad sub-typing tool for all *Cryptosporidium* species. Microsatellites and minisatellites typing, GP60 gene sequencing, and analysis of double-stranded RNA elements are commonly used sub-genotyping tool for the common human infective *Cryptosporidium* species: *C. parvum* and *C. hominis*[50]. However, these tools are not effective for subtyping the remaining species, that are distantly divergent from *C. parvum* such as *C. felis, C. canis, C. muris* and *C. suis*[51], and has been shown to not completely replace multilocus genotype analysis[52]. Nevertheless, the GP60 gene is one of the most popular subtyping tools for *C. parvum* and *C. hominis* as it contains both microsatellite sequence-like serine-coding trinucleotide repeats (TCA/TCG/TCT) at the 5' end and extensive sequence differences in the non-repeat regions[19,53]. In addition to these hyper variable region features, GP60 is also under selective pressure as it encodes the surface glycoproteins gp45 and gp15, that are involved in zoite attachment and invasion of host cells[54]. Hence, the GP60 gene sequence is a preferred subtyping tool.

The nomenclature of *Cryptosporidium* species is based on SSU RNA and GP60 sequence. Based on the phylogenetic relationship of the GP60 gene sequence[5555] *Cryptosporidium* can be subtyped into: Ia, Ib, Id, Ie,If, and Ig for *C. hominis* and IIa, IIb, Ic (or IIc), IId, IIe, IIf, IIg, IIh and IIi for *C. parvum* (Figure 1.3)[19,55]. Finally, the number of TCA, TCG, and TCT repeats present (represented by letters A, G and T respectively), and the number of ACATCAs immediately after the trinucleotide repeats lead to the final part of the subtype name (**Table 1.2**)[56].

Table 1.1 Valid named species of *Cryptosporidium*, and type host (modified from Plutzer[43] and Robison[44])

Species name	Primary host name	Primary site of infection
C. andersoni	Cattle	Abomasum
C. baileyi	Chicken	Cloaca, bursa, trachea
C. bovis	Cattle	Small intestine
C. canis	Dog	Small intestine
C. cuniculus	Rabbit	Small intestine
C. fayeri	Kangaroo	Small intestine
C. felis	Cat	Small intestine
C. fragile	Black- spined toad	Stomach
C. galli	Chicken	Proventriculus
C. hominis	Human	Small intestine
C. macropodum	Kangaroo	Small intestine
C. meleagridis	Turkey	Small intestine
C. molnari	Gilthead sea bream	Stomach (and intestine)
C. muris	Mouse	Stomach
C. parvum	Mouse	Small intestine
C. ryanae	Cattle	Small intestine
C. scophthalmi	Turbot	Intestine (and stomach)
C. serpentis	Corn Snake	Stomach
C. suis	Pig	Small and large intestine
C. varanii	Emerald Monitor	Stomach and small intestine
C. wrairi	Guinea pig	Small intestine

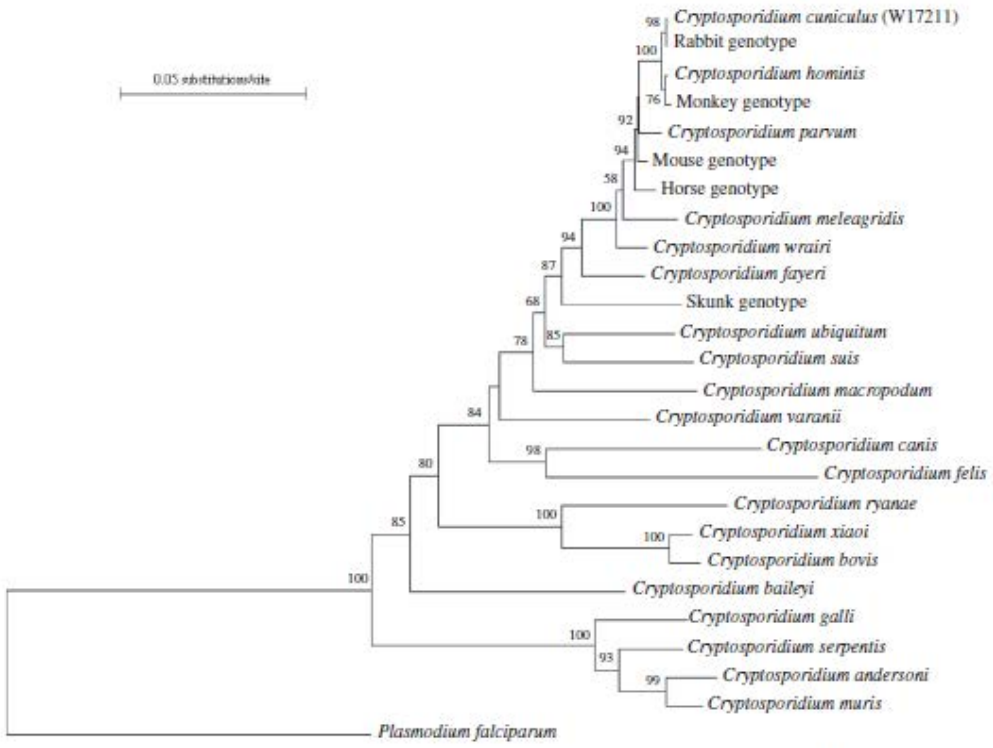

Figure 1.3 Phylogenetic relationships between *Cryptosporidium* spp.

The phylogenetic relationship was inferred by a neighbour-joining analysis of a concatenated sequence constructed from partial DNA sequence of the SSU rRNA, actin and Heat Shock Protein 70 genes. Bootstrapping values of over 50% are shown at branch. Reproduced from Robinson[44].

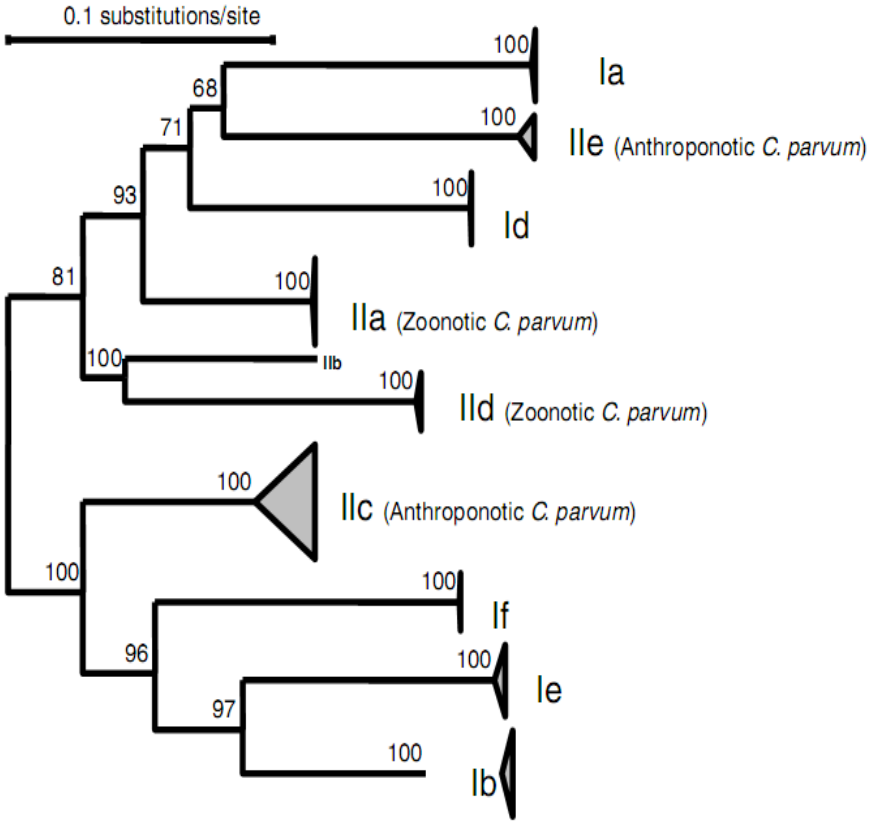

Figure 1.3 Phylogenetic relationship among nine major subtype families of *C. hominis* (Ia, Ib, Id, Ie, and If) and *C. parvum* (IIa, IIc,IId, and IIe) based on neighbor-joining analysis of the GP60 gene sequences (reporoduced from Nichols[56]).

Table 1.2 Different subtypes of *C. parvum* and *C. hominis* and their dominant trinucleotide repeat (reproduced from Nichols[56]).

Species	allele family	GeneBank accession No.
C. hominis	Ia	AF164502 (IaA23R4)
	Ib	AY262031 (IbA10G2)
	Id	DQ665692 (IdA16)
	Ie	AY738184 (IeA11G3T3)
	If	AF440638 (IfA19G1)
	Ig	EF208067 (IgA24)
C. parvum	IIa	AY262034 (IIaA15G2R1)
	IIb	AF402285 (IIbA14)
	IIc	AF164491 (IIcA5G3a)
	IId	AY738194 (IIdA18G1)
	IIe	AY382675 (IIeA12G1)
	IIf	AY738188 (IIfA6)
	IIg	AY873780 (IIgA9)
	IIh	AY873781 (IIhA7G4)
	IIi	AY873782 (IIiA10)

1.5 Epidemiology

1.5.1 Clinical manifestations

In humans, cryptosporidiosis is predominantly caused by seven species of *Cryptosporidium* (*C. parvum, C. hominis, C. fayeri, C. cuniculus, C. meleagridis, C. felis,* and *C. canis*)[57]. However, *C. hominis* and *C. parvum* account for over 95% of *Cryptosporidium* infections in humans[56]. These two species are highly similar, with a 96.7% identical genome and sharing of a large number of genes in common[58]. Due to their high similarity, the identification if two distinct species was not recognised until 1995[59] and consequently they were separated into two species in 2002[60].

Among different species and genotypes of *Cryptosporidium*, *C. parvum* is the most commonly studied because it is geographically widespread, it is able to infect different host species, and it is able to grow and be evaluated in *in vitro* and animal models[20].

The genomes of *C. parvum* and *C. hominis* have been completely sequenced[58,61] and revealed their genome size of approximately 9 Mb and 9.2 Mb respectively, which is relatively small for a eukaryotic organism[62]. However, due to the poor homology to other Apicomplexa, combined with a paucity of *in vitro* cultivation methods, the annotation of the genome has been hampered. For example, chromosome 6 has been analysed, and 55% of the genes predicted are without identifiable motifs[63].

1.5.2 Transmission and sources of *Cryptosporidium*

Cryptosporidium can be transmitted via a wide range of routes including faecal-oral, foodborne and waterborne[18]. The environmentally robust oocyst is resistant to commonly used disinfectants such as chlorine[64]. As large numbers of oocysts are shed in the faeces of infected hosts, and *Cryptosporidium* has a very low ID_{50}, transmission is highly effective[18]. *C. parvum* is zoonotic and is responsible for infecting a wide range of host species, hence wild and domestic animals can serve as a reservoir of *Cryptosporidium* for transmission to humans[10].

1.5.3 Pathogenesis

The range of hosts and the symptoms of cryptosporidiosis varies depending on the species of *Cryptosporidium* causing the infection, the type of host, as well as the immune status of the host[65]. Typical symptoms can range from asymptomatic, to acute self-limiting diarrhoea, to chronic illness and even death in immunocompromised hosts[10,20]. For example, infection of *C. parvum* in humans and calves commonly leads to unique watery diarrhoea, but the infection of *C. parvum* in wild rodents shows no symptoms[10].

In humans, when the host's immune system is intact, cryptosporidiosis symptoms normally last 10-14 days. However, oocyst shedding may continue for as long as a few weeks[66]. In immunologically impaired hosts and HIV infected persons, diarrhoeal frequency and the volume escalates, rapidly becoming chronic. Nevertheless, cryptosporidiosis may be resolved spontaneously without any clinical reason, that further complicates the interpretation of treatment data[66].

Large human populations can be carriers of this parasite without exhibiting any symptoms. One study estimated that the prevalence in developed countries (Nordic countries) was 0.99% in the asymptomatic human population[67]. Conversely, in the less developed part of world, more than 30% of the population can carry *Cryptosporidium* asymptomatically, and are assumed to be the result of either shedding after resolving the diarrhoea, and/or due to continuous exposure to the

parasite[68].

Three mechanisms resulting in diarrhoeal symptoms observed during *Cryptosporidium* infection have been proposed: osmotic diarrhoea caused by parasite-induced damage of intestinal architecture; secretory diarrhoea from metabolites of inflammatory or hormonal host response; and secretory diarrhoea caused by a hypothetical enterotoxin produced by the parasite[69]. It has been observed that the faecal supernatant from *Cryptosporidium* infected calves can cause an enterotoxic response in human jejunal and Caco-2 cells. Alternatively, in some cases it can display a cytotoxic effect such as reduction in the intestinal absorption surface[69]. However, such toxins have yet to be identified.

1.8 *Cryptosporidium* Polyketide Synthase and its Polyketide Product

1.8.1 Polyketide synthase and polyketides

Polyketides are secondary metabolites that display a wide range of structural and functional diversity[70]. They are called secondary metabolites, in contrast to primary metabolites that have either a role in energy production/storage or a structural related role or other cell core process[71]. Polyketide compounds are commonly found to be synthesised in bacteria[72], fungi[73], higher plants[74] and protists[75]. They have received

significant attention due to their wide range of applications in antibiotic[76], anticancer[77], antifungal[78], antiparasitic[79] and immunosuppressive activities[80].

Polyketide biosynthesis is carried out by polyketide synthase (PKS). PKS is closely related to fatty acid synthase (FAS) that performs fatty acid biosynthesis. Both pathways shares strong homology, for the common chemistry involved, the common precursor compound used, and their similar enzyme structures[80]. Both polyketide and fatty acid biosynthesis involves sequential condensation of acyl units onto a growing carbon chain[81]. Once the polyketide is released from PKS, it is typically modified by a tailoring enzyme system to impart additional functionality and yield biologically active compounds. This is a major source of diversity in polyketide biosynthesis[82,83].

1.8.2 Classification of PKS

PKSs are classified into Type I, II or III. Type I PKS is found in both bacteria and fungi, where all catalytic sites for each round of chain extension are contained in one bulk module and several modules join together to complete the polyketide biosynthesis[84]. Type II PKS is exclusively found in bacteria, it made of several proteins each catalyse one step of the reaction, and each catalytic site is used iteratively[85,86]. However, there are some Type I PKS that also use the single module interactively such as the PKS responsible for avilamycin biosynthesis[87]. More recently, type III PKS has been identified in streptophytes, some bacteria and plants, it has a

homodimeric structure and uses catalytic sites iteratively[74].

1.9 PKS in *Cryptosporidium*

The PKS gene was first identified in *C. parvum* in 2002 and was named CpPKS1[88]. This was the first time that a PKS gene was identified in protists[70,88]. The predicted protein product of CpPKS1 consists of 13,414 amino acids with a predicted *Mr* of 1516.5 kDa[88]. The transcription of this 40 kbp putative Type I PKS gene was confirmed by RT-PCR using total RNA isolated from excysted sporozoites and the intracellular stage of *C. parvum*, and the PKS protein has recently been identified in *C. parvum* by Mass Spectroscopy (MS)[89]. Zhu et al.[90] proposed that the CpPKS1 gene in *Cryptosporidium* was of a bacterial origin. It is evolutionarily related to the FAS gene of *Cryptosporidium* and the appearance of CpPKS1 was most likely due to a gene duplication event. It has been hypothesized that the interaction of *Cryptosporidium* with various gut-dwelling bacteria provided an increased likelihood of a lateral gene transfer (LGT) event[88]. Furthermore, John et al.[70] suggested that the LGT would have happened early in *Cryptosporidium* evolution as the PKS I genes from protists do not group with any previous known PKS I group[70].

As genome sequencing of the major *Cryptosporidium* species progresses, a PKS gene has also been identified in *C. hominis*[70] and *C. muris*[91]. In 2010, a proteomic

investigation identified PKS protein in *C. parvum, C. hominis*, but not in *C. muris* and *C. andersoni*, using a differential display of intact oocyst proteins and analysis using 1D liquid chromatography-mass spectrometry (LC-MS). It was hypothesized that the expression of the PKS gene may be specific to intestinal-lineage species, but the inconsistency between the presence of PKS gene and the absence of an PKS protein in *C. muris* was not determined[89].

1.9.1 Structure of PKS and CpPKS1

PKS have been reported to have a maximum of seven enzymatic domains including KS (ketoacyl synthase), AT (acyl transferase), ketoacyl reductase (KR), dehydratase (DH), enoyl reductase (ER), acyl carrier protein (ACP) and thioesterase (TE) to complete the sequential condensation of acyl units onto a growing carbon chain[80]. However, PKS can complete the chain extension reaction with a minimum of three domains only (i.e., ACP, KS and AT)[70]. The PKS gene in *Cryptosporidium* is encoded by a 40 kb intronless open reading frame (ORF) that predicts a single polypeptide[88]. Based on sequence analysis, Zhu et al.[88] assigned 29 enzymatic domains to CpPKS1 (Figure 1.4). Subsequently, CpPKS1 was organised into a loading unit, seven chain elongation modules and a termination domain. Within modules 3-5, there were still regions whose functions could not be assigned based on sequence analysis. The protein product is predicted to be released by a reductase instead of a thioesterase at the termination domain suggesting it produces aldehydes or alcohol as a product.

Since aldehydes are usually unstable and toxic to cells, they need to be readily converted into an acid or alcohol, although such an enzyme has not yet been identified[88]. Based on the module structure of CpPKS1, the hypothetical biosynthetic intermediates have been proposed (**Figure 1.4**), and the part synthesised by CpPKS1 has a molecular weight of 299 Da. Due to the presence of several keto and hydroxyl groups in the intermediates, the final product has been hypothesised to contain a ring structure[88].

Due to the large size of CpPKS1, it cannot be cloned and expressed as a whole gene, but attempts have been made to express each domain individually. Each domain of FAS and the ACP domain of CpPKS1 has been expressed successfully and exhibits activity[92]. Expression studies showed that the acyl-[acyl carrier protein] ligase part ACP domain prefers long chain fatty acids as a starter unit[93]. It was also shown that CpPKS1 was capable of utilising a wide range of short to very long chain fatty acids as substrates while the optimal affinity was achieved with C20 fatty acids. However, *Cryptosporidium* is incapable of *de novo* fatty acid synthesis, and the mechanism of scavenging from the host is unclear[90]. Thus it is difficult to predict what the starter unit for CpPKS1 is. The reductase domain of FAS is highly similar to the reductase of CpPKS1, it can utilise long chain fatty acid CoA as substrate. Its activity increases in respect to the increased carbon chain length of substrate, and exhibits no activity when fatty acid CoA containing 18 or fewer carbons was used for substrate[94]. The

reductase domain is capable of releasing its product as either fatty aldehyde or alcohol, but as aldehydes are toxic to cells, it has been speculated that the product would most likely be a long chain fatty alcohol rather than an aldehyde[94].

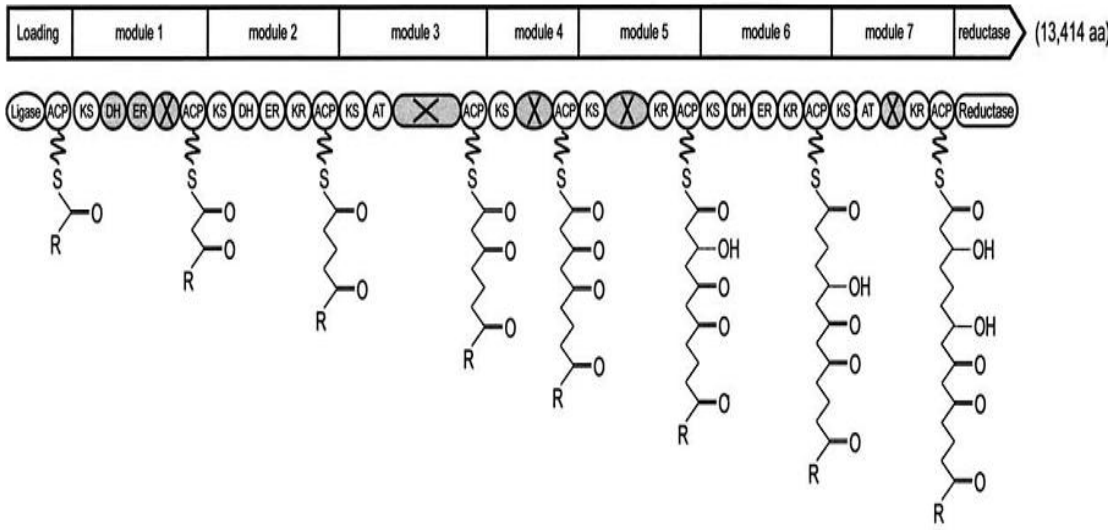

Figure 1.4 CpPKS1 structure and hypothetical biosynthesis intermediates.

Shadowed boxes are either inactive domains or nonfunctional sequences. R is the unknown starter unit (reproduced from Zhu et al.[88]).

1.10 Function and localisation of CpPKS1

Presently, the function of the CpPKS1 gene product and the identity of its hypothetical polyketide product are unknown. In 2005, Thompson et al[18] hypothesised a link between the presence of CpPKS1 to the unique watery diarrhoea caused by *C. parvum*, and has proposed the function of the polyketide is to "enhance the ability of *Cryptosporidium* to colonise the small intestine and/or better compete with other

microorganism or act as a toxin that lead to watery diarrhoea".

In 2002, immunofluorescence labeling with chicken anti-CpPks1 polyclonal antibodies targeting *Cryptosporidium* PKS indicated that CpPKS1 was expressed cytosolicly and was distributed along the anterior half of the sporozoites, where co-locolization occurs between rhoptries, dense granules and micronemes (**Figure 1.5**). These three organelles all have a function in the penetration of host cells, thus, CpPKS1 may have a similar function which should be investigated further[88]. By comparison, a differential proteomic investigation comparing the intact oocysts, the oocyst walls, and the sporozoites of *C. parvum* revealed that that a CpPKS1 protein of the predicted size was only identified at high levels in the fluid surrounding the sporozoites within the intact oocysts[89]. Such a contradiction in localisation has not yet been explained, and the literature supports neither observation.

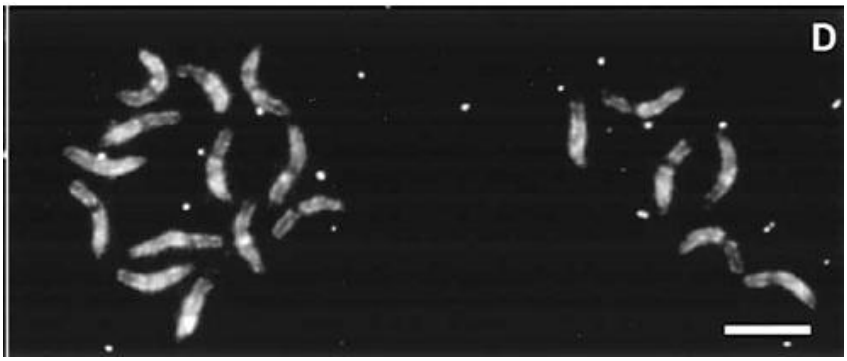

Figure 1.5 Immunofluorescence labeling of CpPKS1 protein in *C.parvum* sporozoites.

CpPKS1 protein was labelled with chicken anti-CpPks1 polyclonal antibodies targeting *Cryptosporidium* polyketide synthase. The fluorescent staining was localised at the anterior half of the sporozoites suggesting the cytosolic expression of CpPKS1 (reproduced from Zhu et al. [88]).

1.11 Mass Spectroscopy (MS) and its application in *Cryptosporidium* polyketide identification

1.11.1 Theory of Mass Spectroscopy

Mass spectrometry (MS) measures the molecular weight of individual compounds by detecting the ion formed by that compound. In MS, the analytes are ionised at the ion source, and fragment ions can be produced simultaneously. The analyte ion and its fragment ions then enter an analyser, at where they are separated based on their *m/z*

(mass-to-charge) ratios. Different types of analysers are available to use that vary in cost, accuracy and resolving power. The separated ions are detected in the detector and the signals generated are amplified and displayed as a mass spectrum (Figure 1.6)[95].

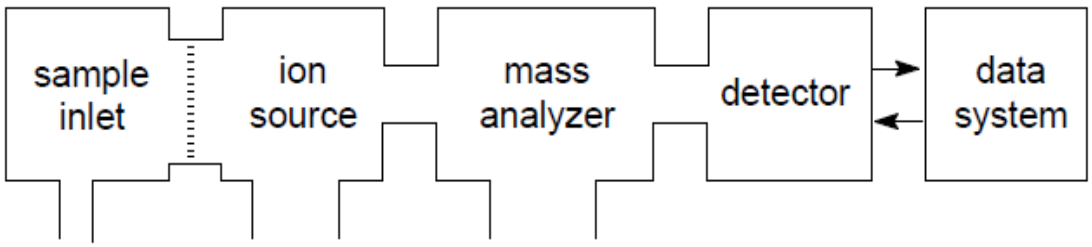

Figure 1.6 Basic concept of mass spectrometry, reproduced from Gross[96].

Several different types of ionisation techniques are available. However, ElectroSpray ionization (ESI) is one of the most widely adopted ionization techniques in biological studies. It is applicable to liquid-phase samples and allows ultrahigh detection sensitivity (attomole to femtomole)[95]. Nanoelectrospray (nano-ES) is a miniaturised version of ESI and can operate at a submicroliter flow rate. Both ESI and nano-ES are based on same mechanism that produces ions by adding or removing one or more H^+ from the analyte molecule and producing ions in form of $[M+nH]^{n+}$ or $[M-nH]^{n-}$. Compared with ESI, Nano-ES utilizes even less sample, thus it allows prolonged accumulation of the data and more detailed analysis on the fragment ions by tandem MS experiments to be conducted on the same amount of sample[97].

ESI based ionization techniques are considered as “soft” ionization, such that it produces molecular ions and provides little structural information. In order to obtain structural information, tandem MS has been introduced[98]. Tandem MS ultilises Collision-Induced Dissociation (CID) to produce a fragment spectrum from a selected molecular ion[99,100]. In CID, the selected molecular ion collides with inert gas atom and generates fragments. The fragment ions produced are detected and generate a fragment spectrum.

Database search is a common approach for interpreting MS data especially in proteomic studies. However, in metabolomics investigations, it requires *de novo* interpretation as metabolite spectra databases only cover a small fraction of naturally occurring metabolites[101]. There are well-established spectral libraries for EI sourced spectra, but, for spectral generated by CID, there is a lack of a standardised spectral library, owing to a high instrument dependent variability[102].

Compared with protein identification, *de novo* interpretation of metabolite MS data is more complicated, as it neither possess a linear structure such as proteins, nor a tree-like structure such as glycans[101]. To date, there is no well-established program to interpret MS data without using a database. Several approaches have been attempted in automated structure determinations, nevertheless, they either require excellent mass accuracy (below 2 ppm)[103] or can only provide the molecular formula of the

compound[101].

1.11.1 The Application of MS in metabolomics studies

Two complementary approaches are used for metabolomics investigations: metabolic profiling and metabolic finger-printing[104]. Metabolic profiling focuses on the characterisation of a single metabolite or a group of related metabolites[105]. In contrast, metabolic finger-printing is a more global approach that aims to identify metabolite(s) that changes in response to disease, toxin exposure, environmental or genetic alternations[105].

Before a biological sample can be analysed by MS, the metabolites from the biological sample need to be extracted and concentrated. MS can also be combined with a separation technique such as gas chromatography (GC), liquid chromatography (LC) or capillary electrophoresis (CE) to significantly increase the number of metabolites that can be identified in the sample as it reduces the number of metabolites that enter the MS system each time[104,106].

MS together with Nuclear Magnetic Resonance (NMR) are the most commonly employed methods of detection in metabolomics investigations. Compared with NMR, MS is a high-throughput technique that is capable of providing information or identification on metabolites at extremely low concentrations with extremely high

sensitivity[106]. However, it provides little information for downstream structural characterisation of unknown compounds[107].

1.12 Aims and implications of this study

The aims of this thesis are to characterise PKS gene diversity and identify a potential toxin through carrying out both a molecular and a mass spectrometric investigation. Specifically I will:

1. Investigate the CpPKS1 gene diversity within the *C. parvum* and *C. hominis* species at the subtype level.
2. Characterise the relationship between CpPKS1 gene diversity and *Cryptosporidium* host specificity.
3. Explore the possibility of using MS to study metabolites of *C. parvum* and develop a metabolomics profile.
4. Identify potential *Cryptosporidium* polyketide candidate(s) and determine their structures.
5. If a suitable polyketide candidate is identified, further cell-based assay could be performed to investigate its effects on human cell lines. The identification of this potential toxin could lead to a pathogen-specific detection method, and an effective treatment option for cryptosporidiosis.

Chapter 2. Material and methods

2.1 Source of oocysts and DNA for molecular characterisation

Cryptosporidium oocysts used for CpPKS1 gene characterisation were obtained from the Macquarie University *Cryptosporidium* library, the UK *Cryptosporidium* Reference Unit, and the University of NSW (UNSW) *Cryptosporidium* oocyst collection. The oocyst samples from the UNSW collection were identified at species level by the analysis of the 18S rDNA, the samples from Macquarie University and the UK collection were identified at subtype level by GP60 sequencing at their facilities[108,109].

2.2 Molecular characterisation of *Cryptosporidium* PKS gene

2.2.1 DNA extraction

Genomic DNA was extracted from purified oocysts using prepGEM^{Tm} Tissue Kit (ZyGEM Corporation Ltd., Hamilton, New Zealand) as described previously[34].

Briefly, an aliquot (10 µl) of purified oocysts was added to a tube containing 89 µl PCR grade sterile water, 10 µl 10 x Buffer (Supplied with *prep*GEM enzyme), and was frozen at -80 °C for 30 min and thawed. After two freeze and thaw cycles, 1 µl prepGEM enzyme was added to the mixture. The mixture was vortexed and incubated at 75 °C for 15 min and 95 °C for 5 min using a thermocycler. DNA extracts were then centrifuged at high speed for 3 min to separate cell debris, and the lysates stored at 4 °C until used.

2.2.2 60 kDa glycoprotein gene sequence based genotyping

The subtype of *Cryptosporidium parvum* and *Cryptosporidium hominis* samples from UNSW *Cryptosporidium* oocysts collection were determined using a GP60-specific PCR, utilising the forward primer (gp15ATG) 5'-CGG GAT CCA TAT GAG ATT GTC GCT CAT TAT C-3' and reverse primer (gp15STOP) 5'-GGA ATT CTT ACA ACA CGA ATA AGG CTG-3' as described by Strong[19]. PCR mixtures contained 50% GoTaq® Green Master 2 x (Promega, Madison, USA), 500 nM forward and reverse primers, 1 mg/ml BSA and 1 µl template DNA. Reaction conditions comprised an initial denaturation step at 94 °C for 3 min, followed by 35 cycles consisting of 94 °C for 30 s, 60 °C for 45 s and 72 °C for 1 min, with a final extension step at 72 °C for 7 min. All PCR reactions performed included a negative control that did not contain *Cryptosporidium* DNA but PCR water only, and a positive control containing DNA of a *C. parvum* A18G3R1 isolate that was previously characterised. PCR reactions were

carried out using a BIO-RAD Mycycler thermal cycler (BIO-RAD, Gladesville, Australia). PCR products were visualised as described in section 2.3.2 and PCR amplicons with the correct size fragment (~ 1000 bp) purified as described in section 2.3.2.5, and sequenced as described in section 2.3.2.6.

Subtype family assignment on gp60 sequences were performed by comparing the sequence with standard sequences retrieved from NCBI database. Isolates were assigned a subtype according to the nomenclature system described by Sulaiman et al[39].

2.2.3 CpPKS1gene characterisation

2.2.3.1 Primers used in CpPKS1 characterisation and novel primers design

The diversity of the CpPKS1-like gene in *C. fayeri*, *C. cuniculus*, *C. bovis*, *C. andersoni*, and *C. ryanae* was investigated using five nested PCRs with 9 sets of in-house designed PCR primers (**Table 2.1**). The sequences of the primers were based on the sequence similarity between *C. parvum*, *C. hominis* and *C. muris*. The DNA sequence of the *C. hominis* PKS gene was incomplete in both NCBI (http://www.ncbi.nlm.nih.gov/) and the cryptodb (http://cryptodb.org/cryptodb/) database, thus primer set KS2 (that targets the KS domain of module 2) were designed based on *C. parvum*, *C. hominis* and *C. muris* PKS sequence. The primer sets

targeting KS region module 5, ACP-KS region module 3, ER region module 1 and the reductase domain were designed based on *C. parvum* and *C. muris* sequence. The retrieved sequences were aligned using ClustalX 2.1. The regions of at least 20 bp long, with less than three sites of mutation and no mutation at the 3' end were selected as primer sites. Furthermore, the second primer sites were selected that were no further than 2 kb away from the first primer site. Five regions of PKS gene were amplified and are summarised on **Figure 2.1**.

2.2.3.2 Primers used in PKS gene characterisation in human infectious *Cryptosporidium* species at subtype level

The CpPKS1 like PKS gene diversity in human infectious *C. parvum*, *C. hominis* and *C. cuniculus* were investigated using two nested and one single PCRs with five sets of PCR primers. The PCR primer used in the investigation was KS23610/KS25050, AK3F/AK3R, for the primary PCRs, and KS23842/KS24855, and AK3F/KS14530 for secondary PCRs, ER6150/ER7328 for the single PCR.

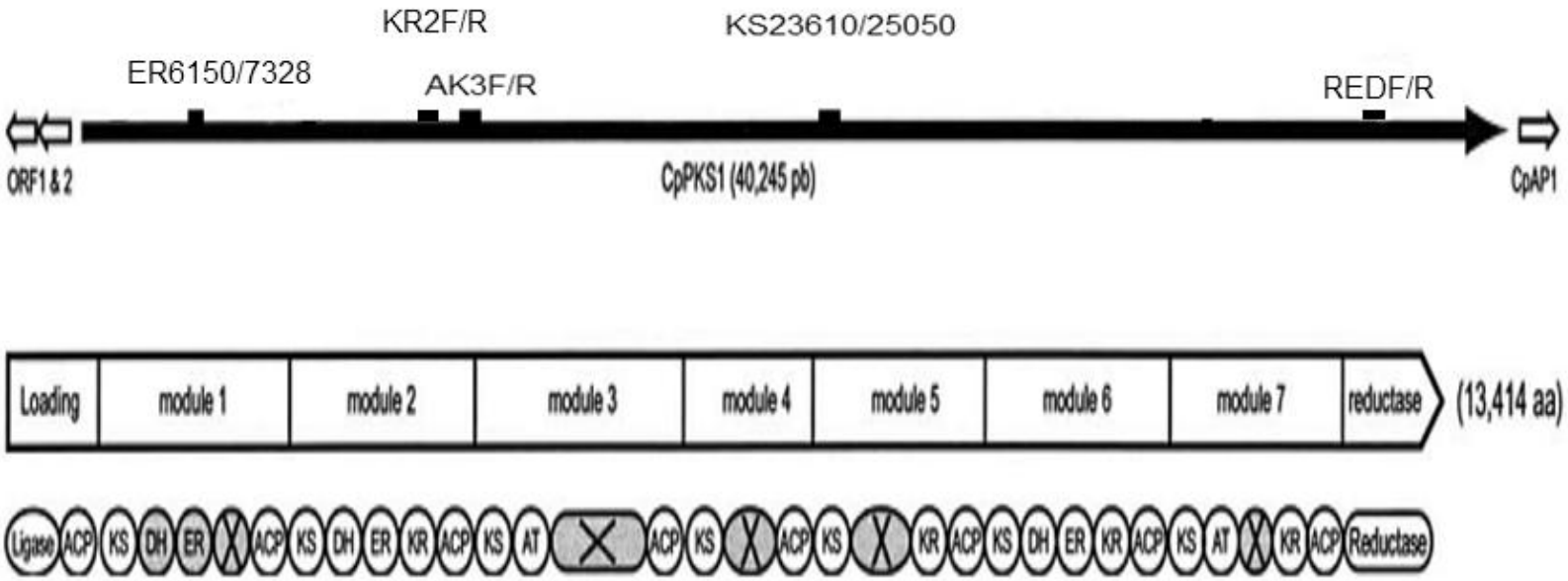

Figure 2.1 Graphic representations of regions targeted by all PCR primer sets used in this investigation. The structure of domain organisation is reproduced from Zhu et al.[88]

A, The location of each primer set used are labelled along the gene; B, the module and domain of each corresponding amplicon

Table 2.1 In-house designed primers used in nested PCR for PKS sequence comparison

Primer name	Forward primer sequence	Reverse primer sequence	Expected size	Region amplified
KR2F/KR2R	5'- GAT CAK GTW TGG GGA TTT GC -3'	5'- GAG CAW AGT AAG AAA TAT TGA A -3'	1.3 kb	KR domain of module 2
REDF/REDR	5'- ATW CAA TGG GGA CCA TGG G -3'	5'- ACT AAA TGW ATT GCC ATW TTT GTT -3'	1.56 kb	reductase domain
AK3F/AK3R	5'- ATY AGT ATT CAA TGG GG -3'	5'- AWG TTC CAG TAC CAT GGC -3'	1.55 kb	ACP and KS domain module 3
KS23610/25050	5'- GAY ACT CCW ATT CGT GAA -3'	5'- ATT GCA TGT GCR TTC GTT CC -3'	1.44 kb	KS domain module 5
ER5960/7940	5'- GAT CAK GTW TGG GGA TTT GC -3'	5'- GAG CAW AGT AAG AAA TAT TGA A -3'	1.98 kb	ER domain module 1
ER6150/7328	5'- ATC CAT GCT KCA ACT GGT GG-3	5'- AAG GGC ARA CAT ATT ATT CC -3'	1.67 kb	ER domain module 1
Secondary PCR				
KR12107/KR13145	5'- ATC CAT GCT KCA ACT GGT GG-3'	5'- AAG GGC ARA CAT ATT ATT CC -3'	1.03 kb	KR domain of module 2
RED39111/RED39904	5'- TCT YTA ATG CTT GAT AAT CC -3'	5'- TCT GCT GCC CAT TTA GAT TG -3'	793 bp	reductase domain
AK3F/KS14530	5'- ATY AGT ATT CAA TGG GG -3'	5'- CCT TCT CCT CTT ACA AAT CCA -3'	1.31 kb	ACP and KS domain module 3
KS23842/KS24855	5'- GGT GCT AGT TGT ACK CTT CC -3'	5'- TAA ACC TGC AAT YCC TGC -3'	1 kb	KS domain module 5

2.2.3.3 Optimisation of *Cryptosporidium*-specific PKS PCRs using in-house designed primer sets

To establish optimised PCR conditions, a gradient PCR was conducted using extension temperatures spanning 46 °C to 56 °C. All PCRs using in-house designed primer sets were nested to increase amplicon specificity and quantity. For the primary PCR, reaction conditions comprised of an initial denaturation at 94 °C for 3 min, followed by 30 cycles of 94 °C for 30s, temperature gradient for 45s and 72 °C for 2 min, with a final extension at 72 °C for 7 min. Secondary PCR reactions comprised of an initial denaturation at 94 °C for 3 min, followed by 30 cycles of 94 °C for 30s, temperature gradient for 45s and 72 °C for 1.5 min and a final extension step at 72 °C for 7 min.

2.2.4 Visualisation of PCR products

PCR amplicons together with a pGEM DNA marker (Promega, Sydney, Australia) were resolved by electrophoresis on 1.5% agarose gels (w/v), made up with TAE buffer (40 mM Tris-Acetate, 1 mM EDTA) containing 0.01% SYBR safe DNA stain (Invitrogen, Mount Waverly, VIC). The agarose gels were run in TAE buffer at a constant voltage of 220 V. Gels were visualized on a Syngene GelDoc System (Syngene, Frederick, USA), under blue light transilluminator-emission.

2.2.5 PCR amplicon purification

PCR products were purified using the QIAquick PCR purification Kit (Qiagen, Melbourne, Australia). The concentration of purified PCR amplicons was determined

using a Nanodrop (Biolab, Australia). Purified PCR products were stored at 4 °C.

2.2.6 Sequencing of purified PCR amplicons

Sequencing reactions were performed in 20 µl volumes containing 1 µl BigDye terminator V3.1 (Applied Biosystems, Australia), 20 ng purified PCR product for PCR using primer sets KS23842/KS24855, AK1F/KS14530 and ER6150/7328, 10 ng for PCR using primer sets ACP1, AT7 and KS2, 3.2 pmol forward primer, 3.5 µl 5x buffer (Applied Biosystems, Australia) and PCR grade water. The PCR reaction consisted of 25 cycles of 96 °C for 10 s, 50 °C for 5 s and 60 °C for 4 min.

The sequencing PCR products were mixed with 5 µl 125 mM EDTA (Ethylene diamine tetraacetic acid), and 60 µl 100% ethanol, mixed and incubated for 9 hours at room temperature. The mixture was centrifuged at 14,000 x g for 20 min, and the supernatant discarded. The remaining pellet was washed with 70% ethanol and centrifuged for 14,000 x g for 10 min and the supernatant discarded. The final pellet was dried by incubation at 95 °C, and samples were sequenced by the Ramaciotti Centre for phylogenetic analysis (University of New South Wales, Sydney, Australia) using an ABI 3730 sequence scanner.

2.2.7 DNA Sequence analysis and phylogenetic tree construction

DNA sequencing results were analysed by FinchTV version 1.4 (Geospiza Inc.,), sequence alignments were performed using ClustalX 2.1. Phylogenetic trees were constructed with maximum likelihood method using MEGA 5[110], and the model of best fit was selected by MEGA 5 with the lowest Bayesian Information Criterion

scores, and the phylogenetic trees were tested with 500 bootstraps.

The phylogenetic tree of the ketoreductase domain was constructed by comparing the ketoreductase sequence identified in *Cryptosporidium* with CpPKS1-similar sequences retrieved from NCBI database using a BLAST search.

2.3 Polyketide identification

2.3.1 Oocyst purification

2.3.1.1 Initial screening for *Cryptosporidium* oocysts in faeces

The oocysts for polyketide identification were purified from faecal samples collected from neonatal calves from a diary farm in Camden, New South Wales, Australia that were aged between 7 to 14 days and were exhibiting diarrhoeal symptoms. Prior to oocyst purification, a faecal slurry was created by resuspending the faecal material in Milli-Q water at ratio of 10 ml per gram of faecal material and screened for the presence of oocysts. For immunofluroescence detection, 10 µl of faecal slurry were stained with the monoclonal antibody CRY104 conjugated to fluorescein isothiocyanate (FITC; Biotechnology Frontiers, North Ryde, Australia) at a final concentration of 2 µg/ml and incubated for 5 min at room temperature. After incubation, 10 µl of stained faecal slurry was placed onto the microscopic slide and covered with a cover slide without mounting medium. The slides were examined by Epi-Fluorescence Microscopy (EFM) using an Olympus BH2 Microscope with a Nikon DXM 1200F digital camera (Olympus, North Ryde, Australia). Only those

faecal slurries containing greater than 100 oocysts per field of view under 10 x magnifications were pooled and used for oocyst purification.

2.3.1.2 Purification of *Cryptosporidium* oocysts from calf faeces

Cryptosporidium oocysts were purified using a modified sucrose flotation method [27]. Faecal flurries were sieved through a series of stainless steel meshes with decreasing pore size from 250, 106, 75 and 38 μm (Cole-parmer, Vernon Hills, USA). Sieving removes the majority of faecal detritus and thus simplifies the purification procedure. The resulting faecal filtrate was pelleted by centrifugation at 3,000 x g at 4 °C for 10 min, resuspended in 30 ml 55% sucrose (specific gravity 1.13 - 1.17), overlaid with 10 ml Milli-Q water and centrifuged again at 3,000 x g at 4 °C for 30 min. Oocysts were collected from between the sucrose-water interface with the rest discarded. The inferface was resuspended in at least 2 volumes of Milli-Q water, then pelleted again by centrifugation at 3,000 x g at 4 °C for 10 min. Oocysts were next resuspended in 20 ml of 50% sucrose, and overlaid with a further 20 ml of 30% sucrose (specific gravity 1.08 - 1.10) and then finally overlaid with 10 ml Milli-Q water. A subsequent sucrose gradient was centrifuged at 3,000 x g at 4 °C for 30 min, and oocysts were collected from between the 30% sucrose and Milli-Q water layer interface with the rest discarded. Oocysts were next washed in at least 2 volumes Milli-Q water and pelleted by centrifugation at 3,000 x g at 4 °C for 10 min. Oocysts were then resuspended in 10 ml 10% Sodium bicarbonate (NaHCO3) and mixed with 10 ml diethyl ether by vigorous shaking, then pelleted by centrifugation at 3,000 x g at 4 °C for 10 min. The final purified oocysts pellet was resuspended in phosphate buffered saline and stored at 4 °C until required.

2.3.2 Determining total oocyst counts and purity by Flow Cytometry (FCM)

2.3.2.1 Oocyst fluorescent staining

The buffer used for staining oocysts was Monoclonal Antibody Buffer (MABB) (0.5 ml Tween-80 detergent, 5 g BSA, 22.6 g tetra sodium pyrophosphate, 800 ml distilled water). Oocysts were stained with FITC conjugated monoclonal antibody (CRY104) at a final concentration of 2 μg/ml as described previously[111]. Oocysts were labelled in a total volume of 100 μl with FITC-antibody at final concentration of 10 μg/ml and vortexed. Labelled oocysts were incubated at 4 °C in the absence of light for a minimum of 10 min prior to the analysis by FCM. Positive and negative controls were set up using previously purified, stained oocysts only, or MABB only respectively.

2.3.2.2 FCM setup

Total oocysts were counted and purity estimation was obtained using the Cell Lab QuantaTM SC, Flow Cytometer (Beckman-Coulter, Gladesville, Australia). The detectors used were side scatter (SS), electronic volume (EV), and the FL-1 (green). The green fluorescent detector was used for the analysis of oocyst stained with the FITC labeled antibody CRY104. On the day of analysis, flow check beads (Beckman-Coulter) were used for instrument setup as described in the manufacturer's manual.

2.3.2.3 Data acquisition and analysis

The positive oocyst sample was used to adjust gate control settings on SS and EV

detectors so that oocysts could be identified on a bivariate dotplot of log SS vs EV (Figure 2.2 A). An ellipse region was defined around the centre of the oocyst population. The counts from FL1 detector were used to confirm that all oocysts were positively stained with the antibody (**Figure 2.2** B). The negative control containing MABB only was analysed using the same settings to ensure that no events were present in the defined region.

An aliquot (50 µl) of fluorescently stained oocysts was analysed using the same settings in triplicate. Oocyst counts were obtained by enumerating only those particles present within the previously defined region and the counts were compared with counts detected by the FL1 detector to ensure that the counts obtained were stained oocysts only.

The purity of the oocyst sample was estimated by using the number of oocysts detected divided by the total number of particles detected after subtracting the number of particles from the negative control: $\frac{\text{Counts from sample-Counts from negative control}}{\text{Counts from sample}}$.

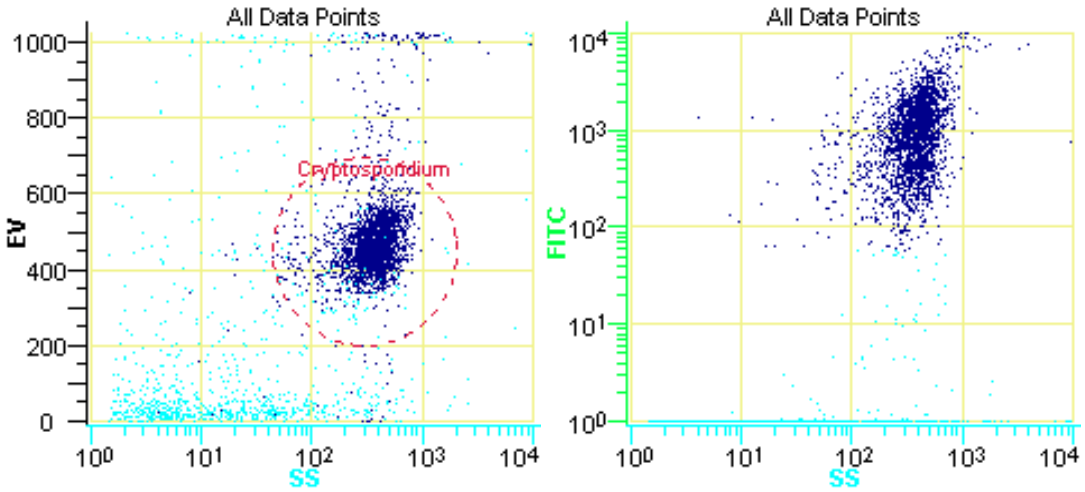

A B

Figure 2.2 Bivariate dot plots of electronic volume (EV) versus side scatter (SS) in arbitrary units.

One dot represents a single cell or particle. The ellipse region in A defines the expected location of *Cryptosporidium* oocysts in the bivariate dotplot. B shows the number of particles detected that are also fluorescently labelled.

2.3.3 Oocyst excystation

Excystation was performed as described by Kato[112]. Ten million oocysts (1×10^7) were pelleted by centrifugation at 3000 x g for 3 min and incubated in PBS (pH 2.8) at 37 °C for 30 min. Oocysts were then pelleted by centrifugation (3000 x g, 3 min), and then was washed with Hank's balanced salt solution (HBSS) and pelleted again by centrifugation (3000 x g, 3 min). Oocysts were then incubated in 1 ml of excystation medium (10 mM HEPES, 0.2 mM sodium deoxycholate, 22 mM sodium hydrocarbonate in HBSS) at 37 °C for 2 hours, and a portion was examined by microscopy to ensure a minimum 90% excystation efficiency. Sporozoites and oocyst

walls were pelleted by centrifugation (3000 x g, 3 min), and the excystation supernatant fraction was also collected.

2.3.4 Polyketide extraction

An aliquot (300 μl) of ethyl acetate and acetic acid mixture (99:1) was added to 1 x 10^8 freshly purified oocysts. Oocysts were mixed by vortexing and sonicated using a probe sonicator at 20% maximum output for 10 x 30s and kept on ice between sonications. Oocyst samples were then centrifuged at 3,000 x g for 5 min and the supernatant collected. The ethyl acetate and acetic acid extraction step was then repeated twice and all supernatants were pooled. The pellet was then mixed with methanol and acetic acid mixture (99:1) and vortexed. Oocyst samples were then centrifuged at 3,000 x g for 5 min, and the supernatant was pooled with the supernatant extracted earlier with ethyl acetate. The methanol and acetic acid extract step was then repeated twice and all supernatants were pooled. The final supernatant was air dried by evaporation in a fume hood. Ethyl acetate extraction was also performed on the excystation supernatant, sporozoite and acid wash fractions collected in section 2.3.3. The remaining pellet after air drying was re-dissolved in methanol at a final concentration of 10 mg/ml.

2.3.5 Nanospray and tandem MS

Oocyst extracts were run on an Orbitrap LTQ XL (Thermo Fisher Scientific, San Jose Ca, USA) ion trap mass spectrometer using a nanospray (nano-electrospray) ionization source to generate ions from the analytes in solution. The instrument was calibrated with a standard calibration solution as outlined in the instrument manual on

the day of analysis using direct infusion into the source. The instrument conditions were optimised for sensitivity using LC tune software (thermo Fisher Scientific, San Jose Ca. USA). The analysis was carried out in positive ion mode using the orbitrap FTMS analyser at a resolution of 60000. An aliquot (2µl) of extract at a concentration of 1 mg/ml, was injected into a glass needle and inserted into the nanospray source with a spray voltage of 1.5 kV used. Ions generated were measured over the mass range 150 to 1000 Da using full scan mode. Data were acquired in full scan mode over 120 s. Product ion spectra were collected using MSn^2 on the parent ion of interest, with a CID/PQD energy set to range from 0 to 50 eV with 10 eV increments. Data were analysed using the Qual Browser feature in Xcaliber 2.1 (Thermo Fisher Scientific, San Jose, Ca, USA).

The MS spectra collected were compared with reference spectra from Metabolite and Tandem MS Database (METLIN) at http://metlin.scripps.edu/ and lipid standards from LIPID MAPS at http://www.lipidmaps.org/data/standards/index.html. When a standard was unavailable, *de novo* structural elucidation was conducted.

Chapter 3 Results on PKS gene diversity in *Cryptosporidium* species

3.1 Background and aims

Over 95% of cryptosporidiosis in humans is caused by *C. parvum* and *C. hominis* infections, and both are responsible for several large waterborne outbreaks of the disease[56]. Recently, *C. cuniculus* has been recognised as a third species that can cause outbreaks in humans[108]. Six and nine allele families within *C. hominis* and *C. parvum* have been identified respectively[56]. However, *C. hominis* infection are predominantly caused by the IbA10G2 subtype[109], whereas the *C. parvum* infections are caused by IIaA18G3R1 and IIaA15G3R1 subtypes[109,113]. Currently, it is unknown what factors contribute to the higher prevalence of these three *Cryptosporidium* subtypes.

In 2005, Thompson linked the unique watery diarrhoeal symptom occurring during *C. parvum* infection to the presence of a PKS gene and proposed the role of a polyketide product may be to either cause this symptom or to enhance the competitiveness of *C. parvum* against other microbes present in the intestinal tract[18]. There have been two hypotheses on the origin of the PKS gene: 1) from bacteria that co-localise with *Cryptosporidium* in the intestinal tract[88], 2) inheritance from an ancestor gene from other Apicomplexans[70]. The two hypotheses were based on the phylogenetic relationships of the ketoacyl synthase domain with the PKS gene in other

organisms[70,75,88].

The PKS gene has been identified in *C. parvum*[88], *C. hominis*[58] and *C. muris*[91]. The PKS gene in human infectious *C. parvum* is approximately 60% identical to the PKS gene in human non-infectious *C. muris*[91]. In a proteomic investigation on the intact oocyst in 2009, the PKS protein was only positively identified in the intestinal tract species (*C. parvum* and *C. hominis*) but not in the gastric lineage species (*C. muris* and *C. andersoni*)[89], suggesting a potential correlation between the PKS gene and human infectivity.

The aims of this chapter are to:

1. Investigate the distribution of PKS gene in various *Cryptosporidium* species using degenerate primers specific for the *Cryptosporidium* PKS gene.
2. Explore the PKS gene diversity at subtype level in the most common human infectious *Cryptosporidium* species: *C. parvum*, *C. hominis*, and *C. cuniculus*.

3.2 Design and optimisation of degenerate primer sets for PKS gene identification using PCR

Degenerate primers used for PCR targeting the ER domain of the first module, KR domain of the second module, ACP and KS domain of the third module, KS domain of the fifth module and the reductase domain were designed based on the complete PKS gene sequences of *C. parvum*, *C. muris* and partial sequences of *C. hominis* in the NCBI database. The regions on the PKS gene amplified by degenerate primers are shown in **Figure 2.1** and the sequence of the primer sets are summarised in **Table 2.2**. An optimised annealing temperature for both primary and secondary PCRs for all primer sets employed was determined using an annealing temperature gradient between 46 °C to 56 °C.

In the primary PCR for amplification of the KR domain, a similar yield by band intensity was achieved at annealing temperatures of 53.9 and 52 °C (**Figure 3.1 A**). In order to reduce non-specific binding, a higher annealing temperature was selected at 53.9 °C. At the reductase and ACP-KS domain, the PCR yields increased when the annealing temperature decreased, as indicated by the increased band intensity (**Figure 3.1 B** and **C**). At the KS domain, the band appeared at higher size than expected (1.44 kb). However, sequencing of the PCR product confirmed that the correct region was

amplified (Figure 3.1 D). The ER domain failed to be amplified by the primer set, hence a new set of primers were designed to amplify a smaller segment of a similar region.

Therefore, to reduce the time required for all five PCR reactions, while minimising non-specific primer-template binding, an annealing temperature of 54 °C was selected for all subsequent reactions.

To increase the quantity of resulting PCR products, while increasing the specificity of the PCR reactions, a second set of nested PCR primers were designed to amplify the PCR products from KR, AK, KS and RED domain PCR reactions. In the secondary PCRs (and new primer sets for the ER domain), the PCR reactions for all five domains achieved high yields for all annealing temperatures tested with the maximum yield achieved at the temperature range between 49.6 to 53.9 °C (**Figure 3.2**). Thus, a middle point annealing temperature of 52 °C was finally selected for all secondary PCRs. In the PCR targeting the ER domain (Figure 3.2 E) the expected product was successfully amplified.

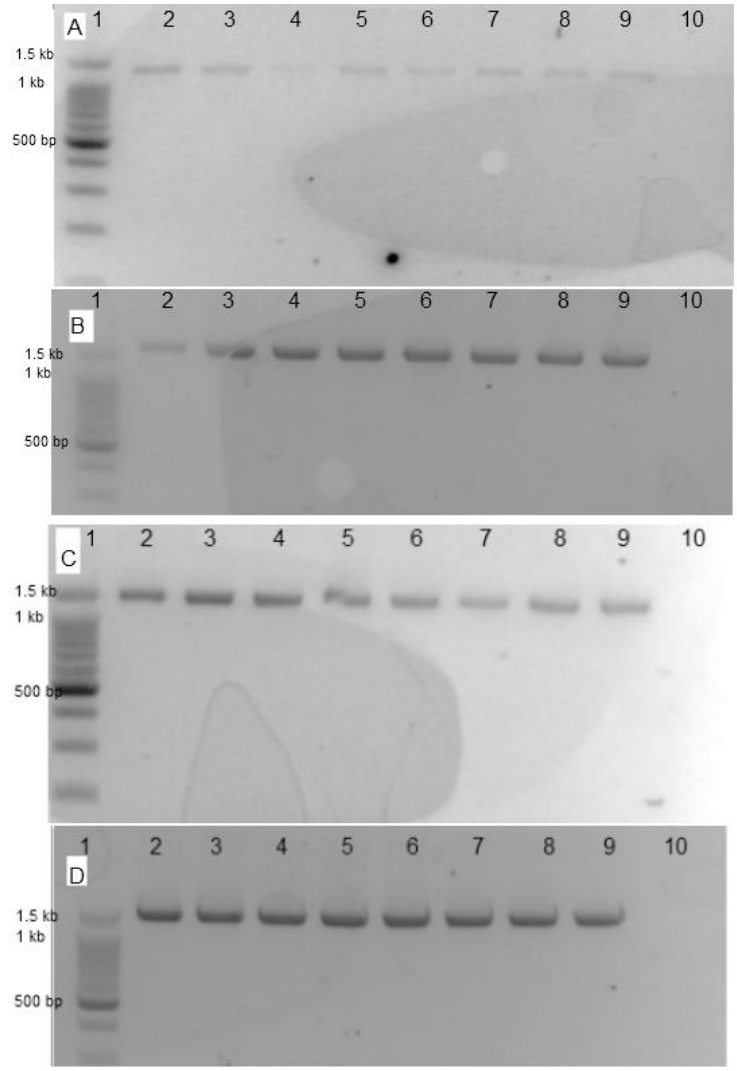

Figure 3.1 Optimisation of the primary PCR reactions for in-house designed degenerate primer sets using various annealing temperatures.

A: KR domain of module; B: Reductase domain; C: ACP-KS domain of module 3; D: KS domain of module 5. In each gel image, Lane 1, 1 kb molecular weight markers; lane 2-9, PCR products of PCR reactions with annealing temperatures of 56, 55.2, 53.9, 52, 49.6, 47.9, 46.7, 46 °C respectively; lane 10, negative control. The expected size of each amplicon for the five domains was: A: 1.3 kb, B: 1.6 kb, C: 1.55 kb, D: 1.4 kb. The sizes of two major DNA markers are labelled.

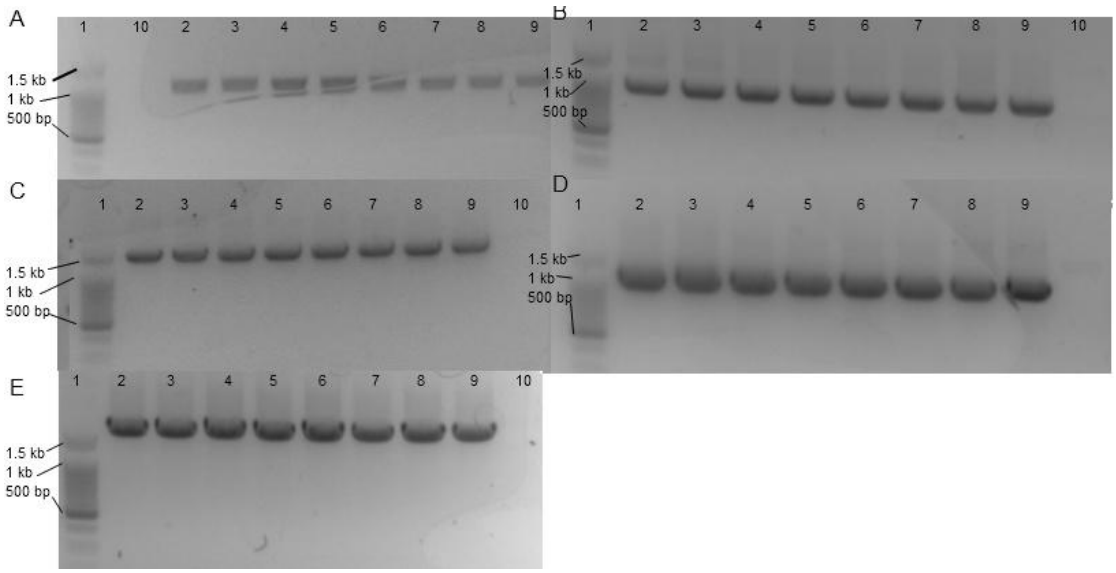

Figure 3.2 Optimisation of the secondary PCR reactions for in-house designed degenerate primer sets using various annealing temperatures.

A: KR domain of module; B: Reductase domain; C: ACP-KS domain of module 3; D: KS domain of module 5; E: ER domain of module 1. In each gel image, Lane 1, 100 bp molecular weight markers; lane 2-9, PCR products of PCR reactions with annealing temperatures of 56, 55.2, 53.9, 52, 49.6, 47.9, 46.7, 46 °C respectively; lane 10, negative control. The expected size of each amplicon for the five domains was: A: 1 kb, B: 800 bp, C: 1.3 kb, D: 1 kb, E: 1.7 kb. The sizes of major DNA markers are labelled.

3.3 Identification of PKS gene in *Cryptosporidium* species

The presence of a PKS gene in *C. cuniculus, C. fayeri*, *C. bovis, C. andersoni* and *C. ryanae* was determined using in-house designed degenerate primers targeting the Enoyl reductase (ER), Ketoacyl reductase (KR), Acyl carrier protein and Ketoacyl synthase (AK), Ketoacyl synthase (KS) and reductase (RED) domains of the PKS gene. As shown in **Figure 2.1**, **Chapter** 2. *C. fayeri, C.cuniculus*, and *C. andersoni* were positive for CpPKS1-like PKS gene, *C. bovis* was positive for the KS and KR domain, while *C. ryanae* failed the PCRs at all five regions investigated. All PCR amplicons of *C. fayeri*, *C. cuiculus*, and *C. andersoni* were sequenced successfully. However, unusual multiple bands were detected at the KR and KS domain of *C. bovis* (**Figure 3.3**), and the largest band in the KS domain was confirmed to be a CpPKS1 like PKS gene.

A comparison of resulting gene sequences is summarised in **Table 3.1**. At ER domain, 600 bp sequence was compared, and 644, 508, 720 and 599 bp were compared at AK, KR, KS and RED domain. At the all five domains analysed, *C. parvum*, *C. hominis*, *C. cuniculus*, and *C. fayeri* exhibited over 90% similarity to each other. The PKS sequences of these four species exhibited only 60% similarity to the PKS from *C. muris*. Unexpectedly, *C. andersoni* carried an identical PKS gene sequence to that of *C. parvum* at the ER, AK and KS domains, but was identical to the PKS gene sequence of *C. muris* at the KR and RED domains. To confirm this unexpected result,

all regions were amplified three times and identical results were obtained. The 509 bp region of the KS domain in *C. bovis* was sequenced successfully, and was 99% identical to the KS domain in *C. parvum*.

To assess the overall phylogenetic relationship of PKS at the gene level, a concatenated sequence of 3108 bp was constructed using the five domains tested by joining the amplicons together based on the order of the domains amplified. The phylogenetic relationships of the concatenated PKS sequences from the six species positive for the PKS gene were compared (**Figure 3.4**). Two groups were clearly identified, with intestinal lineage species *C. parvum*, *C. hominis*, *C. cuniculus*, and *C. fayeri* forming one cluster, whereas the generally considered as human non-infectious and gastric lineage species *C. muris* and *C. andersoni* are not in this cluster.

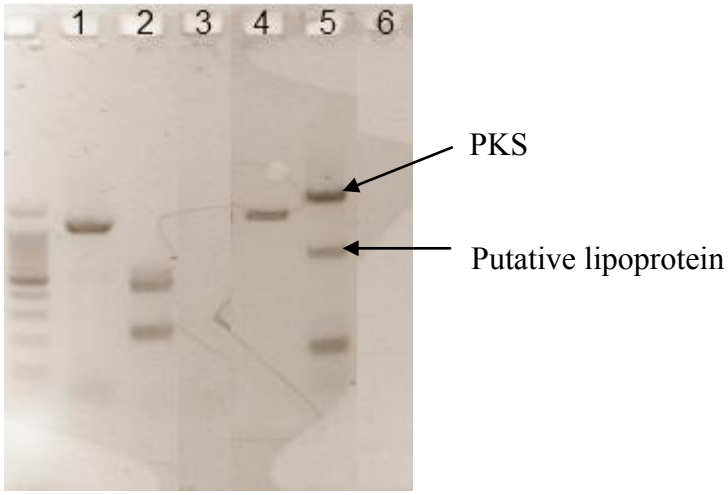

Figure 3.3 Comparison of PCR products between *C. bovis* and *C. parvum*

Lane 1-3 PCR products of the KR domain; lane 4-6 PCR products of KS domain. Lane 1, *C. parvum*; 2, *C. bovis*; 3, negative control; 4, *C. parvum*; 5, *C. bovis*; 6, negative control.

Different banding pattern was observed between the two species at both domains.

Table 3.1 DNA sequence similarities at the five domains of the PKS gene between six *Cryptosporidium* species and the *Cryptosporidium parvum* IowaII isolate

Species	Similarity to the *Cryptosporidium* IowaII sequence (CpPKS1)				
	ER	KR	AK	KS	RED
*C. parvum**	100.00%	100.00%	100.00%	100.00%	100.00%
*C. hominis***	97.80%	97.64%	96.86%	99.03%	97.48%
*C. muris****	51.00%	62.80%	58.89%	64.23%	59.03%
C. fayeri	90.72%	90.75%	91.22%	91.11%	94.36%
C. andersoni	100.00%	63.78%	100.00%	100.00%	60.20%
C. coniculus	97.80%	97.64%	96.86%	99.03%	96.83%

*most common subtype IIaA18G3R1 screened

**most common subtype IbA10G2 screened

****C. muris* comparison was based on the sequence available from NCBI database

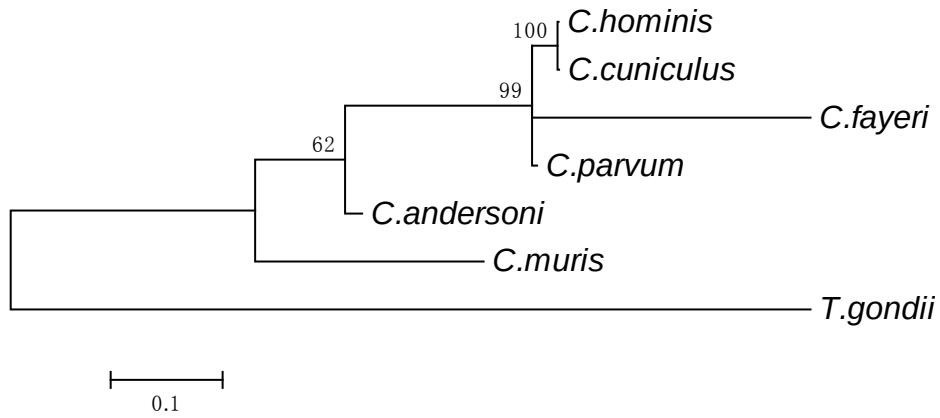

Figure 3.4 Phylogenetic relationships between *C. hominis, C. cuniculus, C. parvum, C. fayeri, C. andersoni,* and *C. muris*

The phylogenetic tree was constructed using a Maximum likelihood method with Tamura 3-parameter model (500 bootstrap) of a concatenated DNA sequence constructed from the 5 domains of PKS sequence investigated here (log likelihood is -10198.53). A concatenated PKS gene sequence from similar domains in *T. gondii* were used as an outgroup.

The PKS gene sequence from six positive species formed two groups which correlated to the site of infection.

3.4 PKS gene diversity in human infectious *Cryptosporidium* species

3.4.1 Summary of human infectious *Cryptosporidium* isolates used

Three regions of the PKS gene within 34 human infectious *Cryptosporidium* isolates were analysed, including 16 *C. hominis*, 16 *C. parvum* and two *C. cuniculus* isolates. The allele family for each isolate was determined by comparing the GP60 gene sequence with the sequences available in NCBI database. The subtypes for all isolates were determined by following the methods used by Strong[19] and Sulaiman[39]. The allele family and subtype of all *Cryptosporidium* isolates are summarised in **Table 3.2**. The amplicons from successful PCRs targeting the ER, AK, and KS domains were analysed in detail and compared against the reference sequence for the CpPKS1 gene.

Table 3.2 Subtypes of human infectious *Cryptosporidium* isolates used for PKS gene sequence analysis.

The Glycoprotein 60 sequences of 16 *C. hominis* isolates analysed consisted of seven GP60 subtypes, the 16 *C. parvum* isolates consisted of 12 GP60 subtypes and the two *C. cuniculus* isolates consisted of two GP60 subtypes.

Species	Subtype	Isolates ID
C. hominis	IaA32	1041
C. hominis	IbA10G2	35, 36, 40, 42, 43, 173, 188, 223, 1043
C. hominis	IdA16	102, 103
C. hominis	IdA17G1	714
C. hominis	IeA11G3T3	11281
C. hominis	IfA19G1	1040
C. hominis	IgA24	3010
C. parvum	IIaA14G3R1	1128
C. parvum	IIaA16G3R1	178
C. parvum	IIaA17G2R1	44
C. parvum	IIaA18G3R1	1125, farm, 202, 4
C. parvum	IIaA19G2R1	41, 191
C. parvum	IIaA20G3R1	230
C. parvum	IIaA22G3R1	203, 1124
C. parvum	IIcA5G3	12436
C. parvum	IIcA5G3a	153
C. parvum	IIdA12G1	3414
C. cuniculus	Va	15570
C. cuniculus	Vb	15735

3.4.2 Genetic diversity of the PKS gene across human infectious *Cryptosporidium* species

Approximately 2 kb of DNA was sequenced for three human infectious species: *C. parvum, C. hominis,* and *C. cuniculus*, which was equivalent to 5% of the entire PKS gene. There were 48 sites of polymorphism detected among the three species analysed, 26 of which were nonsynonymous nucleotide substitutions. The results are summarised in **Table 3.3**.

Table 3.3 Summary of nucleotide polymorphism and predicted protein sequence changes detected in the ER, AK and KS domain of the PKS gene

In total 48 mutations detected in the ER, AK and KS domains of the *Cryptosporidium* PKS gene, 26 were nonsynonymous nucleotide substitutions. The KS domain was the most highly conserved domain observed.

	KS	**AK**	**ER**
number of nucleotide transition/transversion mutation	8	26	14
predicted protein sequence changes	3	14	9
number of nucleotide transition/transversion mutation per 100 bp	1.11	3.55	2.38
number of predicted protein sequence changes per 100 amino acids	1.25	5.74	4.59

3.4.2.1 Gene and protein sequence polymorphism within the KS domain of module 5

The KS 5 domain was the most conserved region observed among the three domains analysed, as indicated by the lowest polymorphism rate at both nucleotide and protein sequence levels (**Table 3.3**). Fourteen *C. parvum*, 16 *C. hominis* and 2 *C. cuniculus* isolates were sequenced successfully at this region (**Table 3.4**). Sequences within the *C. parvum* and *C. hominis* isolates were identical within the species level, regardless of the subtype of each isolate examined. Observed polymorphisms at sites 23268, 23326, 23445, 23466, 23789, 23844 and 23850 were at the species level only.

At this domain, *C. cuniculus* was most similar to *C. hominis* isolates, as it carried an identical nucleotide to *C. hominis* at six sites (position 23,268, 23,326, 23,445, 23,466, 23,789, and 23,844) compared with only 1 site identical to *C. parvum* (position 23,850). Interestingly, a unique nucleotide polymorphism at the species level was identified at position 23877 in both subtypes of *C. cuniculus* examined.

Three nucleotide polymorphism were nonsynonymous nucleotide substitutions at this domain. A phylogenetic tree was constructed based on 720 bp gene sequences as shown in **Figure 3.5**. The species level polymorphism clustered *C. parvum* and *C. hominis* into two distinct clusters. *C. cuniculus* species more closely related to *C. hominis* over *C. parvum* and clustered with *C. hominis* isolates formed cluster I. The separate clustering of *C. parvum* and *C. hominis* at the species level was due to two amino acid variations between *C. parvum* and *C. hominis*.

Table 3.4 sequence polymorphisms between *C. parvum, C. hominis, C. cuniculus* at Ketoacyl Synthase domain of module 5

nucleotide position	23,268	23,326	23,445	23,466
C. parvum	G	G	C	T
C. hominis	A	A	T	C
C. cuniculus	A	A	T	C
Type of mutation	Transition	Transition	Transition	Transition
nucleotide position	23,789	23,844	23,850	23,877
C. parvum	C	T	T	C
C. hominis	G	C	C	C
C. cuniculus	G	C	T	A
Type of mutation	Transversion	Transition	Transition	Transversion

Eight sites of polymorphism between the three species were identified at the 720 bp sequence compared, and 16, 16 and 2 isolates from each species were screened respectively. The nucleotide sequence of *C. parvum* and *C. hominis* isolates were conserved at species level, *C. cuniculus* isolates were most similar to *C. hominis*. However, *C. cuniculus* carried a unique polymorphism from a C to A at position 23,877

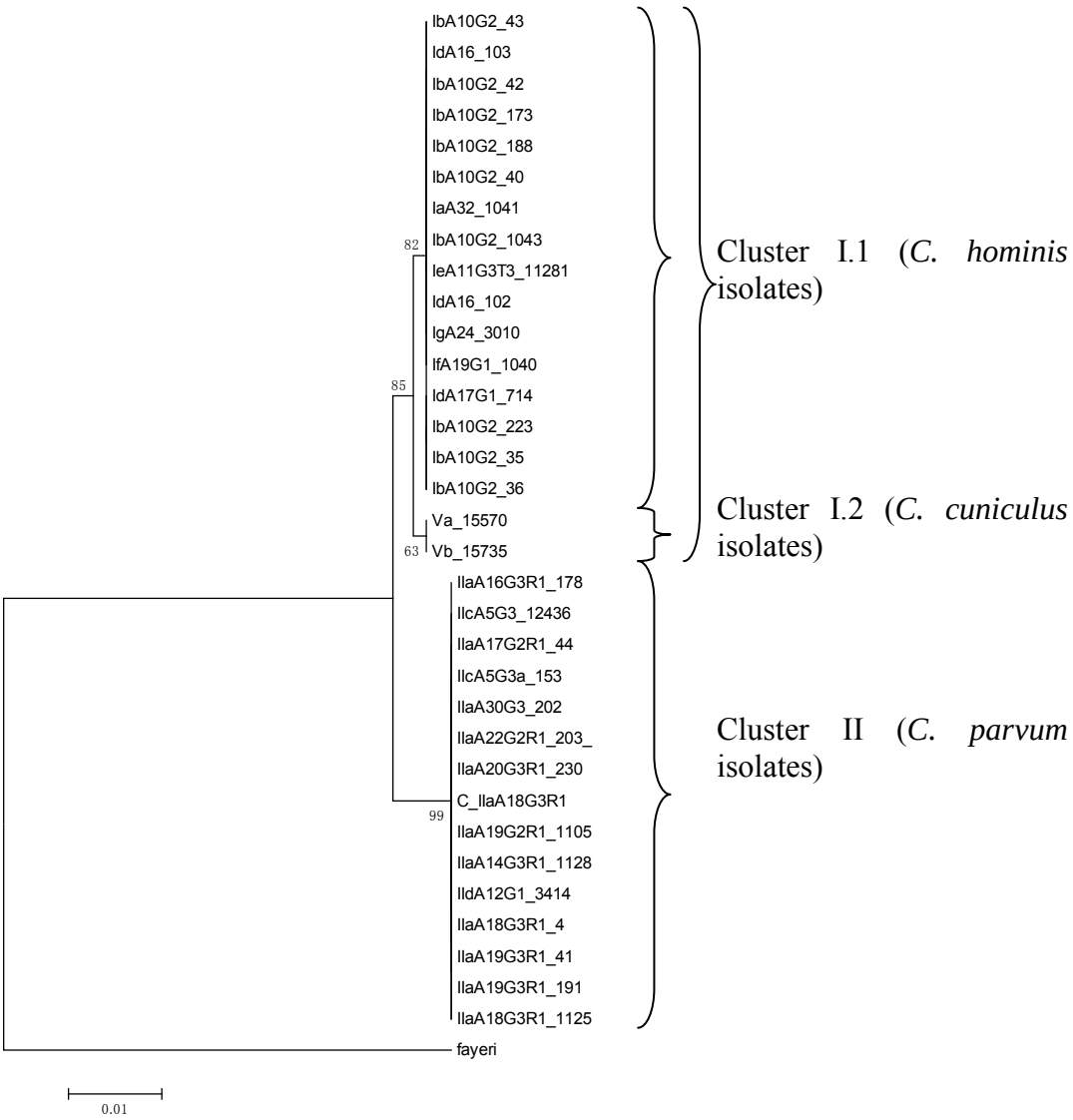

Figure 3.5 Relationship of ketoacyl synthase domain protein sequences between isolates from *C. parvum, C. hominis* and *C. cuniculus*

A phylogenetic tree inferred KS domain of module 5 using Maximum likelihood method with Tamura 3-parameter model and uniform mutation rate. The sequence from *C. fayeri* as an outgroup. The bootstrap values are shown and the log likelihood was -1263.61. The gene sequence polymorphism revealed all isolates were clustered into three groups. The isolates from *C. cuniculus* species were more closely related to the isolates from *C. hominis*. The subtype of each isolate is shown in **Table 3.**

3.4.2.2 Gene and protein sequence polymorphism within the ER domain of module 1

At the ER domain, there were 14 sites of polymorphism observed, nine of which were nonsynonymous nucleotide substitutions (**Table 3.3**). Sixteen *C. parvum*, 16 *C. hominis* and two *C. cuniculus* species were sequenced successfully for this domain (**Table 3.5)**. The sequences of *C. parvum* and *C. hominis* isolates examined displayed consistency within the species level regardless of the subtype of each isolate. This pattern was also observed for the KS domain. The two *C. cuniculus* isolates carried identical nucleotide sequences and were most similar to *C. hominis* at 13 positions compared with one position to *C. parvum*. At position 7,551, the two *C. cuniculus* isolates carried different nucleotides. The Va subtype carried a C and was identical to *C. parvum* and *C. hominis*, whereas the Vb subtype carried a T.

A 599 bp gene sequence was used to construct a maximum likelihood tree and is shown in **Figure 3.6**. Two clusters were clearly observed; Cluster I contained various subtypes of *C. hominis* and *C. cuniculus* isolates, whereas cluster II contained only *C. parvum* isolates. Within cluster I, Vb subtype (isolate 15735) was separated from the rest as result from the nucleotide polymorphism as position 7511.

Table 3.5 sequence polymorphisms between *C. parvum*, *C. hominis*, *C. cuniculus* at enoyl reductase of module 1

nucleotide position	6980	6996	7005	7050	7074
C. parvum	G	T	A	C	A
C. hominis	A	C	G	T	G
C. cuniculus	A	C	G	T	G
Type of mutation	Transition	Transition	Transition	Transition	Transition
nucleotide position	7090	7114	7214	7244	7278
C. parvum	T	A	C	G	A
C. hominis	A	G	T	A	G
C. cuniculus	A	G	T	A	G
Type of mutation	Transversion	Transition	Transition	Transition	Transition
nucleotide position	7377	7381	7499	7511	
C. parvum	C	A	C	C	
C. hominis	T	G	T	C	
C. cuniculus	T	G	T	C/T	
Type of mutation	Transition	Transition	Transition	Transition	

Fourteen sites of polymorphism between the three species were identified at the 624 bp sequence compared, and 16, 16 and 2 isolates from each species were screened respectively. The nucleotide sequence of *C. parvum* and *C. hominis* isolates were conserved at species level, *C. cuniculus* isolates were most similar to *C. hominis*. However, each of the *C. cuniculus* subtypes carried a different nucleotide at position 7511.

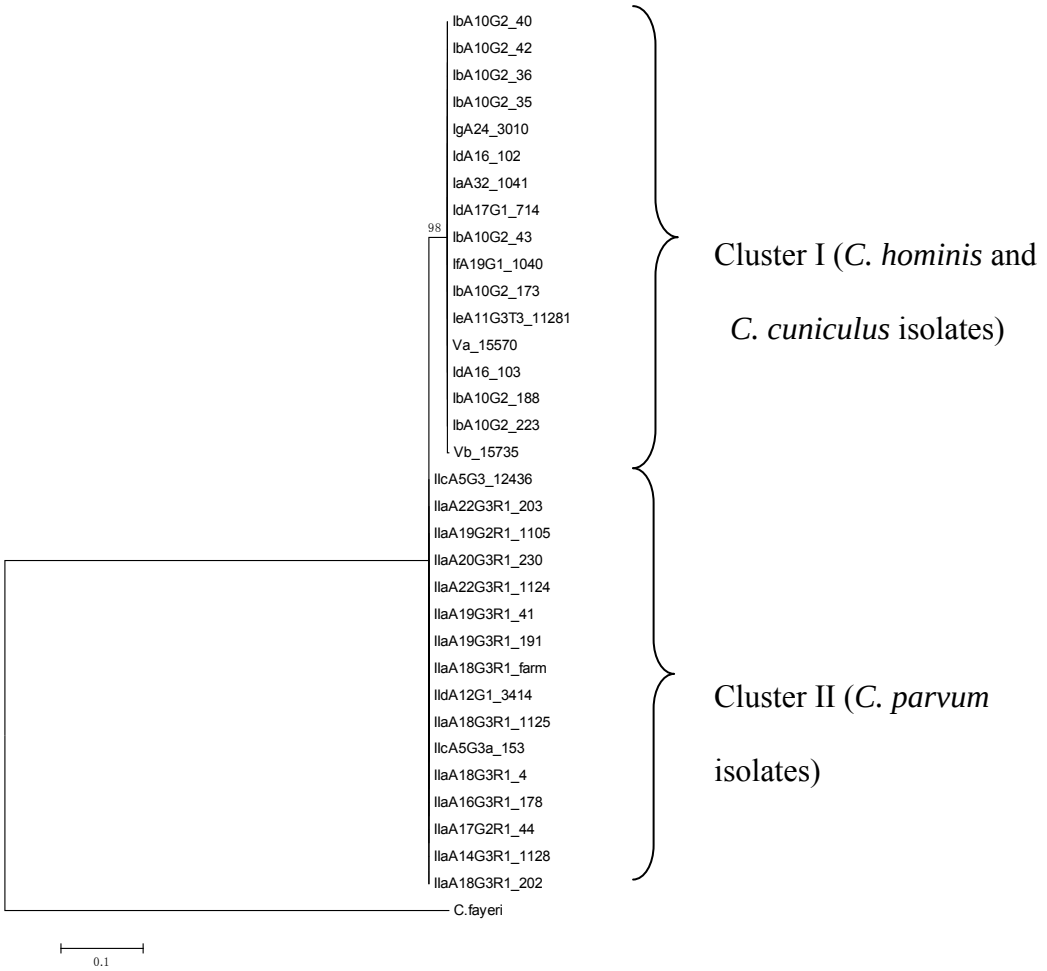

Figure 3.6 Relationship of ER domain protein sequences between isolates from *C. parvum, C. hominis* and *C. cuniculus.*

A phylogenetic tree inferred ER domain of module 5 using maximum likelihood method with bootstrap vales are shown (500 bootstraps), and the log likelihood is -1562.82. The published gene sequence from same region of *C. fayeri* was used as an outgroup, and the model used for tree building was Tamura 3-parameter model with uniform mutation rate. Observed polymorphism in the ER domain resulted in two separated clusters of the isolates analysed. The two *C. cuniculus* isolates were clustered with *C. hominis* isolates, however Vb was separated with the rest isolates in the cluster due to the polymorphism at site 7,511. The subtype of each isolate is shown in **Table 3.2.**

3.4.2.3 Gene and protein sequence polymorphism within the ACP and KS domains of module 3

The AK domain was the most variable domain observed in this study with 26 nucleotide polymorphism detected, 14 of which were nonsynonymous nucleotide substitutions (**Table 3.3**). Fifteen *C. parvum*, 16 *C. hominis* and 2 *C. cuniculus* isolates were sequenced successfully at this region (**Table 3.6**).

As with the pattern observed in the ER and KS domain, 23 polymorphism between *C. parvum* and *C. hominis* were observed at the species level only. However, the *C. hominis* isolates exhibited extensive polymorphism between subtypes at three sites, this within species polymorphism was not observed in the ER or AK domain investigated. At position 13,229 (**Table 3.6**), all except one Ib subtype isolates carried a T, whereas the remaining *C. hominis* isolates carried an A, which was an identical sequence to *C. parvum.* In addition, at position 13,119 and 13,231 (**Table 3.6**), a unique nucleotide was identified in one of the Ib and Ie subtypes respectively. The remaining *C. hominis* isolates examined were identical to that of the *C. parvum* isolates. The two subtypes of *C. cuniculus* carried identical nucleotides to the *C. hominis* isolates at 25 sites. However, at position 13,559 (**Table 3.6**), a unique nucleotide polymorphism was observed from a G to an A.

A 706 bp gene fragment was used to construct a phylogenetic tree using maximum likelihood method displaying the gene sequence similarity between the isolates analysed, and the *C. fayeri* PKS gene sequence retrieved from NCBI database used as an outgroup. The model used for tree building was Tamura 3-parameter model with

uniform mutation rate. The gene sequence polymorphism resulted in the 33 isolates being separated into two major clusters: I and II (**Figure 3.7**). Cluster II contained only *C. parvum* isolates confirming the sequences were identical at the species level. Within Cluster I, two sub-groups were identified. Cluster I.1 contained only *C. cuniculus* isolates cluster I.2 contained the majority of the IbA10G2 subtype *C. hominis* isolates.

Table 3.6 sequence polymorphism between *C. parvum, C. hominis, C. cuniculus* at AK domain of module 3.

nucleotide position	13082	13100	13109	13119	13122
C. parvum	T	C	A	T	A
C. hominis	C	G	G	T/G	G
C. cuniculus	C	G	G	T	G
Type of mutation	Transition	Transverision	Transition	Transversion	Transition
nucleotide position	13134	13145	13167	13188	13200
C. parvum	A	C	G	A	G
C. hominis	T	A	A	G	C
C. cuniculus	T	A	A	G	C
Type of mutation	Transversion	Transversion	Transition	Transition	Transversion
nucleotide position	13229	13231	13353	13395	13411
C. parvum	A	G	T	C	A
C. hominis	T/A	A/G	A	T	G
C. cuniculus	A	G	A	T	G
Type of mutation	Transversion	Transition	Transversion	Transition	Transition
nucleotide position	13422	13448	13551	13556	13559
C. parvum	G	A	C	C	G
C. hominis	C	C	T	T	G
C. cuniculus	C	C	T	T	A

Type of mutation	Transversion	Transversion	Transition	Transition	Transition
nucleotide position	13605	13611	13621	13626	13656
C. parvum	T	G	G	C	A
C. hominis	A	A	A	T	G
C. cuniculus	A	A	A	T	G
Type of mutation	Transversion	Transition	Transition	Transition	Transition
nucleotide position	13791				
C. parvum	G				
C. hominis	A				
C. cuniculus	A				
Type of mutation	Transition				

Twenty-six sites of polymorphism between the three species were identified at the 706 bp sequence compared, and 15, 16 and 2 isolates from each species were screened respectively. The nucleotide sequence of *C. parvum* and *C. hominis* isolates were conserved at species level at 22 sites. *C. hominis* isolates exhibited extensive polymorphism at sites 13,119, 13,229 and 13,231. *C. cuniculus* isolates were most similar to *C. hominis*. However, a unique nucleotide was identified in *C. cuniculus* at position 13,559.

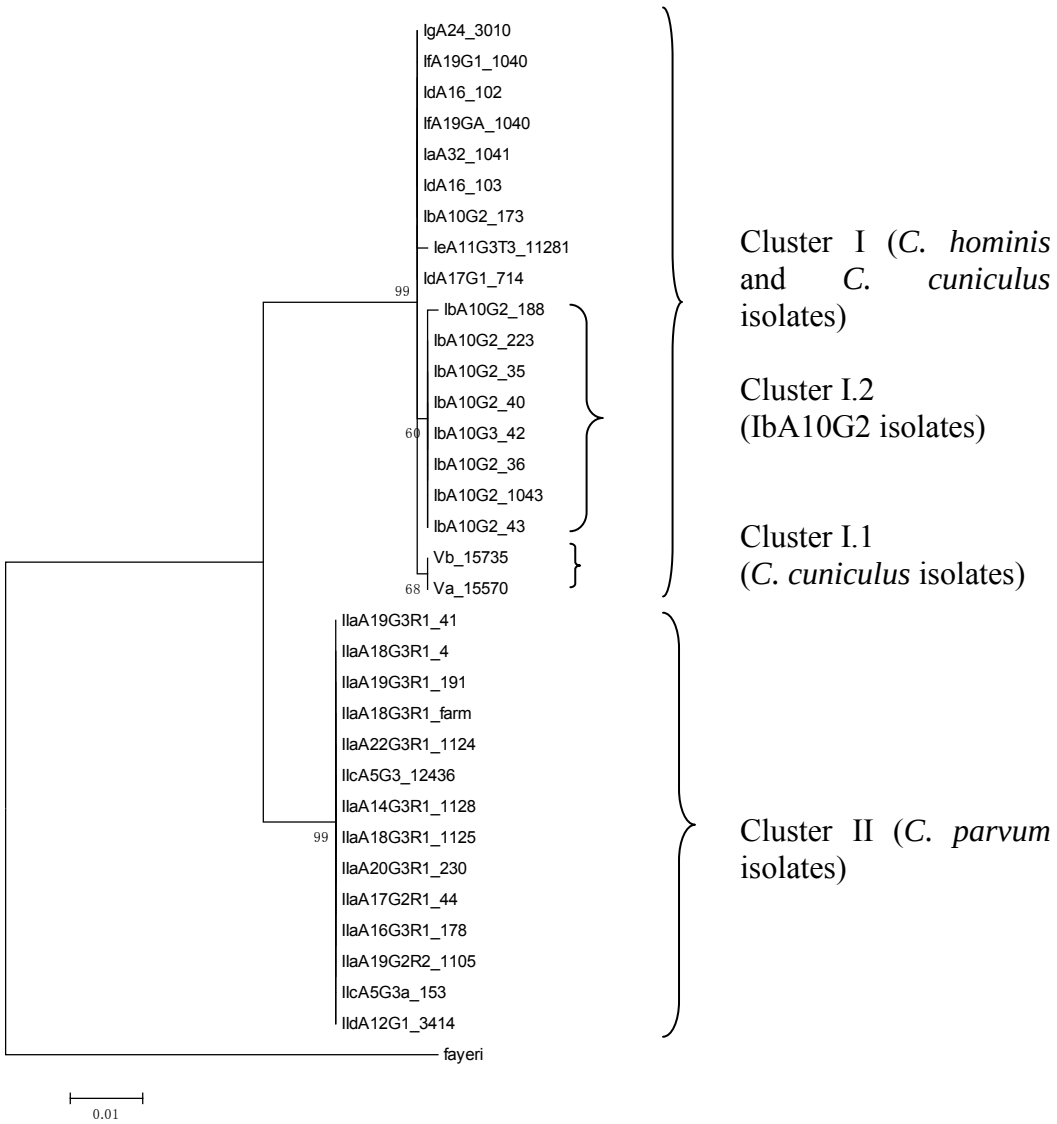

Figure 3.7 Relationship of AK domain protein sequences between isolates from *C. parvum, C. hominis* and *C. cuniculus.*

A phylogenetic tree inferred AK domain of module 3 using maximum likelihood method with Tamura 3-parameter model and uniform mutation rate. The bootstrap vales are shown (500 bootstraps), and the log likelihood is -1305.56. Sequence from same region of *C. fayeri* PKS was used as outgroup. The observed polymorphism in the AK domain clustered the isolates into two major clusters. Within the cluster I, two sub-clusters was formed, consisting of *C. cuniculus* isolates (Cluster I.1), IbA10G2 subtype isolates (Cluster I.2). The subtype of each isolate is shown in **Table 3.2**.

3.5 Conclusion

In summary, a PKS gene that is similar to CpPKS1 was identified in further three species of *Cryptosporidium* using in-house designed *Cryptosporidium* specific degenerate primer sets. Among the four species PKS positively identified: *C. andersoni* is a gastric lineage species and is generally considered as non-human infectious. While the other three are intestinal lineage, *C. cuniculus* and *C. fayeri*, were human infectious but *C. bovis* is non-human infectious. Nevertheless, *C. bovis* was only successfully sequenced at the KS domain, the size of the amplicon is larger than that of *C. parvum*, and different band pattern was observed, further studies are required to investigate the overall diversity of the PKS gene in *C. bovis*.

The phylogenetic trees constructed using a concatenated PKS from the five domains sequenced showed the PKS gene in *Cryptosporidium* was divided into two groups. One group contained PKS gene separated from intestinal and human infectious *Cryptosporidium* species: *C. parvum*, *C. homins*, *C. cuniculus* and *C. fayeri*, and the other group contained gastric non-human infectious *Cryptosporidium* species *C. muris* and *C. andersoni*. This separation suggests a possibility of the correlation between the diversity of the PKS gene and human infectivity or the site of infection.

The PKS sequence from the three most common and outbreak causing *Cryptosporidium* species: *C. parvum*, *C. hominis*, and *C. cuniculus* were compared. The results revealed a large number of DNA sequence polymorphism between *C. parvum* and *C. hominis*, and many of them are nonsynonymous nucleotide

substitutions. The majority of the nucleotide polymorphism between *C. parvum* and *C. hominis* were at species level. However, subtype level polymorphism was also identified within *C. hominis*. The PKS gene in *C. cuniculus* was more similar to *C. hominis* compared with *C. parvum*. However, unique nucleotide polymorphism were also identified in *C. cuniculus* subtypes. The phylogenetic relationship showed the PKS protein was divided into two groups with the isolates of *C. parvum* forming one cluster, and the isolates from *C. hominis* and *C. cuniculus* forming another distinct cluster. This separation suggests the potential of using the PKS gene sequence polymorphism as a novel identification tool for human infectious isolates at species level.

Chapter 4
Results on metabolomics and polyketide identification in *C. parvum*

4.1 Introduction and aims

Cryptosporidium has a complex lifecycle and cannot be cultured in large numbers in the laboratory [25]. Thus, studies on *Cryptosporidium* have thus been limited to the oocyst stage and are predominantly genomic based [58,61,90] with several studies at the proteomic level[114,115].

There is a potential that the diarrhoeal symptoms present during *C. parvum* infection are caused by an enterotoxin as an enterotoxic response in Caco-2 and jejunal cells has been observed[69]. In 2002, a polyketide synthase (PKS) gene was identified in *C. parvum* and the structure for a polyketide product was predicted[88]. Polyketides have been shown to have a wide range of bioactivities including antibiotic, anticancer and have a wide application in medical field[116]. A polyketide synthesised by the PKS from dinoflagellate similar to the PKS from *C. parvum* has been identified to be a neurotoxin[75]. In 2005, Thompson proposed the PKS gene in *C. parvum* was potentially related to toxin production and is responsible for diarrhoeal symptoms[18].

Mass Spectroscopy(MS) is a powerful analytical tool for metabolomics investigations due to its high accuracy, sensitivity, and the ability to identify metabolites at trace concentrations[117]. MS has also been used widely in polyketide identification and characterisation[118,119]. The lipids of the Apicomplexan *Toxoplasma gondii* has been previously studied using MS indicating the utility of using MS to identify metabolites in *Cryptosporidiu* [120,121].

The aims of the research in this chapter are:

1. To explore the feasibility of using MS to develop a metabolomics profile of *Cryptosporidium* at oocyst stage.
2. Identify a potential diarrhoea causing polyketide based on the polyketide structure predicted by Zhu et al.[88].

4.2 Quantification of purified oocysts and purity estimation

The average oocyst concentration following purification from calf faeces was determined after FCM analysis to be 8.4 x 10^5 cells per ml. Prior to FCM analysis, purified oocysts were diluted 1 in 100 in MAB buffer before the addition of CRY104-FITC antibody for the fluorescent staining. Therefore, the original concentration of purified oocysts was estimated to be 1.05 x 10^8 per ml.

The total particles concentration following FCM analysis of stained oocyst and MAB buffer alone was 1.109 x 10^6 per ml and 1.74 x 10^5 per ml respectively. Thus the purity of diluted oocyst was estimated to be 89.84%, using the calculation method described in **section 2.3.2.3**.

4.3 Oocyst disruption by sonication for Mass Spectroscopy (MS) analysis

After sonication, oocysts were examined under EFM to determine the efficiency of oocyst disruption (**Figure 4.1**). Compared with oocyst prior to sonication, the oocyst were effectively disrupted, as indicated by debris surrounding CRY104-FITC labelled oocyst walls (Region A; **Figure 4.1**), combined with a small proportion of oocysts being completely fragmented (Region B; **Figure 4.1**).

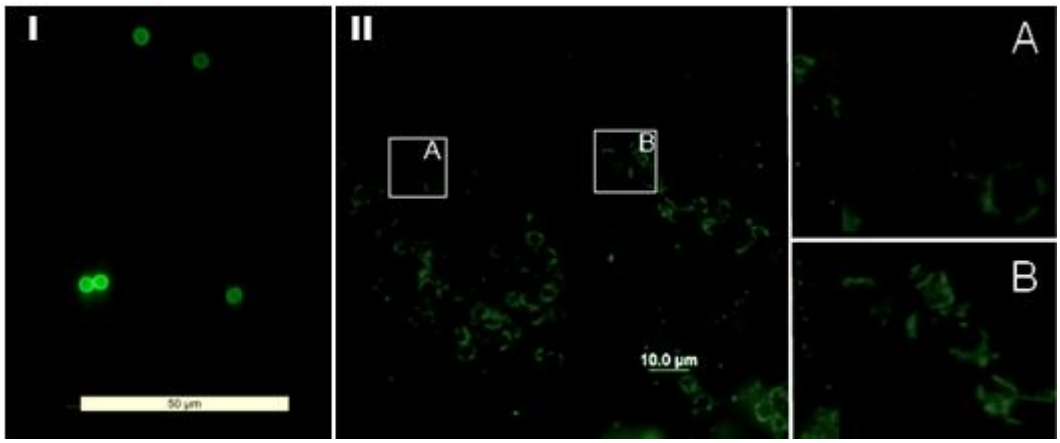

Figure 4.1 EFM image of oocysts before and after disruption by sonication examined at 100 times magnification

I; oocysts before sonication, II; oocysts after sonication. Region A; oocysts were opened up after sonication as indicated by the CRY104-FITC labelled discontinuous circles. Region B; oocysts were completely disrupted after sonication, as indicated by CRY104-FITC labelled fragments.

4.4 Detection of potential metabolites of *Cryptosporidium* by MS

4.4.1 Detection of potential metabolites and their location during the excystation process

Potential metabolites were identified from three fractions related to the excystation process: intact oocysts, excystation medium and the sporozoites/oocyst wall fraction. An extract of approximately 1 x 10^7 oocysts for each stage were investigated after extraction using MS. Based on the isotopic labelling pattern, it was estimated that 161, 191, and 92 potential metabolites were identified in intact oocyst, excystation supernatant and sporozoite fractions respectively (Appendix I), using positive ion detection mode. The number of potential metabolites identified in each fraction and the number of potential metabolites that were in common between fractions are summarised in **Figure 4.2**.

While there were 34 potential metabolites shared among the three fractions, a large number of potential metabolites were still unique to each fraction. The excystation medium fraction exhibited the largest number of potential metabolites that was not identified in the other two fractions. Compared with the sporozoite fraction, the excystation medium shared many more potential metabolites with the oocyst fraction (12 compared with 41). The least number of potential metabolites was identified in the sporozoite fraction, and it shared a small number of potential metabolites with the

other two fractions (14 and 12 respectively). The result suggests metabolomics profile has been changed during the excystation process.

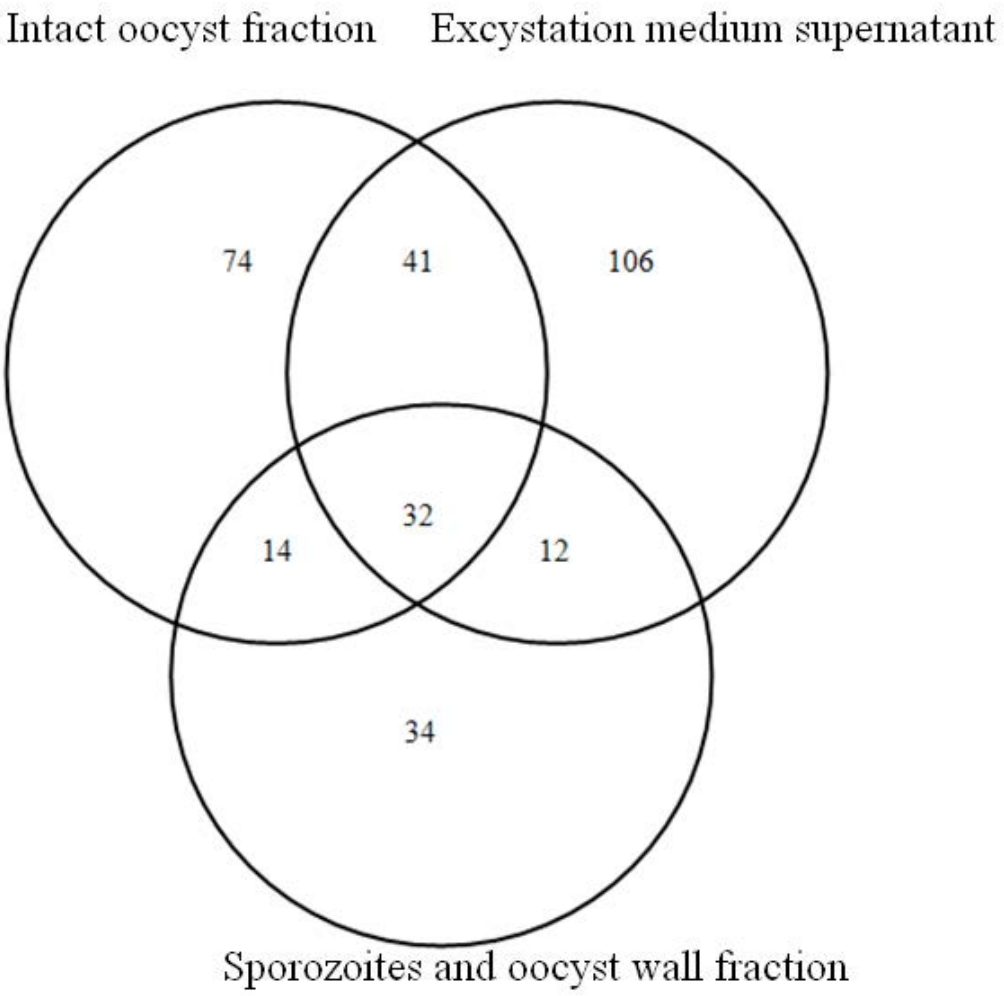

Figure 4.2 Venn diagram of potential metabolites identified by MS in each fraction following extraction.

The numbers of potential metabolites that were unique to each fraction and shared between fractions are labelled. The number of potential metabolites shared by all three fractions was 32, while the intact oocysts, excystation medium and sporozoite fractions contained 74, 106 and 34 unique potential metabolites respectively.

In this study, only positive ions were detected, and the top ten most abundant potential metabolites determined from absolute intensity are summarised in **Table 4.1**. The potential metabolites with a *m/z* value of 851.398 and 867.373 were shared across all three fractions examined. Under the current MS equipment setting, the intact oocyst fraction shared four major potential metabolites with the sporozoite fraction, but did not have any potential metabolites with high intensities in common in the excystation medium fraction. The excystation fraction contained the largest number of unique potential metabolites with high intensity, and the top 2 potential metabolites were not observed in other fractions. The unique compound identified in the excystation supernatant fraction suggested a changed metabolomics profile of *Cryptosporidium* during the excystation process, and these compounds may have important role in the excystation process or even host cell invasion process.

The molecular weights of the potential metabolites identified in each fraction were compared in **Figure 4.3**. The sporozoite fraction was rich in medium to high molecular weight compounds (*m/z* >600), while a relatively low number of low molecular weight compounds (*m/z* <600). The excystation medium fraction contained a large number of potential metabolites across the entire mass range examined. Finally, the oocyst fraction contained a large number of small to medium molecular weight compounds, while the number of high molecular weight (*m/z* > 800) compounds observed was low.

Table 4.1 Summary of top 15 potential metabolites identified in the three fractions by absolute intensity

Sporozoite (molecular weight Da)	Excystation medium (molecular weight Da)	Intact oocyst (molecular weight Da)
437.1916	453.1676	851.3955
851.3957	531.2738	437.1915
453.1653	851.3976	735.3331
867.3683	867.3728	453.1652
261.0869	950.7359	771.4842
795.501	357.2785	815.5105
675.2903	846.4431	727.4583
735.3331	507.3284	321.1295
288.2885	807.503	867.3682
807.5008	463.3023	415.2099
767.4697	869.3789	685.4354
854.404	978.7666	859.5351
321.1296	551.3545	683.4319
353.2657	785.5919	432.2368
587.2818	540.4251	641.2852

The potential metabolites that were common between all three fractions are labelled blue; those common between sporozoite and excystation fractions only are labelled red; those common between excystation medium and intact oocysts fractions are labelled in green

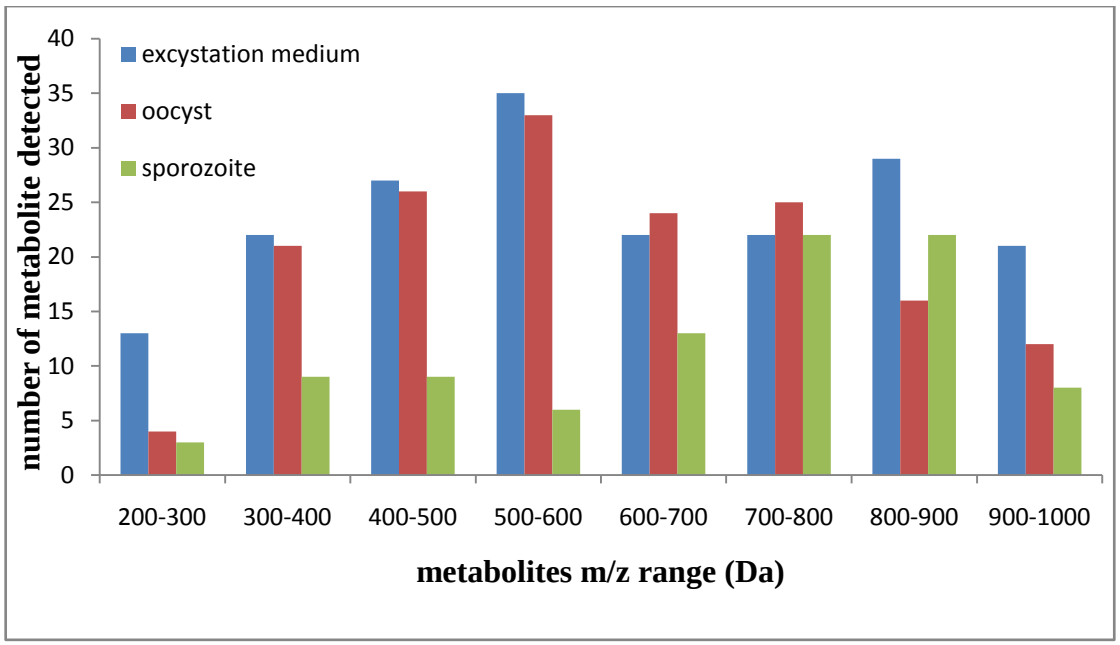

Figure 4.3 Comparison of the molecular weight of the potential metabolites identified in the intact oocyst, excystation medium and sporozoite fractions.

The excystation medium was rich in metabolties across the entire mass range examined; the sporozoite fraction was rich in high molecular weight compounds whereas the oocyst fraction was rich in medium molecular weight compounds.

4.4.2 Identification of potential metabolites from intact oocyst

4.4.2.1 Number of potential metabolites identified in the intact oocysts

In order to determine the maximum number of potential metabolites that could be identified in the intact oocyst stage, MS spectra were collected on an extract prepared from 1 x 10^8 oocysts. When only singly charged molecular ions were recognised as a potential metabolite, approximately 218 potential metabolites were identified based

on the ^{13}C isotopic labelling (protonated ion, $M+H^+$). However, the numbers of potential metabolites at mass range 800-1000 Da was underestimated (**Figure 4.4**), as the existence of peak clusters distorted the ^{13}C isotopic labelling pattern. For example, as shown in **Figure 4.4**, the 895.3157 Da peak had a molecular weight greater by one compared to the 894.3158 Da peak. This may have resulted from isotopic labelling due to the natural abundance of the ^{13}C isotope. However, as the intensity of 895.3157 Da peak was greater than that of the 894.3158 Da peak (which did not meet the isotopic labelling pattern), this suggests the identification of 894.3158 Da peak as a potential metabolite is inappropriate. As a result of this, several peaks were not recognised as potential metabolites in the mass range 800-1000 Da.

Among the 218 potential metabolites detected from the extract of 1 x 10^8 oocysts, 61 had match(es) in the METLIN datasbase (Appendix II). The search was performed based on the exact mass with a 5 ppm error range. Among the 61 potential metabolites that exhibited matches in the database, 47 were potentially lipids. However, due to the lack of MS/MS spectra in all major MS databases, the majority of the compounds could not be positively identified.

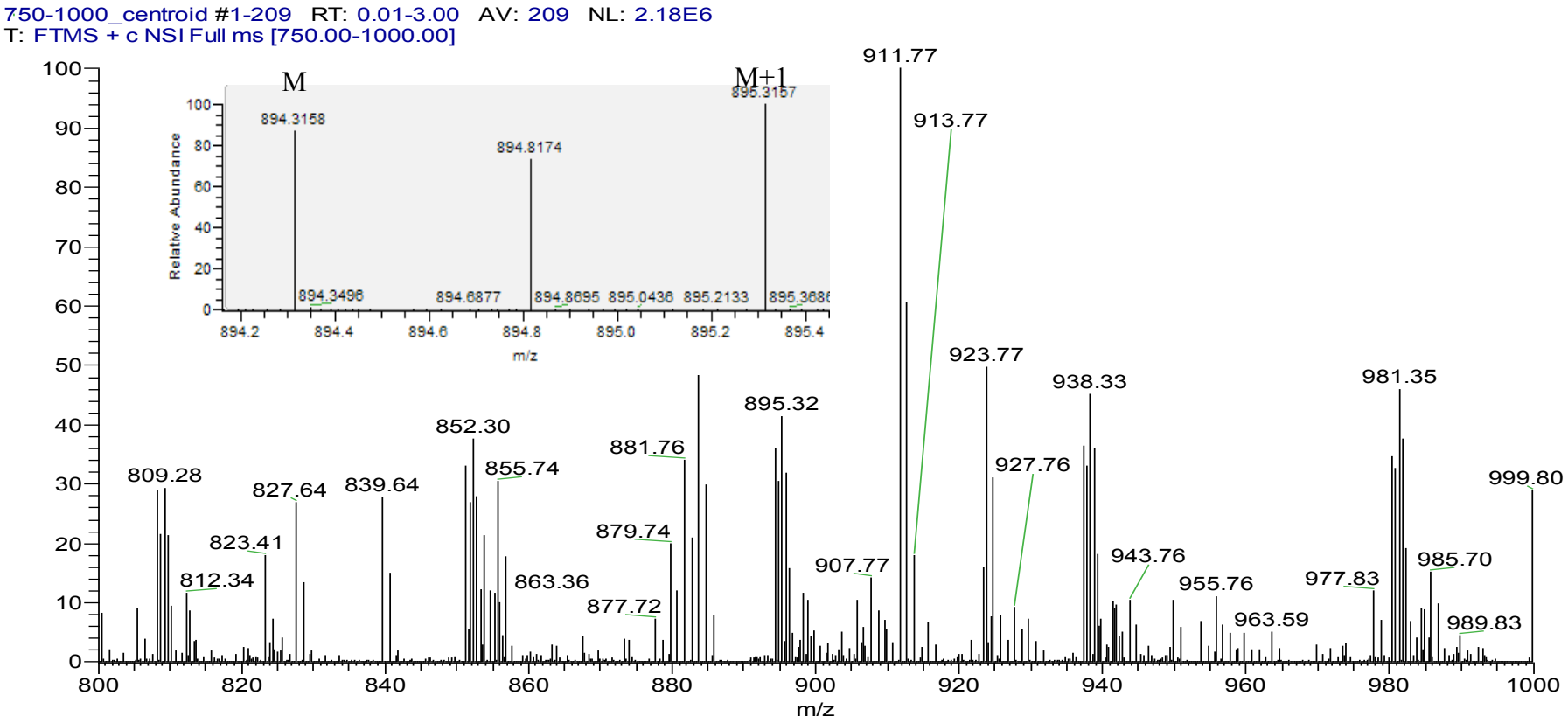

Figure 4.4 MS spectrum at mass range 800-1000, the inlet showing the presence of M+1 peak interfere with the potential metabolite identification.

The number of potential metabolites was underestimated at mass range 800-100. Due to the present M+1 peak due to additional proton interfere with the isotopic peak of ion M, the identity of compound M could not be determined.

For 61 of the potential metabolites that had a match in METLIN database, 22 were observed in the differential display investigation (Appendix I). They were identified in one or more than one fractions of the oocysts, the excystation medium, or the sporozoite fractions. The number of potential metabolites that exhibited a match in the METLIN database for each fraction(s) is shown in **Figure 4.5**. The majority of the potential metabolites identified here were not observed in the differential display investigation, possibly due to lower concentration of the oocysts used in differentiation display experiment. In total, 5, 7, and 5 potential metabolites were explicitly identified in the oocyst, excystation medium and sporozoite fraction respectively. The remaining potential metabolites were identified in more than one fractions.

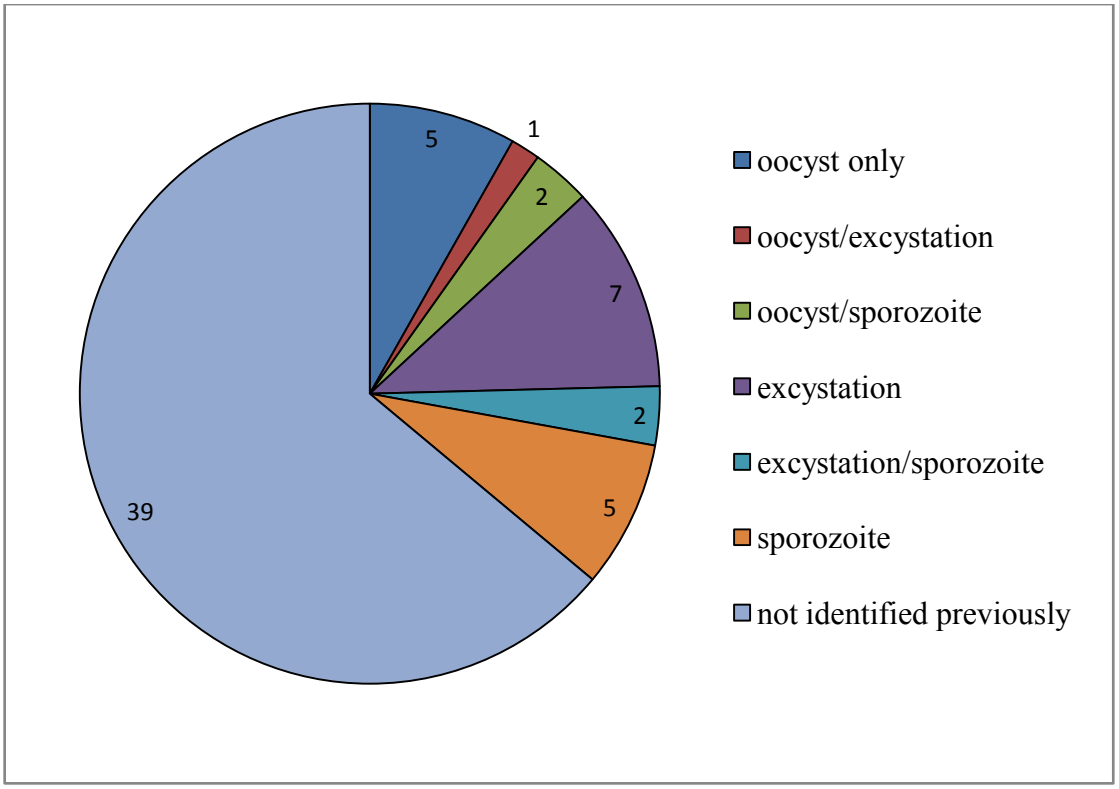

Figure 4.5 The location during excystation process of the potential metabolites identified in the high oocyst crude extraction.

For the 61 potential metabolites that had a match in METLIN database, 63.93% was not identified in the differential display experiment, 11.48% were explicitly identified in the excystation medium, 8% were identified in the sporozoite, and 8.2% were identified in the oocyst only. The rest were identified in more than 1 fraction.

4.4.3 Structure elucidation of 288.28 Da metabolite

This metabolite was identified in all fractions examined during the excystation process, and identified in three different batches of intact oocysts. However, it was only observed as a major peak in the sporozoite fraction with high relative intensity (**Table 4.1**). It was the only metabolite that exhibited a match in METLIN database with the positive mode MS/MS spectra available. The match in the METLIN database was to heptadecasphinganine (C17 sphinganine) with the molecular formula $C_{17}H_{38}NO_2$ in a protonated state. Comparison of the MS/MS spectrum of C17 sphinganine (retrieved from standard lipid database http://www.lipidmaps.org) (**Figure 4.6**) and the MS/MS spectra obtained from MS/MS experiment (**Figure 4.6 inlet**) showed that, both compounds had identical peaks at 270.3, 252.3 and 226.3 Da. However, the 288.28 Da compound exhibited a peak at 244 Da compared with the C17 spinganine at 240 Da. In addition, the 288 Da compound had intensive peaks at both 88 and 70 Da that was not observed in C17 sphinganine. Hence, these two compounds are related but structurally different.

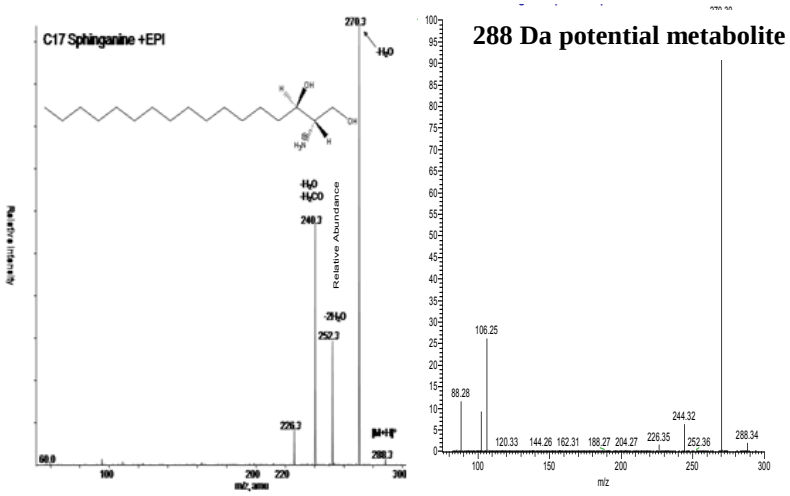

Figure 4.6 Comparison of standard spectrum of C17 sphinganine and 288 Da potential metabolite.

The C17 sphinganine spectrum was retrieved from Lipid map database (http://www.lipidmaps.org/data/standards/fetch_gif_mult.php?MASS=288&LM_ID=LMSP01040003&TRACK_ID=327). The peaks at 270, 252 and 226 Da suggests the structure of 288 Da molecular ion is very similar to C17 sphinganine. However, the 4 Da difference between fragment ions of 288 Da potential metabolites and C17 sphinganine (244 and 240 Da respectively) suggests the two molecules were related but structurally different.

The 288.3 Da compound identified in MS spectrum was in a protonated state with a formula of $C_{17}H_{38}O_2N^+$, predicted by exact mass (1.58 ppm error), and thus the molecular formula is $C_{17}H_{37}O_2N$ in a native state. Evidenced by the MS/MS and MS3 spectra collected (**Figure 4.7**), three major fragmentation pathways during CID process have been identified (**Figure 4.8**), and the ions and fragments identified in the CID spectra of this compound is summarised in **Table 4.2**.

The 288.3 Da molecular ion can lose 182, 18, or 44 Da fragment to produce 106, 270, and 244 Da product ions respectively (**Figure 4.7 A**). The 182 Da fragment represents $C_{13}H_{26}$; the 18 Da fragment is a water molecule; and the 44 Da fragment ion represents $C_2H_6N^+$. The 44 Da fragment loss is a common feature of 1-deoxysphingoid bases, and resulted from the C2-C3 bond cleavage[122].

The 106 Da product ion can undergo two dehydration reactions to produce 88 ($C_4H_{10}OH^+$) and 70 ($C_4H_8N^+$) Da product ions respectively (**Figure 4.7C**). The 270 Da product ion can lose 168 Da fragment ($C_{12}H_{24}$) then a 14 Da fragment (CH_2) to produce the 88 ($C_4H_{10}OH^+$) Da product ion which was also observed in the 106 Da product ion MS3 spectrum (**Figure 4.7B**). Alternatively, the 270 Da product ion can lose 44 Da fragment ion that observed in the MS/MS spectrum of the molecular ion (**Figure 4.7A**) to produce 226 Da product ion. The 244 Da product ion can undergo dehydration reaction to lose a water molecule to produce 226 Da product ion which was also observed in the 270 Da MS3 spectrum (**Figure 4.7B**).Based on the chemical formula of the compound (**Figure 4.8**), the name of compound is 2-amino-3,4-dihydroxy heptadecane, and is a member of sphingoid base compounds.

Table 4.2 Formula of ions and neutral fragments identified in the MS/MS and MS3 spectrum of 288.3 Da molecular ion.

Ion/fragment type	*m/z*	iIon/molecular formula
Molecular ion	288	$C_{17}H_{38}O_2N^+$
Product ion	106	$C_4H_{12}O_2N^+$
Product ion	270	$C_{17}H36ON^+$
Product ion	244	$C_{15}H_{32}O_2^+$
Product ion	88	$C_4H_{10}ON^+$
Product ion	102	$C_5H_{12}ON^+$
Product ion	226	$C_{15}H_{30}O^+$
Product ion	70	$C_4H_8N^+$
Fragment ion	182	$C_{13}H_{26}$
Fragment ion	18	H_2O
Fragment ion	44	C_2H_6N
Fragment ion	168	$C_{12}H_{24}$

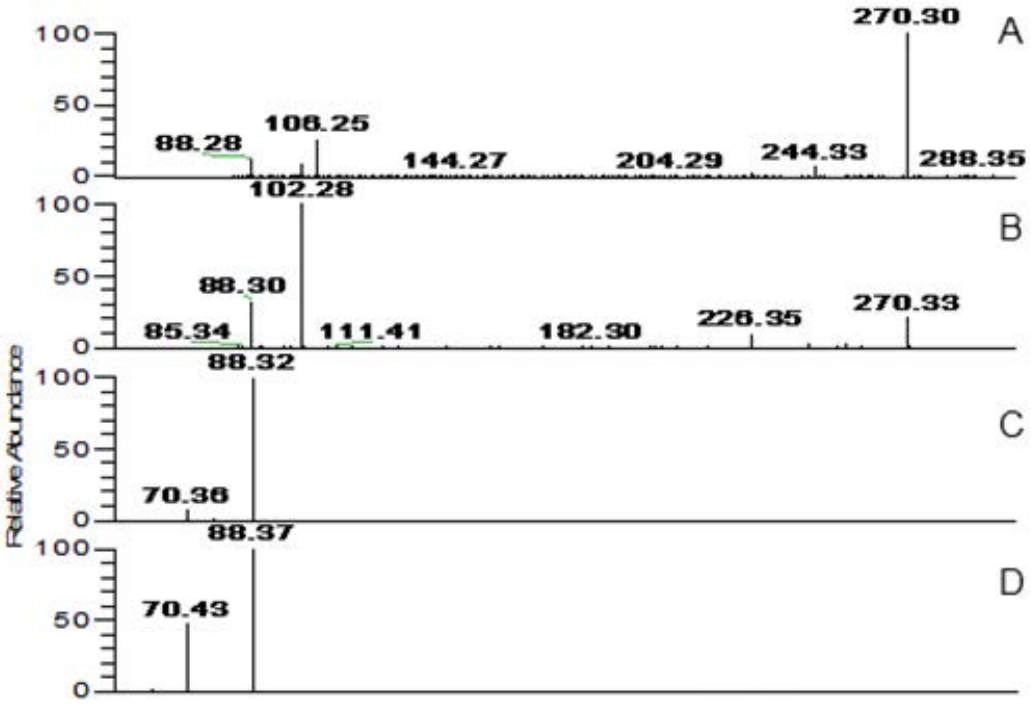

Figure 4.7 Comparison of MS3 of ions generated by CID fragmentation of 288 Da ion.

A, MS/MS spectrum of 288 Da ion; **B**, MS3 spectrum of 270 Da fragment ion generated by spectrum; **C**, MS3 spectrum of 106 Da fragment ion generated by spectrum A; **D**, MS3 spectrum of 88 Da fragment ion generated by spectrum **A**.

A 88 Da fragment was observed in all spectra suggesting it is a common structure within all fragment ions. The 244 Da fragment was not observed in the 270 Da MS3 spectrum suggesting it was generated from the molecular ion (288 Da) from a single step reaction.

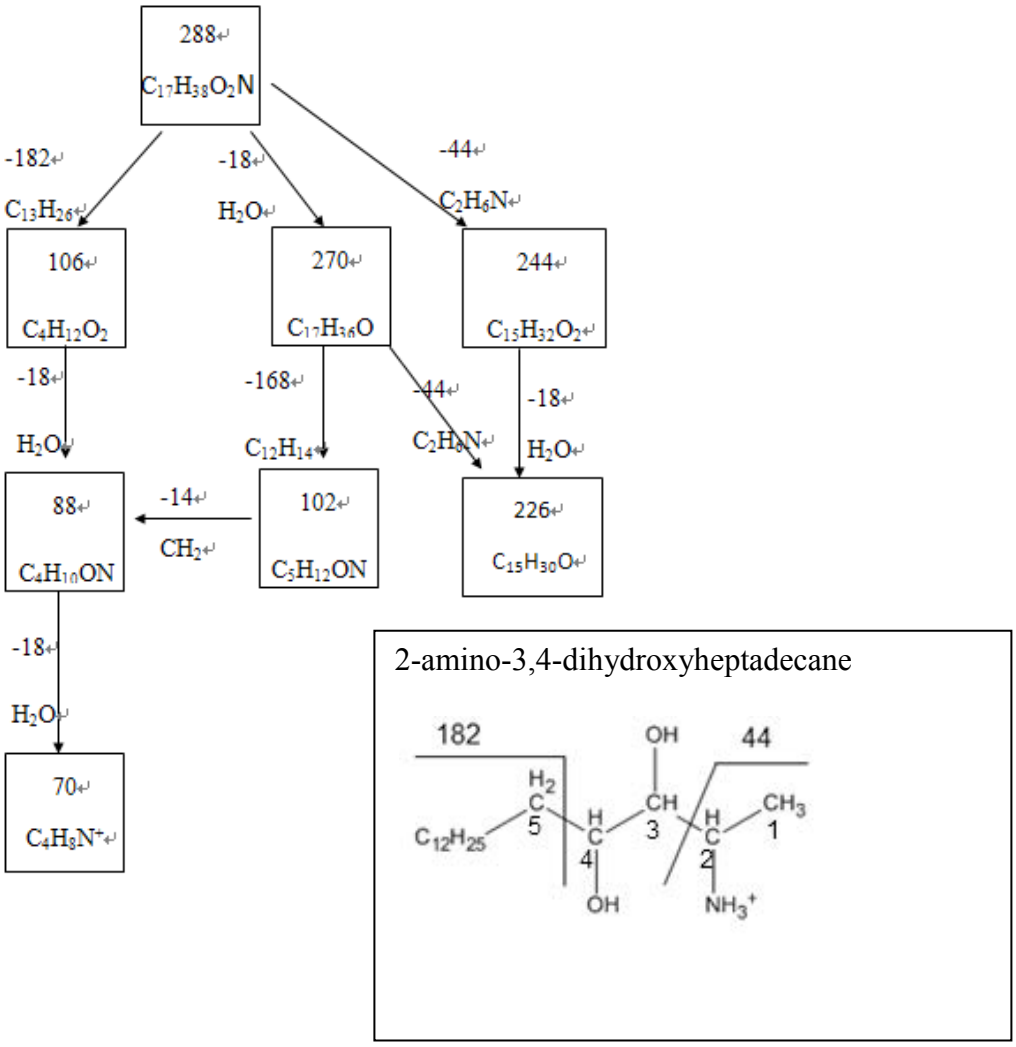

Figure 4.8 Proposed fragmentation pathway of the 288 Da potential metabolite (2-amino-3,4-dihydroxyheptadecane)

The structure of the 288 Da potential metabolite is shown, as well as three fragmentation pathways identified. The 270.3 Da product ion can undergo different fragment pathways to produce either $C4H8N^+$ or $C_{15}H_{30}O^+$.

4.5 Conclusion

There were 161 and 218 potential metabolites identified in the intact oocyst stage of *Cryptosporidium* when a crude extract of 1 x 10^7 and 1 x 10^8 oocysts was prepared. It confirms the construction of a metabolomics profile of *Cryptosporidium* using MS is possible but requires larger number of oocysts. Due to time limitation and the lack of an appropriate MS/MS database, only one metabolite was identified. The difference in the potential metabolites identified in the three excystation process related fractions suggests the metabolomics profile is changing during the excystation process. Since the CpPKS1 has a preference of C20 fatty acid as substrate and the structure synthesised by CpPKS1 has a molecular weight of 299 Da, a polyketide has been searched at the mass range of 400-800 Da, and the potential fatty acid substrate has been searched at mass range of 150-400 Da. Unfortunately, there was no polyketide products positively identified in this study, nevertheless, there were still 217 potential metabolites to be characterised. Further work is required to reveal the identity of a potential polyketide product.

The sphingoid base related molecule: 2-amino-3,4-dihydroxyl heptadecane was identified in the intact oocysts. It is a 17 carbon molecule that is unique compared with 18 carboned sphingoid base compounds identified previously in mammalian cells[123]. The identification of this unique molecule suggests lipid metabolism is unique in *Cryptosporidium*. As a sphingoid base related compound, the 2-amino-3,4-dihydroxyl heptadecane compound is potentially involved in cell signalling as observed for other sphingoid bases[124]. Further investigation is required to determine the stereochemistry of the compound and cell toxicity assay is required to

determine the function of it in *Cryptosporidium*.

Chapter 5 Discussion

5.1. The diversity of PKS gene in *Cryptosporidium* spp.

PKS was previously identified in *C. parvum*, *C. hominis* and *C. muris*, with the complete sequence publicly available for *C. parvum* and *C. muris*[58,91,92]. Degenerate primer sets designed here identified PKS in *C. andersoni*, *C. cuniculus* and *C. fayeri* suggesting there are reasonably conserved regions within the *Cryptosporidium* PKS gene. Among the six species positive for the PKS gene with five regions amplied, the diversity of the PKS gene led to the formation of two distinct groups (**Figure 3.3**, Chapter 3). All *Cryptosporidium* species identified within the *C. parvum* cohort were human-infectious species, whereas the members within the *C. muris* cohort were generally considered as non-human infectious, and the difference between the PKS in *C. parvum* and *C. muris* was approximately 40%.

In *C. andersoni*, within the five *C. andersoni* PKS domains investigated here, two of the domains were identical to that in *C. muris* whereas the other three domains were identical to *C. parvum*, and needs further investigation. The complete PKS gene sequence of *C. andersoni* needs to be determined. With the complete *C. andersoni* PKS gene sequence available, it will allow detailed assessment of the relationship of the PKS gene between *C. parvum*, *C. muris* and *C. andersoni*, and potentially provide insights on how the PKS gene was evolved in the two distantly related

Cryptosporidium species: *C. parvum* and *C. muris*.

C. muris and *C. parvum* are distantly related *Cryptosporidium* species as revealed by the phylogenetic relationship (**Figure 1.3** Chapter 1) [44]. However, PKS genes with 60% similarity were identified in both species. It suggests the PKS gene should be present in all *Cryptosporidium* species, which would be in consistent with John et al.[70] who proposed that the PKS gene of *Cryptosporidium* evolved from a common ancestor gene rather than a lateral gene transfer event.

5.2 A potential identification tool for human infectious *Cryptosporidium*

Currently, there is no rapid identification tool available for differentiations of human-infectious *Cryptosporidium*. Traditional PCR based methods are sensitive and accurate when they are combined with restriction fragment length analysis and/or sequencing for the identification of *Cryptosporidium* species[19,125]. These methods are time consuming and labour-intensive, making them inadequate for a rapid diagnostic response during outbreak investigation[126]. In addition, they are based on species differentiation, instead of human infectivity.

A novel three-colour fluorescence in-situ hybridisation (FISH) method has been developed to provide a reliable and fast approach to distinguish the most common *Cryptosporidium* species i.e., *C. parvum* and *C. hominis*[127]. However, three-colour FISH suffers from several drawbacks such as the need for expensive equipment

(epi-fluorescence microscopy and/or flow cytometry), and oocysts need to be purified prior to analysis. Additionally, at this stage cross-reactivity between two closely related species: *C. hominis* and *C. cuniculus* occurred for this probe.

Several real-time PCR and reverse transcription PCR based methods have been developed. The genes that real time PCR method targets include 18S rRNA[128], β-tubulin[129], or dihydrofolate reductase gene[130]. The only mRNA targeted by reverse transcription PCR is heat shock protein[37]. Utilising mRNA is advantageous over DNA based method as it avoids PCR inhibitors that are commonly co-purified with the nucleic acid and thus increases PCR efficiency[37]. However, these methods suffer from several drawbacks. The main problem with 18S RNA target methods is specificity, such as an inability to identify *C. hominis*[128] from other *Cryptosporidium* species or failure to separate *C. parvum* and *C. wrairi*[126]. For the DNA or mRNA based methods, only human infectious species were tested, other non-infectious species was not examined and potentially lead to false positive result[37,128,129].

In this study, the PKS gene of human infectious *Cryptosporidium* species formed two groups with *C. parvum* forming one cluster and *C. hominis* and *C. cuniculus* forming a second cluster (**Figure 3.5**, **3.6** and **3.7**, Chapter 3). Using this information, a PCR based detection method can now be developed based on the nucleotide polymorphism between *C. parvum* and *C. hominis*. In addition, if a combination of sites were used where *C. cuniculus* is identical to *C. hominis* at one site, but identical to *C. parvum* at another site, *C. cuniculus* can also be distinguished from *C. hominis*.

5.3 Metabolomics profiling of *Cryptosporidium* and polyketide identification

To our knowledge, this is the first known report on using MS to explore the metabolomics profile of *Cryptosporidium* spp.. The identification of 161 and 218 potential metabolites from 1 x 10^7 and 1 x 10^8 intact oocysts respectively highlights the potential of using MS to study the metabolomics profile of *Cryptosporidium*. The 17 carbons of the sphingoid base-related compound: 2-amino-3,4-dihydroxy heptadecane was unique compared to well described 18 carboned sphingoid based compounds identified in mammalian cells[123,131]. This shows the metabolites in *Cryptosporidium* may be different from the metabolites identified from host cells. Due to the lack of a metabolomics database, a large number of oocysts (> 1 x 10^8) will be required to isolate and identify further metabolites successfully. Due to limitation of time and resource, the experiment was not run once, and thus would be subject to sample variation. Hence, the differential display result should be treated with care and should be repeated in the future to ensure the difference in profiles were real and repeatable.

The large number of potential lipids identified in *C. parvum* suggests lipids play an important role in *Cryptosporidium* biology. The important functions of lipids in the

parasite and the involvement in host-parasite interactions have been observed in a closely related apicomplexan parasite *Toxoplasma gondii*. In *T. gondii*, inhibiting cholesterol acquisition from host cells leads to reduced parasite replication, and the cholesterol concentration has been shown to be crucial for the parasite's invasion process[120,121,132]. Hence, the inhibition of lipid metabolism has become a new drug target for *T. gondii*. Lipid metabolism in *Cryptosporidium* needs to be investigated further as it offers an alternative approach to the study *Cryptosporidium* and host interactions, and may potentially provide a new target for therapeutic treatment.

The attempt to identify a polyketide from the intact oocyst was unsuccessful. However, the enterotoxic effects caused by the supernatant of the faeces from *Cryptosporidium* infected calves strongly suggest the presence of such a toxin[69]. It is uncertain whether it was that the polyketide concentration was not high enough to be detected, the polyketide synthase was not active during this life stage, or whether it failed to be identified from the 218 potential metabolites found. At this stage, the proposed structure of the potential polyketide product was based on the organisation of catalytic domain of the CpPKS1 (Chapter 1, **Figure 1.4**). However, due to the lack of knowledge on the substrate involved, and the potential of cyclisation of the polyketide[88], it makes the identification of the polyketide difficult. In the future, the identification of the polyketide can be carried out by eliminating metabolites that can be characterised from the 218 potential metabolites, thereby reducing the possible candidates. Then, attempt to identify the polyketide from the remaining potential metabolites using the structural feature predicted by Zhu et al.[88].

5.4 The potential application of 2-amino-3,4-dihydroxy heptadecane

Sphingoid bases are the backbone of the sphingolipid, and have been shown to have important functions in cell signalling[124]. The metabolite 2-amino-3,4-dihydroxy heptadecane is structurally a sphingoid base-like compound and potentially has a role in cell signalling function.

Numerous 1-deoxy-sphingoid bases have displayed anti-cancer, or anti-virus effects. Both natural and synthetic 1-deoxy-sphingoid based compounds have been evaluated including spisulosine (**Figure 5.2A**), enigmols (**Figure 5.2B**) and xestoaminol C (**Figure 5.2C**)[131]. The proposed mechanism for the cell toxic effect is that since the 1-deoxy-sphigoid bases cannot be degraded by phosphorylation mediated degradation, signalling molecules can accumulate within the cell and inhibit ceramide synthase, which may lead to increased concentrations of sphinganine compounds and resulting hydroxylation products (phytosphingosin). Sphinganine and other sphingoid bases inhibit the protein kinase C dependent process[123] and lead to the inhibition of cell growth [133,134]. Phytosphingosin bases have also been reported to be toxic to the cell and inhibit cell nutrient uptake and growth[134,135]. 2-amino-3,5-dihydroxy heptadecane (**Figure 5.2D**) is structurally similar to phytosphingosin which is dehydroxylated at 1 position. It is structurally similar to the hydrolysed form of enigmol, with one less carbon in its backbone (18 carbons in enigmol). Hence, 2-amino-3,5-dihydroxy heptadecane could be potentially cell toxic or exhibit an anti-cancer effects. In addition, the infection of *Cryptosporidium* have shown to lead to apoptosis in

neighbouring host cells[136], and sphingoid bases, ceramide and phytosphingosin have been known to induce apoptosis[137-139]. The synthesis of 2-amino-3,5-dihydroxy heptadecane and releasing it into host cells may be a process involved in the apoptosis induced by *Cryptosporidium* infection.

The stereochemistry on the amine head of this molecule is unknown. Previous reports have shown that the stereochemistry of the amine and hydroxyl groups on the sphingoid backbone of related molecules can alter the toxic effect via the level of inhibition of ceramide synthase up to 10 fold[140]. There are three chiral centers in the 2-amino-3,4-dihydroxy heptadecane, i.e., the carbon at position 2, 3 and 4. In the future, the compound should be purified in sufficient concentration using HPLC, then NMR can be performed to determine its chirality[141]. Following structural confirmation of the compound and provided sufficient concentrations can be prepared, cell toxicity tests can be performed on Caco-2 cells or other epithelium cells.

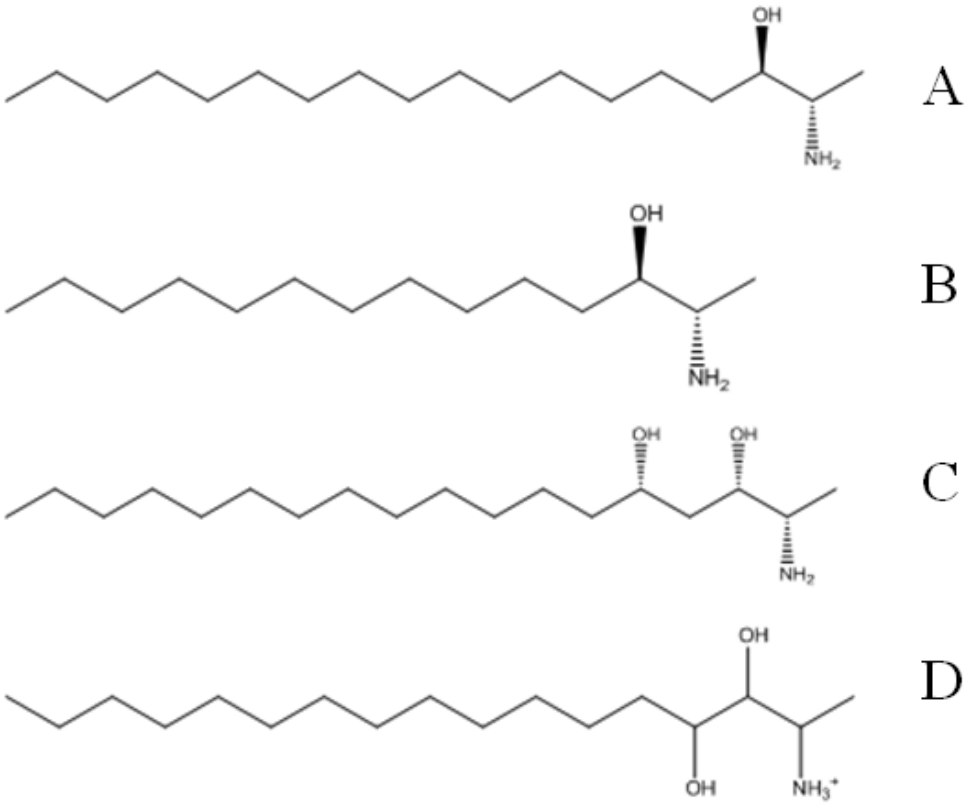

Figure 5.2 Structures comparison of several spingoid bases.

A: spisulosine. B: xestoaminol C. C: 1-deoxy, 5-hydroxy-spninganine (enigmol). D: 2-amino-3,5-dihydroxy heptadecane

5.5 Future direction

5.5.1 PKS gene diversity in *Cryptosporidium* and towards a novel identification tool for human infectious *Cryptosporidium*

PKS gene diversity was divided into two groups that correlated to the site of infection, confirming Truong's proteomic study[89]. More species of *Cryptosporidium* need to be investigated for the presence of PKS genes in order to completely assess the diversity of its sequence and the site of infection, or human infectivity or both. Priority species need to be investigated including *C. meleagridis*, *C. felis,* and *C. canis* that are known to infect immuno-competent humans. Additionally, the PKS diversity in *C. baileyi*, which is the only *Cryptosporidium* species that infects the respiratory track as the primary infection site[142] may clarify the correlation between PKS gene diversity and the site of infection.

Currently, PKS gene diversity of human-infectious species was determined in 21 subtypes of 12 allele families of *C. parvum*, *C. hominis* and *C. cuniculus*. While six allele families of *C. parvum*: IIb, IIe, IIf, IIg, IIh, and IIi were not covered in this study (**Table 1.2** Chapter 1), at the subtype level, there are many more subtypes not yet investigated. Though they rarely cause infection, the diversity still needs to be investigated in order to confirm the nucleotide polymorphism identified between *C. parvum* and *C. hominis* at species level. The nucleotide sequence information from other *Cryptosporidium* species is also required in order to minimise false

identification.

5.5.2 Metabolomics profiling and polyketide identification

A large amount of work is required to elucidate the complete metabolomics profile of *C. parvum*. In order to assist the identification, high-performance liquid chromatography (HPLC) should be applied to the crude extract to separate the extract into pure fractions[143]. With the number of potential metabolites in each fraction reduced, combined with increased metabolite concentration by increasing the number of oocysts used for the extraction, it may ultimately allow the use of NMR to assist with identification[143].

The extraction method used in this study was ethyl acetate and methanol based, and it is commonly used for polyketide extractions[144,145]. In order to confirm the identification of the large number of potential lipids identified from the crude extract of *Cryptosporidium*, a more commonly used lipid extraction methods such as chloroform/methanol could be applied[146,147]. Additionally, analysis in a negative ion detection mode will allow a more effective utilisation of metabolite databases, and enhancing the lipid identification process[120,146].

5.6 Conclusion

This thesis explored the PKS gene diversity in *Cryptosporidium* species; the feasibility of using MS for metabolomics profiling in *C. parvum*; and the identification of a toxin related polyketide. The PKS gene diversity at species and subtype levels suggests a correlation between the site of infection (and/or human infectivity) and the sequence diversity of the *Cryptosporidium* PKS gene. This correlation may be utilised as an alternative tool for a human infectivity-based detection method. Metabolomics profiles were constructed for the three excystation process related fractions. Variations among the three metabolomics profiles suggested new metabolites were synthesised during the excystation process, but this should be repeated in the future to confirm the findings. A novel molecule: 2-amino-3,4-dihydroxy heptadecane was identified in the intact oocysts which may be potentially involved in apoptosis induced by *Cryptosporidium* infection. Further work is required to fractionate the crude extract and identify each compound, including candidate polyketide identified in the metabolomics profiles.

References

1 Hunter, P. & Nichols, G. Epidemiology and clinical features of *Cryptosporidium* infection in immunocompromised patients. *Clinical Microbiology Review* **15**, 145-154 (2002).

2 Meisel, J. L., Perera, D. R., Meligro, C. & Rubin, C. E. Overwelming watery diarrhea associated with a *Cryptosporidium* in an immunosuppressed patient. *Gastroenterology* **70**, 1156-1160 (1976).

3 Panciera, R. J., Thomassen, R. W. & Garner, F. M. Cryptosporidial infection in a calf. *Veterinary Pathology* **8**, 479-484 (1971).

4 Tyzzer, E. E. An extracellular Coccidium, *Cryptosporidium muris* (Gen. Et Sp Nov.), of the gastric glands of the common mouse. *J Med Res* **23**, 487-U426 (1910).

5 Jokipii, L., Pohjola, S. & Jokipii, A. M. M. *Cryptosporidium*: a frequent finding in patients with gastrointestinal symptoms. *The Lancet* **322**, 358-361 (1983).

6 Olson, M. E., Thorlakson, C. L., Deselliers, L., Morck, D. W. & McAllister, T. A. *Giardia* and *Cryptosporidium* in Canadian farm animals. *Veterinary Parasitology* **68**, 375-381, doi:S0304-4017(96)01072-2 [pii] (1997).

7 Olson, M. E., O'Handley, R. M., Ralston, B. J., McAllister, T. A. & Andrew Thompson, R. C. Update on *Cryptosporidium* and *Giardia* infections in cattle. *Trends in Parasitology* **20**, 185-191 (2004).

8 Coklin, T., Farber, J., Parrington, L. & Dixon, B. Prevalence and molecular characterization of Giardia duodenalis and *Cryptosporidium* spp. in dairy cattle in Ontario, Canada. *Veterinary Parasitology* **150**, 297-305, doi:S0304-4017(07)00499-2 [pii]
10.1016/j.vetpar.2007.09.014 (2007).

9 Tyzzer, E. E. A sporozoan found in the peptic glands of the common mouse. *Proc. Soc. Exp. Biol. Med* **5**, 12-13 (1907).

10 Chalmers, R. M., Sturdee, A. P., Bull, S. A., Miller, A. & Wright, S. E. The prevalence of *Cryptosporidium parvum* and *C. muris* in Mus domesticus, Apodemus sylvaticus and Clethrionomys glareolus in an agricultural system. *Parasitology Research* **83**, 478-482 (1997).

11 Fayer, R. Taxonomy and species delimitation in *Cryptosporidium*. *Experimental Parasitology* **124**, 90-97 (2010).

12 Steiner, T. S., Thielman, N. M. & Guerrant, R. L. Protozoal agents: what are the dangers for the public water supply? *Annual Review of Medicine* **48**, 329-340 (1997).

13 Guerrant, R. Cryptosporidiosis: an emerging, highly infectious threat. *Emerging Infectious Diseases* **3**, 51-57 (1997).

14 DuPont, H. L. *et al.* The Infectivity of *Cryptosporidium parvum* in Healthy Volunteers. *The New England Journal of Medicine* **332**, 855-859, doi:10.1056/nejm199503303321304 (1995).

15 MacKenzie, W. R. *et al.* Massive outbreak of waterborne *Cryptosporidium* infection in Milwaukee, Wisconsin: recurrence of illness and risk of secondary transmission. *Clinical Infectious Diseases* **21**, 57-62 (1995).

16 Lumb, R., Smith, K., O'Donoghue, P. J. & Lanser, J. A. Ultrastructure of the

attachment of *Cryptosporidium* sporozoites to tissue culture cells. *Parasitol Research* **74**, 531-536 (1988).
17 Chen, X.-M., Keithly, J., Paya, C. & LaRusso, N. Cryptosporidiosis. *The New England Journal of Medicine* **346**, 1723-1731 (2002).
18 Thompson, R. C. A. *et al.* *Cryptosporidium* and cryptosporidiosis. *Advances in Parasitology* **59**, 77-158 (2005).
19 Strong, W. B., Gut, J. & Nelson, R. G. Cloning and sequence analysis of a highly polymorphic *Cryptosporidium* parvum gene encoding a 60-kilodalton glycoprotein and characterization of its 15- and 45-kilodalton zoite surface antigen products. *Infection and Immunity* **68**, 4117-4134 (2000).
20 Fayer, R. in *Cryptosporidium and cryptosporidiosis* (eds Ronald Fayer & Lihua Xiao) (CRC Press, Boca Raton, 2008).
21 Tzipori, S. & Widmer, G. in *Cryptosporidium and cryptosporidiosis* (eds Ronald Fayer & Lihua Xiao) (CRC Press, Boca Raton, 2008).
22 Upton, S. J., Tilley, M. & Brillhart, D. B. Comparative development of *Cryptosporidium parvum* (Apicomplexa) in 11 continuous host cell lines. *FEMS Microbiology Letters* **118**, 233-236 (1994).
23 Rasmussen, K. R., Larsen, N. C. & Healey, M. C. Complete development of *Cryptosporidium parvum* in a human endometrial carcinoma cell line. *Infection and Immunity* **61**, 1482-1485 (1993).
24 Hijjawi, N. S. *et al.* Complete development of *Cryptosporidium parvum* in host cell-free culture. *International Journal for Parasitology* **34**, 769-777 (2004).
25 Girouard, D., Gallant, J., Akiyoshi, D. E., Nunnari, J. & Tzipori, S. Failure to Propagate *Cryptosporidium* spp. in Cell-Free Culture. *The Journal of Parasitology* **92**, 399-400 (2006).
26 Hijjawi, N., Estcourt, A., Yang, R., Monis, P. & Ryan, U. Complete development and multiplication of *Cryptosporidium hominis* in cell-free culture. *Veterinary Parasitology* **169**, 29-36 (2010).
27 Truong, Q. & Ferrari, B. C. Quantitative and qualitative comparisons of *Cryptosporidium* faecal purification procedures for the isolation of oocysts suitable for proteomic analysis. *International Journal for Parasitology* **36**, 811-819 (2006).
28 Akiyoshi, D. E. *et al.* Characterization of *Cryptosporidium meleagridis* of human origin passaged through different host species. *Infection and Immunity* **71**, 1828-1832 (2003).
29 Garcia, L. S., Bruckner, D. A., Brewer, T. C. & Shimizu, R. Y. Techniques for the recovery and identification of *Cryptosporidium* oocysts from stool specimens. *Journal of Clinical Microbiology* **18**, 185-190 (1983).
30 Huw, V. S. in *Cryptosporidium and cryptosporidiosis* (eds Ronald Fayer & Lihua Xiao) (CRC Press, Boca Raton, 2008).
31 Webster, K. A., Smith, H. V., Giles, M., Dawson, L. & Robertson, L. J. Detection of *Cryptosporidium parvum* oocysts in faeces: Comparison of conventional coproscopical methods and the polymerase chain reaction. *Veterinary Parasitology* **61**, 5-13 (1996).
32 McLauchlin, J. *et al.* Polymerase chain reaction-based diagnosis of infection with *Cryptosporidium* in children with primary immunodficiencies. *The Pediatric Infectious Disease Journal* **22**, 329-334 (2003).
33 Yu, J.-R., Lee, S.-U. & Park, W.-Y. Comparative sensitivity of PCR primer

sets for detection of *Cryptosporidium parvum*. *The Korean Journal of Parasitology* **47**, 293-297 (2009).
34 Ferrari, B. C., Power, M. L. & Bergquist, P. L. Closed-tube DNA extraction using a thermostable proteinase is highly sensitive, capable of single parasite detection. *Biotechnology Letters* **29**, 1831-1837 (2007).
35 Xiao, L. *et al.* Genetic diversity within *Cryptosporidium parvum* and related *Cryptosporidium* species. *Applied and Environmental Microbiology* **65**, 3386-3391 (1999).
36 Xiao, L. *et al.* Molecular characterization of *cryptosporidium* oocysts in samples of raw surface water and wastewater. *Applied and Environmental Microbiology* **67**, 1097-1101, doi:10.1128/AEM.67.3.1097-1101.2001 (2001).
37 Stinear, T., Matusan, A., Hines, K. & Sandery, M. Detection of a single viable *Cryptosporidium parvum* oocyst in environmental water concentrates by reverse transcription-PCR. *Applied and Environmental Microbiology* **62**, 3385-3390 (1996).
38 Spano, F., Putignani, L., McLauchlin, J., Casemore, D. P. & Crisanti, A. PCR-RFLP analysis of the *Cryptosporidium* oocyst wall protein (COWP) gene discriminates between *C. wrairi* and *C. parvum*, and between *C. parvum* isolates of human and animal origin. *FEMS Microbiology Letters* **150**, 209-217, doi:S0378-1097(97)00115-8 [pii] (1997).
39 Sulaiman, I. M. *et al.* Unique endemicity of Cryptosporidiosis in children in Kuwait. *American Society for Microbiology* **43**, 2805-2809 (2005).
40 Yang, W. *et al. Cryptosporidium* source tracking in the Potomac River watershed. *Applied and Environmental Microbiology* **74**, 6495-6504, doi:AEM.01345-08 [pii]
10.1128/AEM.01345-08 (2008).
41 Carreno, R. A., Martin, D. S. & Barta, J. R. *Cryptosporidium* is more closely related to the gregarines than to coccidia as shown by phylogenetic analysis of apicomplexan. *Parasitology Research* **85**, 899-904 (1999).
42 Hijjawi, N. S., Meloni, B. P., Ryan, U. M., Olson, M. E. & Thompson, R. C. Successful in vitro cultivation of *Cryptosporidium andersoni*: evidence for the existence of novel extracellular stages in the life cycle and implications for the classification of *Cryptosporidium*. *Int J Parasitol* **32**, 1719-1726, doi:S0020751902001996 [pii] (2002).
43 Plutzer, J. & Karanis, P. Genetic polymorphism in *Cryptosporidium* species: an update. *Veterinary Parasitology* **165**, 187-199, doi:S0304-4017(09)00400-2 [pii]
10.1016/j.vetpar.2009.07.003 (2009).
44 Robinson, G. *et al.* Re-description of *Cryptosporidium cuniculus* in man and takeuchi, 1979 (Apicomplexa: Cryptosporidiidae): morphology, biology and phylogeny. *International Journal for Parasitology* **40**, 1539-1548 (2010).
45 Fayer, R. & Ungar, B. *Cryptosporidium* spp. and cryptosporidiosis. *American Society for Microbiology* **50**, 458-483 (1986).
46 Ling, Z., Ronald, F., James, M. T., Una, M. R. & et al. Genotypes of *Cryptosporidium* species infecting fur-bearing mammals differ from those of species infecting humans. *Applied and Environmental Microbiology; Washington* **70**, 7574 (2004).
47 Xiao, L., Fayer, R., Ryan, U. & Upton, S. J. *Cryptosporidium* taxonomy: recent advances and implications for public health. *Clinical Microbiology*

Reviews **17**, 72-97 (2004).
48 Gatei, W. *et al. Cryptosporidium muris* infection in an HIV-infected adult, Kenya. *Emerging Infectious Diseases* **8**, 204-206 (2002).
49 Katsumata, T. *et al.* Short report: possible *Cryptosporidium* muris infection in humans. *American Journal of Tropical Medicine and Hygiene* **62**, 70-72 (2000).
50 Smith, H. V., Caccio, S. M., Tait, A., McLauchlin, J. & Thompson, R. C. Tools for investigating the environmental transmission of *Cryptosporidium* and *Giardia* infections in humans. *Trends in Parasitology* **22**, 160-167, doi:S1471-4922(06)00054-7 [pii]
10.1016/j.pt.2006.02.009 (2006).
51 Xiao, L. & Ryan, U. Cryptosporidiosis: an update in molecular epidemilogy. *Current Opinion in Infectious Diseases* **17**, 483-490 (2004).
52 Widmer, G. & Lee, Y. Comparison of single-and multilocus genetic diversity in the protozoan parasites *Cryptosporidium parvum* and *C. hominis*. *Applied and Environmental Microbiology* **76**, 6639-6644 (2010).
53 Xiao, L. Molecular epidemiology of cryptosporidiosis: An update. *Experimental Parasitology* **124**, 80-89 (2010).
54 Cevallos, A. M. *et al.* Molecular Cloning and Expression of a Gene Encoding *Cryptosporidium parvum* Glycoproteins gp40 and gp15. *Infection and Immunity* **68**, 4108-4116, doi:10.1128/iai.68.7.4108-4116.2000 (2000).
55 Alves, M. *et al.* Subgenotype analysis of *Cryptosporidium* isolates from humans, cattle, and zoo ruminants in portugal. *American Society for Microbiology* **41**, 2744-2747 (2003).
56 Nichols, G. in *Cryptosporidium and cryptosporidiosis* (eds Ronald Fayer & Lihua Xiao) (CRC Press, Boca Raton, 2008).
57 Xiao, L. & Feng, Y. Zoonotic cryptosporidiosis. *FEMS Immunology & Medical Microbiology* **52**, 309-323 (2008).
58 Xu, P. *et al.* The genome of *Cryptosporidium hominis Nature* **432**, 415-415 (2004).
59 Awad-el-Kariem, F. M. *et al.* Differentiation between human and animal strains of *Cryptosporidium parvum* using isoenzyme typing. *Parasitology* **110 (Pt 2)**, 129-132 (1995).
60 Morgan-Ryan, U. M. *et al. Cryptosporidium huminis* n. sp. (apicomplexa: Cryptosporidiidae) from Homo sapiens. *The Journal of Eukaryotic Microbiology* **49**, 433-440 (2002).
61 Abrahamsen, M. S. *et al.* Complete Genome Sequence of the Apicomplexan, *Cryptosporidium parvum*. *Science* **304**, 441-445, doi:10.1126/science.1094786 (2004).
62 Kissinger, J. C. in *Cryptosporidium and cryptosporidiosis* (eds Ronald Fayer & Lihua Xiao) (CRC Press, Boca Raton, 2008).
63 Bankier, A. T. *et al.* Integrated mapping, chromosomal sequencing and sequence analysis of *Cryptosporidium parvum*. *Genome Res* **13**, 1787-1799 (2003).
64 Weir, S. C., Pokorny, N. J., Carreno, R. A., Trevors, J. T. & Lee, H. Efficacy of common laboratory disinfectants on the infectivity of *Cryptosporidium parvum* oocysts in cell culture. *Applied and Environmental Microbiology* **68**, 2576-25769 (2002).
65 Corso, P. S. Cost of illness in the 1993 waterborne *Cryptosporidium* outbreak,

Milwaukee, Wisconsin. . *Emerging Infectious Diseases* **9**, 426-431 (2003).
66 Stockdale, H., Spencer, J. & Blagburn, B. in *Cryptosporidium and cryptosporidiosis* (eds Ronald Fayer & Lihua Xiao) (CRC Press, Boca Raton, 2008).
67 Horman, A., Korpela, H., Sutinen, J., Wedel, H. & Hanninen, M.-L. Meta-analysis in assessment of the prevalence and annual incidence of *Giardia* spp. and *Cryptosporidium* spp. infections in humans in the Nordic countries. *International Journal for Parasitology* **34**, 1337-1346 (2004).
68 Esteban, J.-g. *et al.* High *Cryptosporidium* prevalences in healthy Aymara children from the Northern Bolivian Altiplano. *The American Journal of Tropical Medicine and Hygiene* **58**, 50-55 (1998).
69 Guarino, A. *et al.* Human intestinal Cryptosporidiosis: secretory diarrhea and enterotoxic activity in Caco-2 cells. *The Journal of Infectious Diseases* **171**, 976-983 (1995).
70 John, U. *et al.* Novel insights into evolution of protistan polyketide synthases through phylogenomic analysis. *Protist* **159**, 21-30 (2008).
71 Hopwood, D. A. & Sherman, D. H. Molecular genetics of polyketides and its comparison to fatty acid biosynthesis. *Annual Review of Genetics* **24**, 37-66 (1990).
72 Ridley, C. P., Young, L. H. & Khosla, C. Evolution of polyketide synthases in bacteria. *Proceedings of the National Academy of Sciences* **105**, 4595-4600 (2008).
73 Gaffoor, I. *et al.* Functional Analysis of the Polyketide Synthase Genes in the Filamentous Fungus *Gibberella zeae* (Anamorph *Fusarium graminearum*). *Eukaryotic Cell* **4**, 1926-1933, doi:10.1128/ec.4.11.1926-1933.2005 (2005).
74 Tropf, S., Kärcher, B., Schröder, G. & Schröder, J. Reaction mechanism of homodimeric plant polyketide synthases (stilbene and chalcone synthase). *The Journal of Biological Chemistry* **270**, 7922-7928 (1995).
75 Snyder, R. V. *et al.* Localization of polyketide synthase encoding genes to the toxic dinoflagellate *Karenia brevis*. *Phytochemistry* **66**, 1767 (2005).
76 Ginsburg, C. M., McCracken, G. H., Jr., Clahsen, J. & Zweighaft, T. Comparative pharmacokinetics of bacampicillin and ampicillin suspensions in infants and children. *Reviews of Infectious Diseases* **3**, 117-120 (1981).
77 Piel, J. *et al.* Antitumor polyketide biosynthesis by an uncultivated bacterial symbiont of the marine sponge *Theonella swinhoei*. *Proceedings of the National Academy of Sciences of the United States of America* **101**, 16222-16227, doi:10.1073/pnas.0405976101 (2004).
78 Ligon, J. *et al.* Characterization of the biosynthetic gene cluster for the antifungal polyketide soraphen A from *Sorangium cellulosum* So ce26. *Gene* **285**, 257-267 (2002).
79 Volchegursky, Y., Hu, Z., Katz, L. & McDaniel, R. Biosynthesis of the anti-parasitic agent megalomicin: transformation of erythromycin to megalomicin in *Saccharopolyspora erythraea*. *Molecular Microbiology* **37**, 752-762, doi:10.1046/j.1365-2958.2000.02059.x (2000).
80 Staunton, J. & Weissman, K. J. Polyketide biosynthesis: a millennium review. *Natural Product Reports* **18**, 380-416 (2001).
81 Birch, A. J. Biosynthesis of polyketides and related compounds. *Science* **156**, 202-206 (1967).
82 Stassi, D., Donadio, S., Staver, M. J. & Katz, L. Identification of a

Saccharopolyspora erythraea gene required for the final hydroxylation step in erythromycin biosynthesis. *The Journal of Bacteriology* **175**, 182-189 (1993).
83 Xue, Y., Zhao, L., Liu, H.-w. & Sherman, D. H. A gene cluster for macrolide antibiotic biosynthesis in *Streptomyces venezuelae*: Architecture of metabolic diversity. *Proceedings of the National Academy of Sciences of the United States of America* **95**, 12111-12116 (1998).
84 Staunton, J. Combinatorial biosynthesis of erythromycin and complex polyketides. *Current Opinion in Chemical Biology* **2**, 339-345 (1998).
85 Malpartida, F. & Hopwood, D. A. Molecular cloning of the whole biosynthetic pathway of a *Streptomyces* antibiotic and its expression in a heterologous host. *Nature* **309**, 462-464 (1984).
86 Hertweek, C., Luzhetskyy, A., Reberts, Y. & Bechthold, A. Type II polyketide synthaes: gaining a deeper insight into enzymatic teamwork. *Natural Product Reports* **24**, 162-190 (2007).
87 Gaisser, S., Trefzer, A., Stockert, S., Kirschning, A. & Bechthold, A. Cloning of an avilamycin biosynthetic gene cluster from *Streptomyces viridochromogenes* Tu57. *Journal of Bacteriology* **179**, 6271-6278 (1997).
88 Zhu, G. *et al. Cryptosporidium parvum*: the first protist known to encode a putative polyketide synthase. *Gene* **298**, 79-89 (2002).
89 Truong, Q. *Working towards the proteome of Cryptosporidium* Doctor of Philosophy thesis, Macquarie University, (2010).
90 Zhu, G. Current progress in the fatty acid metabolism in *Cryptosporidium parvum*. *The Journal of Eukaryotic Microbiology* **51**, 381-388 (2004).
91 Lorenzi, H. *et al.* (2008).
92 Zhu, G. *et al.* Expression and functional characterization of a giant Type I fatty acid synthase (CpFAS1) gene from *Cryptosporidium parvum*. *Molecular and Biochemical Parasitology* **134**, 127-135, doi:S0166685103003505 [pii] (2004).
93 Fritzler, J. M. & Zhu, G. Functional characterization of the acyl-[acyl carrier protein] ligase in the *Cryptosporidium parvum* giant polyketide synthase. *International Journal for Parasitology* **37**, 307-316 (2007).
94 Zhu, G., Shi, X. & Cai, X. The reductase domain in a Type I fatty acid synthase from the apicomplexan *Cryptosporidium parvum*: Restricted substrate preference towards very long chain fatty acyl thioesters. *BMC Biochemistry* **11**, 1-8, doi:10.1186/1471-2091-11-46 (2010).
95 Dass, C. *Fundamentals of contemporary mass spectrometry*. 5 (John Wiley & Sons, Inc., 2007).
96 Gross, J. H. *Mass spectrometry a text book*. 2 edn, 8 (Springer, 2011).
97 Wilm, M. & Mann, M. Analytical roperties of the nanoelectrospray ion source. *Analytical Chemistry* **68**, 1-8 (1996).
98 de Hoffmann, E. Tandem mass spectrometry: a primer. *Journal of Mass Spectrometry* **31**, 129-137 (1996).
99 Sleno, L. & Volmer, D. A. Ion activation methods for tandem mass spectrometry. *Journal of Mass Spectrometry* **39**, 1091-1112 (2004).
100 Levsen, L. & Schwarz, H. Gass-phase chemistry of collisionally activated ions. *Mass Spectrometry Reviews* **2**, 77-148 (1983).
101 Böcker, S. & Rasche, F. Towards *de novo* identification of metabolites by analyzing tandem mass spectra. *Bioinformatics* **24**, 49-55 (2008).
102 Garcia, D. *et al.* Separation and mass spectrometry in microbial metabolomics.

Current Opinion in Microbiology **11**, 233-239 (2008).
103 Böcker, S., Letzel, M., Lipták, Z. & Pervukhin, A. SIRIUS: decomposing isotope patterns for metabolite identification. *Bioinformatics* **25**, 218-224 (2008).
104 Dettmer, K., Aronov, P. A. & Hammock, B. D. Mass spectrometry-based metabolomics. *Mass Spectrometry Reviews* **26**, 51-78 (2007).
105 Dettmer, K. & Hammock, B. D. Metabolomics-a new exciting field within the "omics" science. *Environmental Health Perspectives* **112**, 396-397 (2004).
106 Villas-Bôas, S., Mas, S., Mas, A., Jorn, S. & Jens, N. Mass spectrometry in metabolome analysis. *Mass Spectrometry Reviews* **24**, 613-646 (2005).
107 Shockcor, J. P. *et al.* Combined HPLC, NMR Spectroscopy, and Ion-Trap Mass Spectrometry with Application to the Detection and Characterization of Xenobiotic and Endogenous Metabolites in Human Urine. *Analytical Chemistry* **68**, 4431-4435, doi:10.1021/ac9606463 (1996).
108 Robinson, G. & Chalmers, R. M. The European rabbit (*Oryctolagus cuniculus*), a source of zoonotic cryptosporidiosis. *Zoonoses and Public Health* **57**, e1-13, doi:JVB1308 [pii]
10.1111/j.1863-2378.2009.01308.x (2010).
109 Waldron, L. S., Ferrari, B. C. & Power, M. L. Glycoprotein 60 diversity in *C. hominis* and *C. parvum* causing human cryptosporidiosis in NSW, Australia. *Experimental Parasitology* **122**, 124-127, doi:S0014-4894(09)00040-X [pii]
10.1016/j.exppara.2009.02.006 (2009).
110 Tamura, K., Dudley, J., Neim, M. & Kumar, S. MEGA4: molecular evolutionary genetics analysis (MEGA) sofeware version 4.0. *Molecular Biology and Evolution* **24**, 1596-1599 (2007).
111 Ferrari, B., Vesey, G., Weir, C., Williams, K. & Veal, D. A. Comparison of *Cryptosporidium*-specific and *Giardia*-specific monoclonal antibodies for monitoring water samples. *Water Research* **33**, 1611-1617 (1999).
112 Kato, S., Jenkins, M. B., Ghiorse, W. C. & Bowman, D. D. Chemical and physical factors affecting the excystation of Cryptosporidium parvum oocysts. *J Parasitol* **87**, 575-581 (2001).
113 O'Brien, E., McInnes, L. & Ryan, U. *Cryptosporidium* GP60 genotypes from humans and domesticated animals in Australia, North America and Europe. *Experimental Parasitology* **118**, 118-121, doi:S0014-4894(07)00161-0 [pii]
10.1016/j.exppara.2007.05.012 (2008).
114 Snelling, W. *et al.* Proteomics analysis and protein expression during sporozoite excystation of *Cryptosporidium* (Coccidia, Apicomplexa). *Molecular & Cellular Proteomics* **6**, 346-355 (2007).
115 Lee, S.-U. *et al. Cryptosporidium parvum*: radiation-induced alteration of the oocyst proteome. *Experimental Parasitology* **127**, 25-30 (2011).
116 Gokhale, R. S., Hunziker, D., Cane, D. E. & Khosla, C. Mechanism and specificity of the terminal thioesterase domain from the erythromycin polyketide synthase. *Chemistry & Biology* **6**, 117-125 (1999).
117 Kamleh, A. *et al.* Metabolomic profiling using Orbitrap Fourier transform mass spectrometry with hydrophilic interaction chromatography: a method with wide applicability to analysis of biomolecules. *Rapid communications in mass spectrometry* **22**, 1912-1918, doi:10.1002/rcm.3564 (2008).
118 Gates, P., Kearney, G., Jones, R., Leadlay, P. & Staunton, J. Structural elucidation studies of erythromycins by electrospray tandem mass

spectrometry. *Rapid communications in mass spectrometry* **13**, 242-246 (1999).
119 Ghosh, R. *et al.* Dissecting the functional role of polyketide synthases in *Dictyosteliu discoideum*. *The Journal of Biological Chemistry* **283** (2008).
120 Welti, R. *et al.* Lipidomic analysis of *Toxoplasma gondii* reveals unusual polar lipids. *Biochemistry* **46**, 13882-13890 (2007).
121 Besteiro, S., MBertrand-Michel, J., Lebrune, M., Vial, H. & Durbremetz, J.-F. Lipidomic analysis of *Toxoplasma gondii* tachyzoites rhoptries: further insights into the role of cholesterol. *Biochemical Journal* **415**, 87-96 (2008).
122 Shaner, R. *et al.* Quantitative analysis of sphingolipids for lipidomics using triple quadrupole and quadrupole linear ion trap mass spectrometers. *The Journal of Lipid Research* **50** (2009).
123 Merrill, A. J. *et al.* Structural requirements for long-chain (sphingoid) base inhibition of protein kinase C *in vitro* and for cellular effects of these compounds. *Biochemistry* **28**, 3138-3145 (1989).
124 Zheng, W. *et al.* Ceramides and other bioactive sphingolipid backbones in halth and disease: lipidomic analysis metabolism and roles in membrane structure, dynamics, signaling and autophagy. *Biochimica et Biophysica Acta* **1758**, 1864-1884 (2006).
125 Xiao, L., Lal, A. A. & Jiang, J. Detection and differentiation of *Cryptosporidium* oocysts in water by PCR-RFLP. *Methods in Molecular Biology* **268**, 163-176, doi:1-59259-766-1:163 [pii]
10.1385/1-59259-766-1:163 (2004).
126 Jothikumar, N., da Silva, A. J., Moura, I., Qvarnstrom, Y. & Hill, V. R. Detection and differentiation of *Cryptosporidium hominis* and *Cryptosporidium parvum* by dual TaqMan assays. *Journal of Medical Microbiology* **57**, 1099-1105, doi:57/9/1099 [pii]
10.1099/jmm.0.2008/001461-0 (2008).
127 Alagappan, A. *Three-colour fluorescent in situ hybridisation detwction of Cryptosporidium species* Doctor of Philosophy thesis, University of Macquarie, (2009).
128 Stroup, S. *et al.* Real-time PCR detection and speciation of *Cryptosporidium* infection using Scorpion probes. *Journal of Medical Microbiology* **55**, 1217-1222, doi:55/9/1217 [pii]
10.1099/jmm.0.46678-0 (2006).
129 Tanriverdi, S. *et al.* Detection and genotyping of oocysts of *Cryptosporidium parvum* by real-time PCR and melting curve analysis. *Journal of Clinical Microbiology* **40**, 3237-3244 (2002).
130 Soliman, R. & Othman, A. Evaluation of DNA melting curve analysis Real-Time PCR for dectection and differentiation of *Cryptosporidium* species. *Parasitologists United Journal* **2**, 47-54 (2009).
131 Pruett, S. *et al.* Biodiversity of sphingoid bases ("sphingosines") and related amino alcohols. *The Journal of Lipid Research* **49**, 1621-1639 (2008).
132 Sonda, S. & Hehl, A. Lipid biology of Apicomplexa: perspectives for new drug targes, particularly for Toxoplasma gondii. *Trends in Parasitology* **22**, 41-47 (2006).
133 Symolon, H. *et al.* Enigmol: a novel sphingolipid analogue with anticancer activity against cancer cell lines and *In vivo* models for intestinal and prostate cancer. *Molecular Cancer Therapeutics* **10**, 648-657 (2011).

134 Chung, N., Mao, C., Heitman, J., Hannun, Y. & Obeid, L. Phytosphingosine as a specific inhibitor of growth and nutrient import in *Saccharomyces cerevisiae*. *The Journal of Biological Chemistry* **276**, 35614-35621 (2001).
135 Zitomer, N. *et al.* Ceramide synthase inhibition by fumonisin B_1 causes accumulation of 1-deoxysphinganine. *The Journal of Biological Chemistry* **284**, 4786-4795 (2009).
136 McCole, D., Eckmann, L., Laurent, F. & Kagnoff, M. Intestinal epithelial cell apoptosis following *Cryptosporidium parvum* infection. *Infection and Immunity* **68**, 1710-1713 (2000).
137 Aida, K. *et al.* Apoptosis inducedment by plant and fungus sphingoid bases in human colon cancer cells. *Journal of Oleo science* **53**, 503-510 (2004).
138 Zang, X., Li, B. & Ren, R. Effect of ceramide on apoptosis of human colon cancer HT-29 cells. *Wei Sheng Yan Jiu Journal of hygiene research* **35**, 537-540 (2006).
139 Nagahara, Y. *et al.* Phytosphingosine induced mitochondria-involved apoptosis. *Cancer science* **96**, 83-92 (2005).
140 Humpf, H.-U. *et al.* Acylation of naturally occuring and synthetic 1-deoxysphinganines by ceramide synthase. *The Journal of Biological Chemistry* **273**, 19060-19064 (1998).
141 Ryu, G., Choi, B. W. & Lee, B. H. Alsolute sterochemistry determination of tetrin B. *The Bulletin of the Korean Chemical Society* **23**, 1429-1434 (2002).
142 Goodwin, M. A., Brown, J., Resurreccion, R. S. & Smith, J. A. Respiratory coccidiosis (*Cryptosporidium baileyi*) among northern Georgia broilers in one company. *Avian Diseases* **40**, 572-575 (1996).
143 Han, X. & Gross, R. Shotgun lipidomics: electrospray ionization mass spectrometric analysis and quantitation of cellular lipidomes directly from crude extracts of biological samples. *Mass Spectrometry Reviews* **24**, 367-412 (2005).
144 Pfeifer, B. A., Admiraal, S. J., Gramajo, H., Cane, D. E. & Khosla, C. Biosynthesis of complex polyketides in a metabolically enginerred strain. *Science* **291**, 1790-1792 (2001).
145 Fu, H., Ebert-Khosla, E., Hopwood, D. A. & Khosla, C. Enginerred biosynthesis of novel polyketides: dissection of the catalytic specificity of the act ketoreductase. *Journal of the american chemiical society* **116**, 4166-4170 (1994).
146 Milne, S., Ivanova, P., Forrester, J. & Brown, A. Lipidomics: an analysis of cellular lipids by ESI-MS. *Methods* **39**, 92-103 (2006).
147 Han, X. & Gross, R. Global analyses of cellular lipidomes directly from crude extracts of biological samples by ESI mass spectrometry. *The Journal of Lipid Research* **44**, 1071 (2003).

Appendices

Appendix IV Potential metabolites identified in the extracts of three excystation process related fractions (intact oocyst, excystation medium and sporozoite) and the extract from 1x 10^8 intact oocysts.

Potential metabolites identified from 1 x 10^7 oocysts			Potential metabolites identified from 1 x 10^8 oocysts at intact oocyst stage
Intact oocyst	Excystation medium	Sporotoite/oocyst wall	
209.1147	153.1273	136.0729	101.0028
235.1303	163.1325	139.0726	151.1112
239.1616	173.0781	227.1248	153.1269
244.2624	179.104	239.1054	155.1425
247.1304	185.1144	254.8231	157.08285
263.1253	197.078	261.0869	163.1323
272.2936	199.1688	554.2718	169.1217
277.141	205.0678	587.2818	172.0941
288.2885	217.1194	599.3182	185.11403
293.2086	237.0728	675.2903	197.07761
295.2242	253.2132	698.277	199.16847
301.1409	267.2289	711.5738	201.08771
304.261	279.1589	727.4581	217.1039
304.2833	281.1382	728.4629	217.11891
307.1152	282.279	735.4435	217.15529
309.2035	295.1175	739.605	217.1791
316.3197	299.1488	780.5492	227.12439
321.1295	337.1051	784.5851	237.07239
321.2399	357.2785	786.6005	239.16062
323.2555	369.3843	797.5074	241.06717
332.3145	371.1011	799.6778	245.07735
349.1619	371.3153	804.551	271.20218
351.2868	373.2735	808.5812	275.16065
363.2868	375.2891	825.6933	279.15815
365.3024	387.1799	853.4035	283.26208
375.2504	391.284	853.7253	285.2779
379.1514	397.2009	854.404	287.2208
379.2817	409.2719	870.3675	288.2884
381.2974	410.3262	877.7243	289.15282
393.2974	411.1805	881.7547	291.15555
395.3129	413.1963	901.7245	299.1605
407.1464	413.2123	956.5254	301.1397
409.1621	429.2408	958.5415	301.21
409.1748	430.243	201.0881	304.2608
413.266	453.188	353.2657	309.20238
415.2099	460.2693	439.1988	316.3201
415.2817	469.183	440.1989	317.185
419.2766	471.3057	542.3212	319.224
423.1412	487.1936	544.3368	321.2386

425.1569	512.1889	615.4951	323.2542
432.2368	516.3324	617.5096	325.23369
434.1837	517.2042	641.5106	327.2268
437.1915	517.4611	643.5261	329.24167
439.2664	529.2587	715.4152	349.13037
440.1987	533.2802	737.4592	353.2646
440.4095	533.4559	767.4697	354.2841
447.3466	545.456	782.5652	359.2387
453.1652	546.3993	787.4581	360.14868
455.1634	547.4717	793.4856	360.3233
463.2747	550.6288	795.501	365.1038
463.3027	553.2557	806.5649	365.30111
468.4408	561.131	807.5008	367.28031
469.3286	565.482	829.4869	371.1001
483.3442	567.3285	855.4987	371.31412
485.2878	571.4328	869.3792	375.2133
491.3704	577.4458	879.738	381.2958
503.3704	590.4253	903.7383	383.2141
507.3288	611.3546	905.7543	383.3144
519.3653	617.4255	907.7706	391.28276
520.2881	634.4516	239.1611	393.2958
520.3395	647.4583	288.2885	395.3121
531.2716	652.8414	301.1399	396.12035
531.3653	655.3808	304.2604	397.29095
540.4256	661.4518	304.2839	409.1604
542.3215	699.407	309.2029	409.26978
544.3371	705.4781	316.3197	411.3456
549.451	722.502	321.1296	413.2644
551.3537	749.5043	323.2549	425.15533
561.451	764.5752	381.2966	429.2383
563.4668	779.5809	413.2646	435.24866
564.4984	783.5759	415.2107	437.01645
567.4381	799.5498	432.2369	439.3769
568.4569	801.4544	437.1916	441.2956
570.4569	805.5583	453.1653	445.1186
572.4364	807.5737	619.272	447.34517
580.4933	817.4492	658.4658	455.31125
583.254	823.4771	659.2864	467.10003
583.4331	823.5691	683.4319	467.4079
585.4487	836.7331	685.4334	469.3268
586.4801	837.5576	686.4971	475.41271
587.4279	843.446	702.492	483.34237
587.4642	850.7488	735.3331	485.30105
589.4434	856.5631	763.605	495.4392
589.4714	860.8732	771.4842	519.1371
595.3797	865.4119	815.5104	521.37937
597.3606	867.3916	827.4686	529.45955
599.4278	872.558	846.4411	531.47562
599.4641	873.379	851.3957	537.3942
601.4435	883.3872	859.5352	537.4833
615.4228	898.587	867.3683	541.11854
615.4955	901.3977	903.5618	548.50167
617.5112	906.7092		548.5052
619.2707	911.3508		553.3893
619.4093	919.3851		553.4568

637.3052	924.5872		557.45006
639.4059	926.3933		563.46494
641.2852	934.7411		567.4363
641.5113	962.5056		569.43095
641.7869	966.7299		569.45065
643.5271	967.3147		569.457
654.3319	967.4602		571.43041
658.4658	968.4638		571.4354
659.2872	969.311		580.49157
663.4535	980.7734		583.43096
665.5326	996.6235		583.4354
671.4856	201.0882		585.4465
680.4802	307.1175		585.48127
683.4319	353.2656		587.42608
685.4354	393.2971		587.46203
686.4971	409.1619		587.46515
693.5638	415.2815		591.49371
702.4922	439.1994		597.4413
718.4871	440.4092		599.42578
719.4704	447.3465		599.46241
724.4741	469.3284		599.4651
727.4583	507.3284		601.425
732.3249	520.2903		601.43968
735.3331	531.2738		615.42093
737.3394	540.4251		615.4937
738.453	549.451		617.50941
740.4691	551.3545		619.52497
743.4317	561.451		621.4378
752.5049	563.4662		623.4515
758.5695	564.4979		625.4636
760.5858	568.4563		641.50914
763.6058	580.4931		643.52516
766.529	585.448		647.5563
771.4842	586.4796		653.53066
779.4751	587.4637		659.28473
780.5512	595.3806		663.4513
782.5678	599.4274		669.45948
785.59	615.4226		671.48323
787.458	637.3045		671.4856
790.3558	639.4069		680.47812
790.8574	654.3317		681.56206
806.5672	663.453		685.4329
810.5553	671.4848		687.4608
815.5105	680.4795		693.4535
827.4687	715.4157		701.40719
831.4845	718.4889		707.21934
840.3993	737.3415		711.57237
841.3665	737.4611		721.5751
846.4411	743.4333		723.24039
848.3878	767.4715		723.35371
848.8893	785.5919		723.57204
851.3955	793.5305		732.55135
859.5351	795.5031		739.60361
867.3682	807.503		745.46577
875.5094	829.4854		750.52089

879.7414	855.5031		751.60468
903.5619	869.3789		758.56685
903.7415	909.3561		760.58263
905.7575	950.7359		761.58806
907.7732	952.7421		763.44835
909.3534	978.7666		763.60464
919.5358	239.1612		764.57522
947.5882	288.2891		765.2608
950.7367	301.1404		765.7625
952.7434	304.2605		766.59106
978.7679	304.284		767.46937
985.7031	309.2031		769.3237
	316.3203		771.5736
	321.1303		780.54839
	323.255		782.56433
	381.2969		782.565
	413.2659		784.58244
	415.2112		784.5859
	419.2762		786.5981
	419.3148		788.60848
	432.2377		789.61896
	437.1928		790.59134
	453.1676		792.60667
	463.3023		799.6047
	619.2723		800.57699
	658.4674		802.59284
	659.2869		803.5435
	683.433		804.54845
	685.4346		806.5639
	686.4991		806.566
	702.4932		808.279
	727.4593		808.5798
	735.335		808.7807
	763.6069		809.2786
	771.4856		810.59762
	815.5117		812.342
	827.4707		823.40708
	846.4431		825.69175
	851.3976		827.63587
	859.5374		830.56487
	867.3728		839.6359
	903.5644		851.70707
			852.2971
			853.72239
			855.3605
			855.73776
			859.6045
			877.72251
			879.73768
			881.75345
			895.3157
			898.3788
			901.72311
			903.74
			905.75346

			905.7561
			907.76813
			911.7664
			912.76954
			921.73166
			923.76605
			929.75387
			938.3342
			938.8354
			941.3971
			943.73456
			981.3528
			981.8537
			984.4154

Appendix V Matches identified in METLIN database searched by the exact masses of potential metabolites identified in the extract from 1 x 10^8 intact oocysts.

Exact mass	Ion type	dppm	Name	Formula
903.74	$[M+H]^+$	4	TG(20:4(5Z,8Z,11Z,14Z)/18:1(9Z)/18:3(9Z,12Z,15Z))[iso6]	C59H98O6
288.2884	$[M+H]^+$	4	C17 Sphinganine	C17H37NO2
153.1269	$[M+H]^+$	3	2E, 4E-decadienal	C10H16O
153.1269	$[M+H]^+$	3	2,6-decadienal	C10H16O
153.1269	$[M+H]^+$	3	4,7-decadienal	C10H16O
153.1269	$[M+H]^+$	3	(+)-Camphor	C10H16O
153.1269	$[M+H]^+$	3	(-)-trans-Isopiperitenol	C10H16O
153.1269	$[M+H]^+$	3	Geranial	C10H16O
153.1269	$[M+H]^+$	3	(S)-(-)-Perillyl alcohol	C10H16O
153.1269	$[M+H]^+$	3	α-Pinene-oxide	C10H16O
153.1269	$[M+H]^+$	3	2-Methyl-5-isopropylhexa-2Z,5-dienal	C10H16O
153.1269	$[M+H]^+$	3	Limonene-1,2-epoxide	C10H16O
153.1269	$[M+H]^+$	3	Neral	C10H16O
153.1269	$[M+H]^+$	3	Fenchone	C10H16O
153.1269	$[M+H]^+$	3	(+)-Piperitone	C10H16O
153.1269	$[M+H]^+$	3	(R)-(+)-Pulegone	C10H16O
153.1269	$[M+H]^+$	3	Thujone	C10H16O
153.1269	$[M+H]^+$	3	(4R,6R)-cis-Carveol	C10H16O
153.1269	$[M+H]^+$	3	(1R,4R)-Dihydrocarvone	C10H16O
153.1269	$[M+H]^+$	3	(1S,4R)-Iso-dihydrocarvone	C10H16O
153.1269	$[M+H]^+$	3	(1R,4S)-Iso-dihydrocarvone	C10H16O
153.1269	$[M+H]^+$	3	(1S,4S)-Dihydrocarvone	C10H16O
153.1269	$[M+H]^+$	3	Myrtenol	C10H16O
153.1269	$[M+H]^+$	3	Pinocarveol	C10H16O
153.1269	$[M+H]^+$	3	(+)-cis-Isopulegone	C10H16O
153.1269	$[M+H]^+$	3	(-)-trans-Carveol	C10H16O
153.1269	$[M+H]^+$	3	Perillyl alcohol	C10H16O
153.1269	$[M+H]^+$	3	α-Pinene oxide	C10H16O
153.1269	$[M+H]^+$	3	2-Methyl-6-methylene-2E,7-octadien-1-ol	C10H16O
153.1269	$[M+H]^+$	3	2E,9-Decadienal	C10H16O
153.1269	$[M+H]^+$	3	2E,4Z-Decadienal	C10H16O
153.1269	$[M+H]^+$	3	(-)-cis-sabinol	C10H16O
153.1269	$[M+H]^+$	3	sabinol	C10H16O
153.1269	$[M+H]^+$	3	(4R)-limonene 1alpha,2alpha-epoxide	C10H16O
153.1269	$[M+H]^+$	3	1-(1,4-dimethylcyclohex-3-enyl)ethanone	C10H16O
153.1269	$[M+H]^+$	3	(1R,4S)-fenchone	C10H16O
153.1269	$[M+H]^+$	3	(+)-beta-thujone	C10H16O
153.1269	$[M+H]^+$	3	(-)-beta-thujone	C10H16O
153.1269	$[M+H]^+$	3	(+)-cis-sabinol	C10H16O
153.1269	$[M+H]^+$	3	(R)-camphor	C10H16O
153.1269	$[M+H]^+$	3	(+)-trans-Carveol	C10H16O
153.1269	$[M+H]^+$	3	(4S,6S)-cis-Carveol	C10H16O
153.1269	$[M+H]^+$	3	trans-2-Methyl-5-isopropylhexa-2,5-dienal	C10H16O
217.11891	$[M+H]^+$	2	γ-Glutamyl-γ-aminobutyraldehyde	C9H16N2O4
217.11891	$[M+H]^+$	2	Thr Pro	C9H16N2O4

217.11891	$[M+H]^+$	2	Pro Thr	C9H16N2O4
279.15815	$[M+H]^+$	3	Phthalic acid Mono-2-ethylhexyl Ester	C16H22O4
279.15815	$[M+H]^+$	3	α-CEHC	C16H22O4
279.15815	$[M+H]^+$	3	Emmotin A	C16H22O4
279.15815	$[M+H]^+$	3	alhpa-tocopheronolactone	C16H22O4
279.15815	$[M+H]^+$	3	Alpha-CEHC	C16H22O4
371.31412	$[M+H]^+$	3	Docosanedioic acid	C22H42O4
391.28276	$[M+H]^+$	3	3α-Hydroxy-6-oxo-5β-cholan-24-oic Acid	C24H38O4
391.28276	$[M+H]^+$	3	3β-Hydroxy-6-oxo-5β-cholan-24-oic Acid	C24H38O4
391.28276	$[M+H]^+$	3	3α-Hydroxy-6-oxo-5α-cholan-24-oic Acid	C24H38O4
391.28276	$[M+H]^+$	3	3β-Hydroxy-6-oxo-5α-cholan-24-oic Acid	C24H38O4
391.28276	$[M+H]^+$	3	3β-Hydroxy-7-oxo-5β-cholan-24-oic Acid	C24H38O4
391.28276	$[M+H]^+$	3	3β-Hydroxy-7-oxo-5α-cholan-24-oic Acid	C24H38O4
391.28276	$[M+H]^+$	3	3α-Hydroxy-11-oxo-5β-cholan-24-oic Acid	C24H38O4
391.28276	$[M+H]^+$	3	3β-Hydroxy-11-oxo-5β-cholan-24-oic Acid	C24H38O4
391.28276	$[M+H]^+$	3	3α-Hydroxy-12-oxo-5β-cholan-24-oic Acid	C24H38O4
391.28276	$[M+H]^+$	3	3β-Hydroxy-12-oxo-5β-cholan-24-oic Acid	C24H38O4
391.28276	$[M+H]^+$	3	12β-Hydroxy-3-oxo-5β-cholan-24-oic Acid	C24H38O4
391.28276	$[M+H]^+$	3	6α-Hydroxy-3-oxo-5β-cholan-24-oic Acid	C24H38O4
391.28276	$[M+H]^+$	3	6β-Hydroxy-3-oxo-5β-cholan-24-oic Acid	C24H38O4
391.28276	$[M+H]^+$	3	6α-Hydroxy-3-oxo-5α-cholan-24-oic Acid	C24H38O4
391.28276	$[M+H]^+$	3	7β-Hydroxy-3-oxo-5β-cholan-24-oic Acid	C24H38O4
391.28276	$[M+H]^+$	3	7α-Hydroxy-3-oxo-5α-cholan-24-oic Acid	C24H38O4
391.28276	$[M+H]^+$	3	7α-Hydroxy-12-oxo-5β-cholan-24-oic Acid	C24H38O4
391.28276	$[M+H]^+$	3	7β-Hydroxy-12-oxo-5β-cholan-24-oic Acid	C24H38O4
391.28276	$[M+H]^+$	3	7α-Hydroxy-12-oxo-5α-cholan-24-oic Acid	C24H38O4
391.28276	$[M+H]^+$	3	7β-Hydroxy-12-oxo-5α-cholan-24-oic Acid	C24H38O4
391.28276	$[M+H]^+$	3	12α-Hydroxy-3-oxo-5β-cholan-24-oic Acid	C24H38O4
391.28276	$[M+H]^+$	3	12α-Hydroxy-3-oxo-5α-cholan-24-oic Acid	C24H38O4
391.28276	$[M+H]^+$	3	12α-Hydroxy-7-oxo-5α-cholan-24-oic Acid	C24H38O4
391.28276	$[M+H]^+$	3	3β,6β-Dihydroxychol-4-en-24-oic Acid	C24H38O4
391.28276	$[M+H]^+$	3	3β,7α-Dihydroxychol-4-en-24-oic Acid	C24H38O4

391.28276	$[M+H]^+$	3	3β,7α-Dihydroxychol-5-en-24-oic Acid	C24H38O4
391.28276	$[M+H]^+$	3	3β,7β-Dihydroxychol-5-en-24-oic Acid	C24H38O4
391.28276	$[M+H]^+$	3	3β,12α-Dihydroxychol-5-en-24-oic Acid	C24H38O4
391.28276	$[M+H]^+$	3	3α,12α-Dihydroxy-5β-chol-6-en-24-oic Acid	C24H38O4
391.28276	$[M+H]^+$	3	3α,12β-Dihydroxy-5β-chol-6-en-24-oic Acid	C24H38O4
391.28276	$[M+H]^+$	3	3α,12α-Dihydroxy-5β-chol-7-en-24-oic Acid	C24H38O4
391.28276	$[M+H]^+$	3	3α,12α-Dihydroxy-5β-chol-8-en-24-oic Acid	C24H38O4
391.28276	$[M+H]^+$	3	3α,12α-Dihydroxy-5β-chol-8(14)-en-24-oic Acid	C24H38O4
391.28276	$[M+H]^+$	3	3α,12α-Dihydroxy-5β-chol-9(11)-en-24-oic Acid	C24H38O4
391.28276	$[M+H]^+$	3	7α,12α-Dihydroxy-5β-chol-3-en-24-oic Acid	C24H38O4
391.28276	$[M+H]^+$	3	(22E)-3α,7α-Dihydroxy-5β-chol-22-en-24-oic Acid	C24H38O4
391.28276	$[M+H]^+$	3	(22E)-3α,7β-Dihydroxy-5β-chol-22-en-24-oic Acid	C24H38O4
391.28276	$[M+H]^+$	3	(22E)-3α,12α-Dihydroxy-5β-chol-22-en-24-oic Acid	C24H38O4
391.28276	$[M+H]^+$	3	1α-Hydroxy-3-oxo-5β-cholan-24-oic Acid	C24H38O4
391.28276	$[M+H]^+$	3	3α,7α-Dihydroxychol-5-en-24-oic Acid	C24H38O4
391.28276	$[M+H]^+$	3	3α,7β-Dihydroxychol-5-en-24-oic Acid	C24H38O4
391.28276	$[M+H]^+$	3	3α,7α-Dihydroxy-5β-chol-11-en-24-oic Acid	C24H38O4
391.28276	$[M+H]^+$	3	3α,7β-Dihydroxy-5β-chol-11-en-24-oic Acid	C24H38O4
391.28276	$[M+H]^+$	3	3α,12α-Dihydroxy-5β-chol-14-en-24-oic Acid	C24H38O4
391.28276	$[M+H]^+$	3	3α,12β-Dihydroxy-5β-chol-9(11)-en-24-oic Acid	C24H38O4
391.28276	$[M+H]^+$	3	3α-Hydroxy-12-oxo-5α-cholan-24-oic Acid	C24H38O4
391.28276	$[M+H]^+$	3	7α,12α-Dihydroxy-5β-chol-2-en-24-oic Acid	C24H38O4
391.28276	$[M+H]^+$	3	12α-Hydroxy-7-oxo-5β-cholan-24-oic Acid	C24H38O4
391.28276	$[M+H]^+$	3	3β,19-Dihydroxychol-5-en-24-oic Acid	C24H38O4
391.28276	$[M+H]^+$	3	3α-Hydroxy-7-oxo-5α-cholan-24-oic Acid	C24H38O4
391.28276	$[M+H]^+$	3	3α,7α-Dihydroxy-5β-chol-16-en-24-oic Acid	C24H38O4
391.28276	$[M+H]^+$	3	Dioctyl phthalate	C24H38O4
391.28276	$[M+H]^+$	3	Pregnan-20-one, 17-(acetyloxy)-3-hydroxy-6-methyl-, (3b,5b,6a)-	C24H38O4
391.28276	$[M+H]^+$	3	Pregnan-20-one, 17-(acetyloxy)-3-hydroxy-6-methyl-, (3a,5b,6a)-	C24H38O4

391.28276	$[M+H]^+$	3	Pregnan-20-one, 17-(acetyloxy)-3-hydroxy-6-methyl-, (3a,5a,6a)-	C24H38O4
391.28276	$[M+H]^+$	3	Pregnan-20-one, 17-(acetyloxy)-3-hydroxy-6-methyl-, (3b,5a,6a)-	C24H38O4
391.28276	$[M+H]^+$	3	7-Oxolithocholic acid	C24H38O4
391.28276	$[M+H]^+$	3	Nutriacholic acid	C24H38O4
391.28276	$[M+H]^+$	3	7a-Hydroxy-3-oxo-5b-cholanoic acid	C24H38O4
391.28276	$[M+H]^+$	3	7b-Hydroxy-3-oxo-5b-cholanoic acid	C24H38O4
429.2383	$[M+H]^+$	3	Irbesartan	C25H28N6O
429.2383	$[M+H]^+$	4	ZK118182 isopropyl ester	C23H37ClO5
563.46494	$[M+H]^+$	3	bacteriohopane-31,32,33,34,35-pentol	C35H62O5
563.46494	$[M+H]^+$	3	DG(14:0/18:3(6Z,9Z,12Z)/0:0)	C35H62O5
563.46494	$[M+H]^+$	3	DG(14:0/18:3(9Z,12Z,15Z)/0:0)	C35H62O5
563.46494	$[M+H]^+$	3	DG(14:1(9Z)/18:2(9Z,12Z)/0:0)	C35H62O5
563.46494	$[M+H]^+$	3	DG(18:2(9Z,12Z)/14:1(9Z)/0:0)	C35H62O5
563.46494	$[M+H]^+$	3	DG(18:3(6Z,9Z,12Z)/14:0/0:0)	C35H62O5
563.46494	$[M+H]^+$	3	DG(18:3(9Z,12Z,15Z)/14:0/0:0)	C35H62O5
447.34517	$[M+H]^+$	3	3-Dehydroteasterone	C28H46O4
447.34517	$[M+H]^+$	3	1α,25-dihydroxy-26,27-dimethyl-20,21-didehydro-23-oxavitamin D3 / 1α,25-dihydroxy-26,27-dimethyl-20,21-didehydro-23-oxacholecalciferol	C28H46O4
447.34517	$[M+H]^+$	3	(24R)-1α,24-dihydroxy-26,27-dimethyl-22-oxavitamin D3 / (24R)-1α,24-dihydroxy-26,27-dimethyl-22-oxacholecalciferol	C28H46O4
447.34517	$[M+H]^+$	3	(24S)-1α,24-dihydroxy-26,27-dimethyl-22-oxavitamin D3 / (24S)-1α,24-dihydroxy-26,27-dimethyl-22-oxacholecalciferol	C28H46O4
447.34517	$[M+H]^+$	3	1α,25-dihydroxy-11α-methoxyvitamin D3 / 1α,25-dihydroxy-11α-methoxycholecalciferol	C28H46O4
447.34517	$[M+H]^+$	3	1α,25-dihydroxy-11α-(hydroxymethyl)vitamin D3 / 1α,25-dihydroxy-11α-(hydroxymethyl)cholecalciferol	C28H46O4
447.34517	$[M+H]^+$	3	1α,25-dihydroxy-11β-methoxyvitamin D3 / 1α,25-dihydroxy-11β-methoxycholecalciferol	C28H46O4
447.34517	$[M+H]^+$	3	(20S)-1α,25-dihydroxy-20-methoxyvitamin D3 / (20S)-1α,25-dihydroxy-20-methoxycholecalciferol	C28H46O4
447.34517	$[M+H]^+$	3	1α,25-dihydroxy-24a,24b-dihomo-22-oxavitamin D3 / 1α,25-dihydroxy-24a,24b-dihomo-22-oxacholecalciferol	C28H46O4
447.34517	$[M+H]^+$	3	1α,25-dihydroxy-24a,24b-dihomo-22-oxa-20-epivitamin D3 / 1α,25-dihydroxy-24a,24b-dihomo-22-oxa-20-epicholecalciferol	C28H46O4
447.34517	$[M+H]^+$	3	1α,25-dihydroxy-26,27-dimethyl-22-oxavitamin D3 / 1α,25-dihydroxy-26,27-dimethyl-22-oxacholecalciferol	C28H46O4

447.34517	$[M+H]^+$	3	1α,25-dihydroxy-24a,24b-dihomo-23-oxavitamin D3 / 1α,25-dihydroxy-24a,24b-dihomo-23-oxacholecalciferol	C28H46O4
447.34517	$[M+H]^+$	3	1α,25-dihydroxy-24a,24b-dihomo-23-oxa-20-epivitamin D3 / 1α,25-dihydroxy-24a,24b-dihomo-23-oxa-20-epicholecalciferol	C28H46O4
447.34517	$[M+H]^+$	3	(20S)-1α,20,25-trihydroxy-24a-homovitamin D3 / (20S)-1α,20,25-trihydroxy-24a-homocholecalciferol	C28H46O4
447.34517	$[M+H]^+$	3	(23R)-1α,23,25-trihydroxy-23-methylvitamin D3 / (23R)-1α,23,25-trihydroxy-23-methylcholecalciferol	C28H46O4
447.34517	$[M+H]^+$	3	1α-hydroxy-18-(4-hydroxy-4-methylpentyloxy)-23,24,25,26,27-pentanorvitamin D3 / 1α-hydroxy-18-(4-hydroxy-4-methylpentyloxy)-23,24,25,26,27-pentanorcholecalciferol	C28H46O4
447.34517	$[M+H]^+$	3	2β-methoxy-1α,25-dihydroxyvitamin D3	C28H46O4
447.34517	$[M+H]^+$	3	KH 1049	C28H46O4
447.34517	$[M+H]^+$	3	3-Dehydroteasterone	C28H46O4
151.1112	$[M+H]^+$	3	Carvone	C10H14O
151.1112	$[M+H]^+$	3	2,4,7-decatrienal	C10H14O
151.1112	$[M+H]^+$	3	(-)-Carvone	C10H14O
151.1112	$[M+H]^+$	3	(-)-Isopiperitenone	C10H14O
151.1112	$[M+H]^+$	3	Perillyl aldehyde	C10H14O
151.1112	$[M+H]^+$	3	Carvacrol	C10H14O
151.1112	$[M+H]^+$	3	Menthofuran	C10H14O
151.1112	$[M+H]^+$	3	Pinocarvone	C10H14O
151.1112	$[M+H]^+$	3	Myrtenal	C10H14O
151.1112	$[M+H]^+$	3	Thymol	C10H14O
151.1112	$[M+H]^+$	3	4-Isopropylbenzyl alcohol	C10H14O
151.1112	$[M+H]^+$	3	1-(4-(prop-1-en-2-yl)cyclopent-1-enyl)ethanone	C10H14O
151.1112	$[M+H]^+$	3	piperitenone	C10H14O
151.1112	$[M+H]^+$	3	(+)-sabinone	C10H14O
155.1425	$[M+H]^+$	3	2-decenal	C10H18O
155.1425	$[M+H]^+$	3	3-decenal	C10H18O
155.1425	$[M+H]^+$	3	5-decenal	C10H18O
155.1425	$[M+H]^+$	3	6-decenal	C10H18O
155.1425	$[M+H]^+$	3	Geraniol	C10H18O
155.1425	$[M+H]^+$	3	(-)-Menthone	C10H18O
155.1425	$[M+H]^+$	3	(-)-Borneol	C10H18O
155.1425	$[M+H]^+$	3	(-)-endo-Fenchol	C10H18O
155.1425	$[M+H]^+$	3	Sabinene hydrate	C10H18O
155.1425	$[M+H]^+$	3	Linalool	C10H18O
155.1425	$[M+H]^+$	3	(R)-(+)-Citronellal	C10H18O
155.1425	$[M+H]^+$	3	Nerol	C10H18O
155.1425	$[M+H]^+$	3	(R)-(+)-α-Terpineol	C10H18O
155.1425	$[M+H]^+$	3	(S)-(-)-Citronellal	C10H18O
155.1425	$[M+H]^+$	3	(-)-Linalool	C10H18O
155.1425	$[M+H]^+$	3	(1R,2R,4R)-Dihydrocarveol	C10H18O
155.1425	$[M+H]^+$	3	(1R,2S,4R)-Neo-dihydrocarveol	C10H18O

155.1425	$[M+H]^+$	3	(1S,2S,4R)-Iso-dihydrocarveol	C10H18O
155.1425	$[M+H]^+$	3	(1S,2R,4R)-Neoiso-dihydrocarveol	C10H18O
155.1425	$[M+H]^+$	3	(1S,2S,4S)-Dihydrocarveol	C10H18O
155.1425	$[M+H]^+$	3	(1S,2R,4S)-Neo-dihydrocarveol	C10H18O
155.1425	$[M+H]^+$	3	(+)-Isomenthone	C10H18O
155.1425	$[M+H]^+$	3	eucalyptol	C10H18O
155.1425	$[M+H]^+$	3	CHRYSANTHEMYL ALCOHOL	C10H18O
155.1425	$[M+H]^+$	3	3,7-Dimethyl-3Z,6-octadien-1-ol	C10H18O
155.1425	$[M+H]^+$	3	7Z,9-Decadien-1-ol	C10H18O
155.1425	$[M+H]^+$	3	4Z-Decenal	C10H18O
155.1425	$[M+H]^+$	3	5Z-Decenal	C10H18O
155.1425	$[M+H]^+$	3	(S)-lavandulol	C10H18O
155.1425	$[M+H]^+$	3	(R)-lavandulol	C10H18O
155.1425	$[M+H]^+$	3	Iridoid skeleton	C10H18O
155.1425	$[M+H]^+$	3	(+)-borneol	C10H18O
155.1425	$[M+H]^+$	3	(-)-α-Terpineol	C10H18O
155.1425	$[M+H]^+$	3	(1R,2R,4S)-Iso-dihydrocarveol	C10H18O
155.1425	$[M+H]^+$	3	(1R,2S,4S)- Neoiso-dihydrocarveol	C10H18O
169.1217	$[M+H]^+$	3	cis, cis-stillingic acid	C10H16O2
169.1217	$[M+H]^+$	3	2Z,4E-decadienoic acid	C10H16O2
169.1217	$[M+H]^+$	3	trans, cis-stillingic acid	C10H16O2
169.1217	$[M+H]^+$	3	2E,4E-decadienoic acid	C10H16O2
169.1217	$[M+H]^+$	3	2Z,6Z-decadienoic acid	C10H16O2
169.1217	$[M+H]^+$	3	2E,6Z-decadienoic acid	C10H16O2
169.1217	$[M+H]^+$	3	2E,6E-decadienoic acid	C10H16O2
169.1217	$[M+H]^+$	3	4E,6E-decadienoic acid	C10H16O2
169.1217	$[M+H]^+$	3	Aleprestic acid	C10H16O2
169.1217	$[M+H]^+$	3	2,3-decadienoic acid	C10H16O2
169.1217	$[M+H]^+$	3	2,5-decadienoic acid	C10H16O2
169.1217	$[M+H]^+$	3	2E,7E-decadienoic acid	C10H16O2
169.1217	$[M+H]^+$	3	2E,7Z-decadienoic acid	C10H16O2
169.1217	$[M+H]^+$	3	2Z,6E-decadienoic acid	C10H16O2
169.1217	$[M+H]^+$	3	3,4-decadienoic acid	C10H16O2
169.1217	$[M+H]^+$	3	3,5-decadienoic acid	C10H16O2
169.1217	$[M+H]^+$	3	3E,5Z-decadienoic acid	C10H16O2
169.1217	$[M+H]^+$	3	3Z,5E-decadienoic acid	C10H16O2
169.1217	$[M+H]^+$	3	4,8-decadienoic acid	C10H16O2
169.1217	$[M+H]^+$	3	4E,9-decadienoic acid	C10H16O2
169.1217	$[M+H]^+$	3	5E,9-decadienoic acid	C10H16O2
169.1217	$[M+H]^+$	3	5E,8E-decadienoic acid	C10H16O2
169.1217	$[M+H]^+$	3	6E,8E-decadienoic acid	C10H16O2
169.1217	$[M+H]^+$	3	7,9-decadienoic acid	C10H16O2
169.1217	$[M+H]^+$	3	3,7-dimethyl-2Z,6E-octadienoic acid	C10H16O2
169.1217	$[M+H]^+$	3	3-decynoic acid	C10H16O2
169.1217	$[M+H]^+$	3	4-decynoic acid	C10H16O2
169.1217	$[M+H]^+$	3	5-decynoic acid	C10H16O2
169.1217	$[M+H]^+$	3	6-decynoic acid	C10H16O2
169.1217	$[M+H]^+$	3	7-decynoic acid	C10H16O2
169.1217	$[M+H]^+$	3	8-decynoic acid	C10H16O2
169.1217	$[M+H]^+$	3	9-decynoic acid	C10H16O2
169.1217	$[M+H]^+$	3	6-Oxocineole	C10H16O2
169.1217	$[M+H]^+$	3	(+)-exo-5-Hydroxycamphor	C10H16O2
169.1217	$[M+H]^+$	3	Chrysanthemic acid	C10H16O2
169.1217	$[M+H]^+$	3	(1S,4R)-1-Hydroxy-2-oxolimonene	C10H16O2

169.1217	$[M+H]^+$	3	Iridodial	C10H16O2
169.1217	$[M+H]^+$	3	(+)-Iridodial	C10H16O2
169.1217	$[M+H]^+$	3	(+)-Iridodial	C10H16O2
169.1217	$[M+H]^+$	3	8-Epiiridodial	C10H16O2
169.1217	$[M+H]^+$	3	3,7-Dimethyl-2E,6-octadienoic acid	C10H16O2
169.1217	$[M+H]^+$	3	2E,7-Octadienyl acetate	C10H16O2
169.1217	$[M+H]^+$	3	2E,4E-Octadienyl acetate	C10H16O2
169.1217	$[M+H]^+$	3	2E,6E-Octadienyl acetate	C10H16O2
169.1217	$[M+H]^+$	3	2E,6Z-Octadienyl acetate	C10H16O2
169.1217	$[M+H]^+$	3	2,6-Dimethyl-8-hydroxy-2E,6E-octadienal	C10H16O2
169.1217	$[M+H]^+$	3	4-oxo-2E-Decenal	C10H16O2
169.1217	$[M+H]^+$	3	(+)-cis-chrysanthemic acid	C10H16O2
169.1217	$[M+H]^+$	3	(-)-cis-chrysanthemic acid	C10H16O2
169.1217	$[M+H]^+$	3	(4R,7R)-4-isopropenyl-7-methyloxepan-2-one	C10H16O2
169.1217	$[M+H]^+$	3	(4S,7R)-4-isopropenyl-7-methyloxepan-2-one	C10H16O2
169.1217	$[M+H]^+$	3	diosphenol	C10H16O2
169.1217	$[M+H]^+$	3	(-)-1,2-campholide	C10H16O2
169.1217	$[M+H]^+$	3	1,2-campholide	C10H16O2
169.1217	$[M+H]^+$	3	(+)-exo-5-hydroxycamphor	C10H16O2
169.1217	$[M+H]^+$	3	(3S,6R)-6-Isopropenyl-3-methyl-2-oxo-oxepanone	C10H16O2
169.1217	$[M+H]^+$	3	(3S,6S)-6-Isopropenyl-3-methyl-2-oxo-oxepanone	C10H16O2
169.1217	$[M+H]^+$	3	trans-2-Methyl-5-isopropylhexa-2,5-dienoic acid	C10H16O2
169.1217	$[M+H]^+$	3	cis-2-Methyl-5-isopropylhexa-2,5-dienoic acid	C10H16O2
217.15529	$[M+H]^+$	2	Val Val	C10H20N2O3
217.1791	$[M+H]^+$	3	α-hydroxy lauric acid	C12H24O3
217.1791	$[M+H]^+$	3	4-hydroxy lauric acid	C12H24O3
217.1791	$[M+H]^+$	3	11-hydroxy-dodecanoic acid	C12H24O3
217.1791	$[M+H]^+$	3	7-hydroxy-dodecanoic acid	C12H24O3
217.1791	$[M+H]^+$	3	9-hydroxy-dodecanoic acid	C12H24O3
217.1791	$[M+H]^+$	3	3R-hydroxy-dodecanoic acid	C12H24O3
217.1791	$[M+H]^+$	3	3S-hydroxy-dodecanoic acid	C12H24O3
217.1791	$[M+H]^+$	3	11R-hydroxy-dodecanoic acid	C12H24O3
217.1791	$[M+H]^+$	3	2R-hydroxylauric acid	C12H24O3
217.1791	$[M+H]^+$	3	2S-hydroxylauric acid	C12H24O3
217.1791	$[M+H]^+$	3	4S-hydroxylauric acid	C12H24O3
217.1791	$[M+H]^+$	3	4R-hydroxylauric acid	C12H24O3
217.1791	$[M+H]^+$	3	3-Hydroxydodecanoic acid	C12H24O3
217.1791	$[M+H]^+$	3	12-Hydroxydodecanoic acid	C12H24O3
245.07735	$[M+H]^+$	2	Uridine	C9H12N2O6
245.07735	$[M+H]^+$	2	Pseudouridine	C9H12N2O6
283.26208	$[M+H]^+$	3	2-methyl-16-heptadecenoic acid	C18H34O2
283.26208	$[M+H]^+$	3	2Z-octadecenoic acid	C18H34O2
283.26208	$[M+H]^+$	3	trans-2-oleic acid	C18H34O2
283.26208	$[M+H]^+$	3	3-octadecylenic acid	C18H34O2
283.26208	$[M+H]^+$	3	4-octadecylenic acid	C18H34O2
283.26208	$[M+H]^+$	3	5-octadecylenic acid	C18H34O2
283.26208	$[M+H]^+$	3	Petroselaidic acid	C18H34O2
283.26208	$[M+H]^+$	3	7Z-octadecenoic acid	C18H34O2

283.26208	$[M+H]^+$	3	7E-octadecenoic acid	C18H34O2
283.26208	$[M+H]^+$	3	cis-8-oleic acid	C18H34O2
283.26208	$[M+H]^+$	3	trans-8-elaidic acid	C18H34O2
283.26208	$[M+H]^+$	3	cis-10-oleic acid	C18H34O2
283.26208	$[M+H]^+$	3	10E-octadecenoic acid	C18H34O2
283.26208	$[M+H]^+$	3	cis-12-oleic acid	C18H34O2
283.26208	$[M+H]^+$	3	trans-12-elaidic acid	C18H34O2
283.26208	$[M+H]^+$	3	15E-octadecenoic acid	C18H34O2
283.26208	$[M+H]^+$	3	16E-octadecenoic acid	C18H34O2
283.26208	$[M+H]^+$	3	13Z-octadecenoic acid	C18H34O2
283.26208	$[M+H]^+$	3	15Z-octadecenoic acid	C18H34O2
283.26208	$[M+H]^+$	3	16Z-octadecenoic acid	C18H34O2
283.26208	$[M+H]^+$	3	17-octadecenoic acid	C18H34O2
283.26208	$[M+H]^+$	3	3Z-octadecenoic acid	C18H34O2
283.26208	$[M+H]^+$	3	4Z-octadecenoic acid	C18H34O2
283.26208	$[M+H]^+$	3	5Z-octadecenoic acid	C18H34O2
283.26208	$[M+H]^+$	3	Oleic Acid	C18H34O2
283.26208	$[M+H]^+$	3	Elaidic Acid	C18H34O2
283.26208	$[M+H]^+$	3	Vaccenic acid	C18H34O2
283.26208	$[M+H]^+$	3	cis-vaccenic acid	C18H34O2
283.26208	$[M+H]^+$	3	6-octadecylenic acid	C18H34O2
283.26208	$[M+H]^+$	3	Palmitoleic Acid ethyl ester	C18H34O2
283.26208	$[M+H]^+$	3	11-Cycloheptylundecanoic acid	C18H34O2
283.26208	$[M+H]^+$	3	11E-Hexadecenyl acetate	C18H34O2
283.26208	$[M+H]^+$	3	5E-Hexadecenyl acetate	C18H34O2
283.26208	$[M+H]^+$	3	6E-Hexadecenyl acetate	C18H34O2
283.26208	$[M+H]^+$	3	8E-Hexadecenyl acetate	C18H34O2
283.26208	$[M+H]^+$	3	9E-Hexadecenyl acetate	C18H34O2
283.26208	$[M+H]^+$	3	10Z-Hexadecenyl acetate	C18H34O2
283.26208	$[M+H]^+$	3	11Z-Hexadecenyl acetate	C18H34O2
283.26208	$[M+H]^+$	3	12Z-Hexadecenyl acetate	C18H34O2
283.26208	$[M+H]^+$	3	3Z-Hexadecenyl acetate	C18H34O2
283.26208	$[M+H]^+$	3	5Z-Hexadecenyl acetate	C18H34O2
283.26208	$[M+H]^+$	3	7Z-Hexadecenyl acetate	C18H34O2
283.26208	$[M+H]^+$	3	9Z-Hexadecenyl acetate	C18H34O2
283.26208	$[M+H]^+$	3	7-Hexadecenyl acetate	C18H34O2
285.2779	$[M+H]^+$	3	11,15-dimethyl-hexadecanoic acid	C18H36O2
285.2779	$[M+H]^+$	3	15-methyl-heptadecanoic acid	C18H36O2
285.2779	$[M+H]^+$	3	Stearic acid	C18H36O2
285.2779	$[M+H]^+$	3	10-methyl-heptadecanoic acid	C18H36O2
285.2779	$[M+H]^+$	3	(+)-Isostearic acid	C18H36O2
285.2779	$[M+H]^+$	3	2,6-dimethyl-hexadecanoic acid	C18H36O2
285.2779	$[M+H]^+$	3	4,8-dimethyl-hexadecanoic acid	C18H36O2
285.2779	$[M+H]^+$	3	2,14-dimethyl-hexadecanoic acid	C18H36O2
285.2779	$[M+H]^+$	3	4,14-dimethyl-hexadecanoic acid	C18H36O2
285.2779	$[M+H]^+$	3	6,14-dimethyl-hexadecanoic acid	C18H36O2
285.2779	$[M+H]^+$	3	lambda isostearic acid	C18H36O2
285.2779	$[M+H]^+$	3	neostearic acid	C18H36O2
285.2779	$[M+H]^+$	3	Palmitic Acid ethyl ester	C18H36O2
285.2779	$[M+H]^+$	3	14-Methylheptadecanoic acid	C18H36O2
285.2779	$[M+H]^+$	3	Hexadecyl acetate	C18H36O2
287.2208	$[M+H]^+$	3	9-hydroxy-16-oxo-hexadecanoic acid	C16H30O4
287.2208	$[M+H]^+$	3	10-hydroxy-16-oxo-hexadecanoic acid	C16H30O4
287.2208	$[M+H]^+$	3	Hexadecanedioic acid	C16H30O4

299.1605	$[M+H]^+$	3	Olomoucine	C15H18N6O
349.13037	$[M+H]^+$	2	PI-103	C19H16N4O3
359.2387	$[M+H]^+$	3	Arg Ile Ala	C15H30N6O4
359.2387	$[M+H]^+$	3	Ala Arg Ile	C15H30N6O4
359.2387	$[M+H]^+$	3	Ala Leu Arg	C15H30N6O4
359.2387	$[M+H]^+$	3	Arg Leu Ala	C15H30N6O4
359.2387	$[M+H]^+$	3	Ile Ala Arg	C15H30N6O4
359.2387	$[M+H]^+$	3	Ala Arg Leu	C15H30N6O4
359.2387	$[M+H]^+$	3	Arg Ala Leu	C15H30N6O4
359.2387	$[M+H]^+$	3	Ile Arg Ala	C15H30N6O4
359.2387	$[M+H]^+$	3	Arg Ala Ile	C15H30N6O4
359.2387	$[M+H]^+$	3	Ala Ile Arg	C15H30N6O4
359.2387	$[M+H]^+$	3	Leu Arg Ala	C15H30N6O4
359.2387	$[M+H]^+$	3	Leu Ala Arg	C15H30N6O4
383.2141	$[M+H]^+$	2	His Arg Ala	C15H26N8O4
383.2141	$[M+H]^+$	2	His Ala Arg	C15H26N8O4
383.2141	$[M+H]^+$	2	Ala Arg His	C15H26N8O4
383.2141	$[M+H]^+$	2	Arg Ala His	C15H26N8O4
383.2141	$[M+H]^+$	2	Ala His Arg	C15H26N8O4
383.2141	$[M+H]^+$	2	Arg His Ala	C15H26N8O4
383.3144	$[M+H]^+$	3	methyl 9-butylperoxy-10,12-octadecadienoate	C23H42O4
383.3144	$[M+H]^+$	3	methyl 13-butylperoxy-9,11-octadecadienoate	C23H42O4
383.3144	$[M+H]^+$	3	MG(0:0/20:2(11Z,14Z)/0:0)	C23H42O4
383.3144	$[M+H]^+$	3	MG(20:2(11Z,14Z)/0:0/0:0)	C23H42O4
411.3456	$[M+H]^+$	3	MG(0:0/22:2(13Z,16Z)/0:0)	C25H46O4
411.3456	$[M+H]^+$	3	MG(22:2(13Z,16Z)/0:0/0:0)	C25H46O4
435.24866	$[M+H]^+$	4	LPA(0:0/18:2(9Z,12Z))	C21H39O7P
435.24866	$[M+H]^+$	4	LPA(18:2(9Z,12Z)/0:0)	C21H39O7P
441.2956	$[M+H]^+$	4	26,26,26-trifluoro-25-hydroxy-27-norvitamin D3 / 26,26,26-trifluoro-25-hydroxy-27-norcholecalciferol	C26H39F3O2
485.30105	$[M+H]^+$	0	Gallopamil	C28H40N2O5
529.45955	$[M+H]^+$	3	32,35-anhydrobacteriohopaneterol	C35H60O3
531.47562	$[M+H]^+$	2	30-(-2-(O-2-hydroxy-ethane)-3-hydroxy-propane)-hopane	C35H62O3
537.3942	$[M+H]^+$	0	Hyperforin	C35H52O4
587.46515	$[M+H]^+$	3	DG(14:0/20:5(5Z,8Z,11Z,14Z,17Z)/0:0)	C37H62O5
587.46515	$[M+H]^+$	3	DG(14:1(9Z)/20:4(5Z,8Z,11Z,14Z)/0:0)	C37H62O5
587.46515	$[M+H]^+$	3	DG(14:1(9Z)/20:4(8Z,11Z,14Z,17Z)/0:0)	C37H62O5
587.46515	$[M+H]^+$	3	DG(16:1(9Z)/18:4(6Z,9Z,12Z,15Z)/0:0)	C37H62O5
587.46515	$[M+H]^+$	3	DG(18:4(6Z,9Z,12Z,15Z)/16:1(9Z)/0:0)	C37H62O5
587.46515	$[M+H]^+$	3	DG(20:4(5Z,8Z,11Z,14Z)/14:1(9Z)/0:0)	C37H62O5
587.46515	$[M+H]^+$	3	DG(20:4(8Z,11Z,14Z,17Z)/14:1(9Z)/0:0)	C37H62O5
587.46515	$[M+H]^+$	3	DG(20:5(5Z,8Z,11Z,14Z,17Z)/14:0/0:0)	C37H62O5
601.425	$[M+H]^+$	0	Capsorubin	C40H56O4
601.425	$[M+H]^+$	0	Capsanthin 3,6-epoxide	C40H56O4
601.425	$[M+H]^+$	0	Cycloviolaxanthin	C40H56O4
601.425	$[M+H]^+$	0	Cucurbitaxanthin B	C40H56O4
601.425	$[M+H]^+$	0	Nostoxanthin	C40H56O4
601.425	$[M+H]^+$	0	Siphonaxanthin	C40H56O4
601.425	$[M+H]^+$	0	Oscillol	C40H56O4
601.425	$[M+H]^+$	0	4-Hydroxymyxol/ 4-OH-myxol/ (Aphanizophyll)	C40H56O4

601.425	$[M+H]^+$	0	Salmoxanthin/ Trollixanthin	C40H56O4
601.425	$[M+H]^+$	0	Prasinoxanthin	C40H56O4
601.425	$[M+H]^+$	0	Preprasinoxanthin	C40H56O4
601.425	$[M+H]^+$	0	9-cis-Violaxanthin	C40H56O4
601.425	$[M+H]^+$	0	Violaxanthin	C40H56O4
601.425	$[M+H]^+$	0	Neoxanthin	C40H56O4
601.425	$[M+H]^+$	0	all-trans-neoxanthin	C40H56O4
601.425	$[M+H]^+$	0	9\'-cis-neoxanthin	C40H56O4
601.425	$[M+H]^+$	0	Luteoxanthin	C40H56O4
601.425	$[M+H]^+$	0	(2S,2\'S)-Oscillol	C40H56O4
721.5751	$[M+H]^+$	2	DG(22:3(10Z,13Z,16Z)/22:5(7Z,10Z,13Z,16Z,19Z)/0:0)[iso2]	C47H76O5
721.5751	$[M+H]^+$	2	DG(22:4(7Z,10Z,13Z,16Z)/22:4(7Z,10Z,13Z,16Z)/0:0)	C47H76O5
721.5751	$[M+H]^+$	2	DG(22:2(13Z,16Z)/22:6(4Z,7Z,10Z,13Z,16Z,19Z)/0:0)[iso2]	C47H76O5
721.5751	$[M+H]^+$	2	DG(22:6(4Z,7Z,10Z,13Z,16Z,19Z)/22:2(13Z,16Z)/0:0)	C47H76O5
732.55135	$[M+H]^+$	3	PE-NMe(16:0/18:1(9Z))[U]	C40H78NO8P
732.55135	$[M+H]^+$	3	PE-NMe(16:0/18:1(9Z))	C40H78NO8P
732.55135	$[M+H]^+$	3	PE-NMe(18:1(9Z)/16:0)	C40H78NO8P
732.55135	$[M+H]^+$	3	PC(14:0/18:1(11Z))	C40H78NO8P
732.55135	$[M+H]^+$	3	PC(14:0/18:1(9Z))	C40H78NO8P
732.55135	$[M+H]^+$	3	PC(14:1(9Z)/18:0)	C40H78NO8P
732.55135	$[M+H]^+$	3	PC(16:0/16:1(9Z))	C40H78NO8P
732.55135	$[M+H]^+$	3	PC(16:1(9Z)/16:0)	C40H78NO8P
732.55135	$[M+H]^+$	3	PC(18:0/14:1(9Z))	C40H78NO8P
732.55135	$[M+H]^+$	3	PC(18:1(11Z)/14:0)	C40H78NO8P
732.55135	$[M+H]^+$	3	PC(18:1(9Z)/14:0)	C40H78NO8P
732.55135	$[M+H]^+$	3	PE(15:0/20:1(11Z))	C40H78NO8P
732.55135	$[M+H]^+$	3	PE(20:1(11Z)/15:0)	C40H78NO8P
745.46577	$[M+H]^+$	2	Adonixanthin 3-glucoside	C46H64O8
745.46577	$[M+H]^+$	2	19\'-Butanoyloxyfucoxanthin	C46H64O8
745.46577	$[M+H]^+$	2	Adonixanthin 3\'-β-D-glucoside/ Adonixanthin 3\'-glucoside	C46H64O8
745.46577	$[M+H]^+$	2	(3S,2\'S)-4-Ketomyxol 2\'-α-L-fucoside	C46H64O8
751.60468	$[M+H]^+$	3	3-Nonaprenyl-4-hydroxybenzoic acid	C52H78O3
771.5736	$[M+H]^+$	4	PC(16:0/19:3(9Z,12Z,15Z))[U]	C43H81NO8P
784.5859	$[M+H]^+$	1	PC(14:1(9Z)/22:2(13Z,16Z))	C44H82NO8P
784.5859	$[M+H]^+$	1	PC(16:0/20:3(5Z,8Z,11Z))	C44H82NO8P
784.5859	$[M+H]^+$	1	PC(16:0/20:3(8Z,11Z,14Z))	C44H82NO8P
784.5859	$[M+H]^+$	1	PC(16:1(9Z)/20:2(11Z,14Z))	C44H82NO8P
784.5859	$[M+H]^+$	1	PC(18:0/18:3(6Z,9Z,12Z))	C44H82NO8P
784.5859	$[M+H]^+$	1	PC(18:0/18:3(9Z,12Z,15Z))	C44H82NO8P
784.5859	$[M+H]^+$	1	PC(18:1(11Z)/18:2(9Z,12Z))	C44H82NO8P
784.5859	$[M+H]^+$	1	PC(18:1(9Z)/18:2(9Z,12Z))	C44H82NO8P
784.5859	$[M+H]^+$	1	PC(18:2(9Z,12Z)/18:1(11Z))	C44H82NO8P
784.5859	$[M+H]^+$	1	PC(18:2(9Z,12Z)/18:1(9Z))	C44H82NO8P
784.5859	$[M+H]^+$	1	PC(18:3(6Z,9Z,12Z)/18:0)	C44H82NO8P
784.5859	$[M+H]^+$	1	PC(18:3(9Z,12Z,15Z)/18:0)	C44H82NO8P
784.5859	$[M+H]^+$	1	PC(20:2(11Z,14Z)/16:1(9Z))	C44H82NO8P
784.5859	$[M+H]^+$	1	PC(20:3(5Z,8Z,11Z)/16:0)	C44H82NO8P
784.5859	$[M+H]^+$	1	PC(20:3(8Z,11Z,14Z)/16:0)	C44H82NO8P
784.5859	$[M+H]^+$	1	PC(22:2(13Z,16Z)/14:1(9Z))	C44H82NO8P

810.59762	$[M+H]^+$	3	1-Stearoyl-2-Arachidonoyl PC	C46H84NO8P
810.59762	$[M+H]^+$	3	PC(16:0/22:4(7Z,10Z,13Z,16Z))	C46H84NO8P
810.59762	$[M+H]^+$	3	PC(18:0/20:4(8Z,11Z,14Z,17Z))	C46H84NO8P
810.59762	$[M+H]^+$	3	PC(18:1(11Z)/20:3(5Z,8Z,11Z))	C46H84NO8P
810.59762	$[M+H]^+$	3	PC(18:1(11Z)/20:3(8Z,11Z,14Z))	C46H84NO8P
810.59762	$[M+H]^+$	3	PC(18:1(9Z)/20:3(5Z,8Z,11Z))	C46H84NO8P
810.59762	$[M+H]^+$	3	PC(18:1(9Z)/20:3(8Z,11Z,14Z))	C46H84NO8P
810.59762	$[M+H]^+$	3	PC(18:2(9Z,12Z)/20:2(11Z,14Z))	C46H84NO8P
810.59762	$[M+H]^+$	3	PC(18:3(6Z,9Z,12Z)/20:1(11Z))	C46H84NO8P
810.59762	$[M+H]^+$	3	PC(18:3(9Z,12Z,15Z)/20:1(11Z))	C46H84NO8P
810.59762	$[M+H]^+$	3	PC(18:4(6Z,9Z,12Z,15Z)/20:0)	C46H84NO8P
810.59762	$[M+H]^+$	3	PC(20:0/18:4(6Z,9Z,12Z,15Z))	C46H84NO8P
810.59762	$[M+H]^+$	3	PC(20:1(11Z)/18:3(6Z,9Z,12Z))	C46H84NO8P
810.59762	$[M+H]^+$	3	PC(20:1(11Z)/18:3(9Z,12Z,15Z))	C46H84NO8P
810.59762	$[M+H]^+$	3	PC(20:2(11Z,14Z)/18:2(9Z,12Z))	C46H84NO8P
810.59762	$[M+H]^+$	3	PC(20:3(5Z,8Z,11Z)/18:1(11Z))	C46H84NO8P
810.59762	$[M+H]^+$	3	PC(20:3(5Z,8Z,11Z)/18:1(9Z))	C46H84NO8P
810.59762	$[M+H]^+$	3	PC(20:3(8Z,11Z,14Z)/18:1(11Z))	C46H84NO8P
810.59762	$[M+H]^+$	3	PC(20:3(8Z,11Z,14Z)/18:1(9Z))	C46H84NO8P
810.59762	$[M+H]^+$	3	PC(20:4(5Z,8Z,11Z,14Z)/18:0)	C46H84NO8P
810.59762	$[M+H]^+$	3	PC(20:4(8Z,11Z,14Z,17Z)/18:0)	C46H84NO8P
810.59762	$[M+H]^+$	3	PC(22:4(7Z,10Z,13Z,16Z)/16:0)	C46H84NO8P
823.40708	$[M+H]^+$	4	GLYCYRRHIZIC ACID	C42H62O16
823.40708	$[M+H]^+$	4	glycyrrhizinic acid	C42H62O16
823.40708	$[M+H]^+$	4	Glycyrrhizin	C42H62O16
839.6359	$[M+H]^+$	4	PC(18:0/22:4(7Z,10Z,13Z,16Z))	C48H89NO8P
839.6359	$[M+H]^+$	4	PC(18:0/22:4(7Z,10Z,13Z,16Z))[U]	C48H89NO8P
839.6359	$[M+H]^+$	4	PC(20:0/20:4(5Z,8Z,11Z,14Z))	C48H89NO8P
839.6359	$[M+H]^+$	4	PC(20:2(11E,14E)/20:2(11E,14E))	C48H89NO8P
839.6359	$[M+H]^+$	4	PC(20:2(2E,4E)/20:2(2E,4E))[S]	C48H89NO8P
839.6359	$[M+H]^+$	4	PC(22:4(7Z,10Z,13Z,16Z)/18:0)[U]	C48H89NO8P
623.4515	$[M+H]^+$	0	PC(10:0/14:0)[U]	C32H65NO8P
623.4515	$[M+H]^+$	0	PC(11:0/13:0)[U]	C32H65NO8P
623.4515	$[M+H]^+$	0	PC(12:0/12:0)	C32H65NO8P
623.4515	$[M+H]^+$	0	PC(12:0/12:0)[U]	C32H65NO8P
623.4515	$[M+H]^+$	0	PC(13:0/11:0)[U]	C32H65NO8P
623.4515	$[M+H]^+$	0	PC(14:0/10:0)[U]	C32H65NO8P
623.4515	$[M+H]^+$	0	PC(15:0/9:0)[U]	C32H65NO8P
623.4515	$[M+H]^+$	0	PC(18:0/6:0)[U]	C32H65NO8P
623.4515	$[M+H]^+$	0	PC(6:0/18:0)	C32H65NO8P
623.4515	$[M+H]^+$	0	PC(9:0/15:0)[U]	C32H65NO8P
758.56685	$[M+H]^+$	3	PE-NMe(18:1(9E)/18:1(9E))	C42H80NO8P
758.56685	$[M+H]^+$	3	PE-NMe(18:1(9Z)/18:1(9Z))[U]	C42H80NO8P
758.56685	$[M+H]^+$	3	PE-NMe(18:1(9Z)/18:1(9Z))	C42H80NO8P
758.56685	$[M+H]^+$	3	PE-NMe(18:1(9E)/18:1(9E))[U]	C42H80NO8P
758.56685	$[M+H]^+$	3	PC(14:0/20:2(11Z,14Z))	C42H80NO8P
758.56685	$[M+H]^+$	3	PC(14:1(9Z)/20:1(11Z))	C42H80NO8P
758.56685	$[M+H]^+$	3	PC(16:0/18:2(9Z,12Z))	C42H80NO8P
758.56685	$[M+H]^+$	3	PC(16:1(9Z)/18:1(11Z))	C42H80NO8P
758.56685	$[M+H]^+$	3	PC(16:1(9Z)/18:1(9Z))	C42H80NO8P
758.56685	$[M+H]^+$	3	PC(18:1(11Z)/16:1(9Z))	C42H80NO8P
758.56685	$[M+H]^+$	3	PC(18:1(9Z)/16:1(9Z))	C42H80NO8P
758.56685	$[M+H]^+$	3	PC(18:2(9Z,12Z)/16:0)	C42H80NO8P
758.56685	$[M+H]^+$	3	PC(20:1(11Z)/14:1(9Z))	C42H80NO8P

758.56685	$[M+H]^+$	3	PC(20:2(11Z,14Z)/14:0)	C42H80NO8P
758.56685	$[M+H]^+$	3	PE(15:0/22:2(13Z,16Z))	C42H80NO8P
758.56685	$[M+H]^+$	3	PE(22:2(13Z,16Z)/15:0)	C42H80NO8P
760.58263	$[M+H]^+$	3	PC(14:0/20:1(11Z))	C42H82NO8P
760.58263	$[M+H]^+$	3	PC(14:1(9Z)/20:0)	C42H82NO8P
760.58263	$[M+H]^+$	3	PC(16:0/18:1(11Z))	C42H82NO8P
760.58263	$[M+H]^+$	3	PC(16:0/18:1(9Z))	C42H82NO8P
760.58263	$[M+H]^+$	3	PC(16:1(9Z)/18:0)	C42H82NO8P
760.58263	$[M+H]^+$	3	PC(18:0/16:1(9Z))	C42H82NO8P
760.58263	$[M+H]^+$	3	PC(18:1(11Z)/16:0)	C42H82NO8P
760.58263	$[M+H]^+$	3	PC(18:1(9Z)/16:0)	C42H82NO8P
760.58263	$[M+H]^+$	3	PC(20:0/14:1(9Z))	C42H82NO8P
760.58263	$[M+H]^+$	3	PC(20:1(11Z)/14:0)	C42H82NO8P
760.58263	$[M+H]^+$	3	PE(15:0/22:1(13Z))	C42H82NO8P
760.58263	$[M+H]^+$	3	PE(22:1(13Z)/15:0)	C42H82NO8P
806.566	$[M+H]^+$	4	Galabiosylceramide (d18:1/12:0)	C42H79NO13
806.566	$[M+H]^+$	4	Lactosylceramide (d18:1/12:0)	C42H79NO13
806.566	$[M+H]^+$	4	PC(16:0/22:6(4Z,7Z,10Z,13Z,16Z,19Z))	C46H80NO8P
806.566	$[M+H]^+$	4	PC(16:1(9Z)/22:5(4Z,7Z,10Z,13Z,16Z))	C46H80NO8P
806.566	$[M+H]^+$	4	PC(16:1(9Z)/22:5(7Z,10Z,13Z,16Z,19Z))	C46H80NO8P
806.566	$[M+H]^+$	4	PC(18:1(11Z)/20:5(5Z,8Z,11Z,14Z,17Z))	C46H80NO8P
806.566	$[M+H]^+$	4	PC(18:1(9Z)/20:5(5Z,8Z,11Z,14Z,17Z))	C46H80NO8P
806.566	$[M+H]^+$	4	PC(18:2(9Z,12Z)/20:4(5Z,8Z,11Z,14Z))	C46H80NO8P
806.566	$[M+H]^+$	4	PC(18:2(9Z,12Z)/20:4(8Z,11Z,14Z,17Z))	C46H80NO8P
806.566	$[M+H]^+$	4	PC(18:3(6Z,9Z,12Z)/20:3(5Z,8Z,11Z))	C46H80NO8P
806.566	$[M+H]^+$	4	PC(18:3(6Z,9Z,12Z)/20:3(8Z,11Z,14Z))	C46H80NO8P
806.566	$[M+H]^+$	4	PC(18:3(9Z,12Z,15Z)/20:3(5Z,8Z,11Z))	C46H80NO8P
806.566	$[M+H]^+$	4	PC(18:3(9Z,12Z,15Z)/20:3(8Z,11Z,14Z))	C46H80NO8P
806.566	$[M+H]^+$	4	PC(18:4(6Z,9Z,12Z,15Z)/20:2(11Z,14Z))	C46H80NO8P
806.566	$[M+H]^+$	4	PC(20:2(11Z,14Z)/18:4(6Z,9Z,12Z,15Z))	C46H80NO8P
806.566	$[M+H]^+$	4	PC(20:3(5Z,8Z,11Z)/18:3(6Z,9Z,12Z))	C46H80NO8P
806.566	$[M+H]^+$	4	PC(20:3(5Z,8Z,11Z)/18:3(9Z,12Z,15Z))	C46H80NO8P
806.566	$[M+H]^+$	4	PC(20:3(8Z,11Z,14Z)/18:3(6Z,9Z,12Z))	C46H80NO8P
806.566	$[M+H]^+$	4	PC(20:3(8Z,11Z,14Z)/18:3(9Z,12Z,15Z))	C46H80NO8P
806.566	$[M+H]^+$	4	PC(20:4(5Z,8Z,11Z,14Z)/18:2(9Z,12Z))	C46H80NO8P
806.566	$[M+H]^+$	4	PC(20:4(8Z,11Z,14Z,17Z)/18:2(9Z,12Z))	C46H80NO8P
806.566	$[M+H]^+$	4	PC(20:5(5Z,8Z,11Z,14Z,17Z)/18:1(11Z))	C46H80NO8P
806.566	$[M+H]^+$	4	PC(20:5(5Z,8Z,11Z,14Z,17Z)/18:1(9Z))	C46H80NO8P
806.566	$[M+H]^+$	4	PC(22:5(4Z,7Z,10Z,13Z,16Z)/16:1(9Z))	C46H80NO8P
806.566	$[M+H]^+$	4	PC(22:5(7Z,10Z,13Z,16Z,19Z)/16:1(9Z))	C46H80NO8P
806.566	$[M+H]^+$	4	PC(22:6(4Z,7Z,10Z,13Z,16Z,19Z)/16:0)	C46H80NO8P
905.7561	$[M+H]^+$	3	TG(18:3(9Z,12Z,15Z)/18:3(9Z,12Z,15Z)/20:1(11Z))[iso3]	C59H100O6
905.7561	$[M+H]^+$	3	TG(18:2(9Z,12Z)/18:3(9Z,12Z,15Z)/20:2(11Z,14Z))[iso6]	C59H100O6
905.7561	$[M+H]^+$	3	TG(16:1(9Z)/20:3(8Z,11Z,14Z)/20:3(8Z,11Z,14Z))[iso3]	C59H100O6
905.7561	$[M+H]^+$	3	TG(18:1(9Z)/18:3(9Z,12Z,15Z)/20:3(8Z,11Z,14Z))[iso6]	C59H100O6
905.7561	$[M+H]^+$	3	TG(18:2(9Z,12Z)/18:2(9Z,12Z)/20:3(8Z,11Z,14Z))[iso3]	C59H100O6
905.7561	$[M+H]^+$	3	TG(16:0/20:3(8Z,11Z,14Z)/20:4(5Z,8Z,11Z,14Z))[iso6]	C59H100O6
905.7561	$[M+H]^+$	3	TG(16:1(9Z)/20:2(11Z,14Z)/20:4(5Z,8Z,11Z,14Z))[iso6]	C59H100O6

905.7561	$[M+H]^+$	3	TG(18:0/18:3(9Z,12Z,15Z)/20:4(5Z,8Z,11Z,14Z))[iso6]	C59H100O6
905.7561	$[M+H]^+$	3	TG(18:1(9Z)/18:2(9Z,12Z)/20:4(5Z,8Z,11Z,14Z))[iso6]	C59H100O6
905.7561	$[M+H]^+$	3	TG(16:0/20:2(11Z,14Z)/20:5(5Z,8Z,11Z,14Z,17Z))[iso6]	C59H100O6
905.7561	$[M+H]^+$	3	TG(16:1(9Z)/20:1(11Z)/20:5(5Z,8Z,11Z,14Z,17Z))[iso6]	C59H100O6
905.7561	$[M+H]^+$	3	TG(18:0/18:2(9Z,12Z)/20:5(5Z,8Z,11Z,14Z,17Z))[iso6]	C59H100O6
905.7561	$[M+H]^+$	3	TG(18:1(9Z)/18:1(9Z)/20:5(5Z,8Z,11Z,14Z,17Z))[iso3]	C59H100O6
905.7561	$[M+H]^+$	3	TG(17:2(9Z,12Z)/17:2(9Z,12Z)/22:3(10Z,13Z,16Z))[iso3]	C59H100O6
905.7561	$[M+H]^+$	3	TG(17:2(9Z,12Z)/19:0/20:5(5Z,8Z,11Z,14Z,17Z))[iso6]	C59H100O6
905.7561	$[M+H]^+$	3	TG(16:1(9Z)/18:3(9Z,12Z,15Z)/22:3(10Z,13Z,16Z))[iso6]	C59H100O6
905.7561	$[M+H]^+$	3	TG(17:1(9Z)/17:2(9Z,12Z)/22:4(7Z,10Z,13Z,16Z))[iso6]	C59H100O6
905.7561	$[M+H]^+$	3	TG(17:0/17:2(9Z,12Z)/22:5(7Z,10Z,13Z,16Z,19Z))[iso6]	C59H100O6
905.7561	$[M+H]^+$	3	TG(17:1(9Z)/17:1(9Z)/22:5(7Z,10Z,13Z,16Z,19Z))[iso3]	C59H100O6
905.7561	$[M+H]^+$	3	TG(17:0/17:1(9Z)/22:6(4Z,7Z,10Z,13Z,16Z,19Z))[iso6]	C59H100O6
905.7561	$[M+H]^+$	3	TG(16:0/18:3(9Z,12Z,15Z)/22:4(7Z,10Z,13Z,16Z))[iso6]	C59H100O6
905.7561	$[M+H]^+$	3	TG(16:1(9Z)/18:2(9Z,12Z)/22:4(7Z,10Z,13Z,16Z))[iso6]	C59H100O6
905.7561	$[M+H]^+$	3	TG(16:0/18:2(9Z,12Z)/22:5(7Z,10Z,13Z,16Z,19Z))[iso6]	C59H100O6
905.7561	$[M+H]^+$	3	TG(16:1(9Z)/18:1(9Z)/22:5(7Z,10Z,13Z,16Z,19Z))[iso6]	C59H100O6
905.7561	$[M+H]^+$	3	TG(16:0/18:1(9Z)/22:6(4Z,7Z,10Z,13Z,16Z,19Z))[iso6]	C59H100O6
905.7561	$[M+H]^+$	3	TG(16:1(9Z)/18:0/22:6(4Z,7Z,10Z,13Z,16Z,19Z))[iso6]	C59H100O6
905.7561	$[M+H]^+$	3	TG(18:1(9Z)/16:0/22:6(4Z,7Z,10Z,13Z,16Z,19Z))[iso6]	C59H100O6
905.7561	$[M+H]^+$	3	TG(18:2(9Z,12Z)/16:0/22:5(7Z,10Z,13Z,16Z,19Z))[iso6]	C59H100O6
905.7561	$[M+H]^+$	3	TG(18:2(9Z,12Z)/18:1(11Z)/20:4(5Z,8Z,11Z,14Z))[iso6]	C59H100O6
905.7561	$[M+H]^+$	3	TG(20:4(5Z,8Z,11Z,14Z)/18:0/18:3(9Z,12Z,15Z))[iso6]	C59H100O6
784.58244	$[M+H]^+$	3	PC(14:1(9Z)/22:2(13Z,16Z))	C44H82NO8P
784.58244	$[M+H]^+$	3	PC(16:0/20:3(5Z,8Z,11Z))	C44H82NO8P
784.58244	$[M+H]^+$	3	PC(16:0/20:3(8Z,11Z,14Z))	C44H82NO8P
784.58244	$[M+H]^+$	3	PC(16:1(9Z)/20:2(11Z,14Z))	C44H82NO8P
784.58244	$[M+H]^+$	3	PC(18:0/18:3(6Z,9Z,12Z))	C44H82NO8P
784.58244	$[M+H]^+$	3	PC(18:0/18:3(9Z,12Z,15Z))	C44H82NO8P
784.58244	$[M+H]^+$	3	PC(18:1(11Z)/18:2(9Z,12Z))	C44H82NO8P
784.58244	$[M+H]^+$	3	PC(18:1(9Z)/18:2(9Z,12Z))	C44H82NO8P
784.58244	$[M+H]^+$	3	PC(18:2(9Z,12Z)/18:1(11Z))	C44H82NO8P
784.58244	$[M+H]^+$	3	PC(18:2(9Z,12Z)/18:1(9Z))	C44H82NO8P
784.58244	$[M+H]^+$	3	PC(18:3(6Z,9Z,12Z)/18:0)	C44H82NO8P

784.58244	$[M+H]^+$	3	PC(18:3(9Z,12Z,15Z)/18:0)	C44H82NO8P
784.58244	$[M+H]^+$	3	PC(20:2(11Z,14Z)/16:1(9Z))	C44H82NO8P
784.58244	$[M+H]^+$	3	PC(20:3(5Z,8Z,11Z)/16:0)	C44H82NO8P
784.58244	$[M+H]^+$	3	PC(20:3(8Z,11Z,14Z)/16:0)	C44H82NO8P
784.58244	$[M+H]^+$	3	PC(22:2(13Z,16Z)/14:1(9Z))	C44H82NO8P
786.5981	$[M+H]^+$	3	1,2-Dioleoyl PC	C44H84NO8P
786.5981	$[M+H]^+$	3	PC(14:0/22:2(13Z,16Z))	C44H84NO8P
786.5981	$[M+H]^+$	3	PC(14:1(9Z)/22:1(13Z))	C44H84NO8P
786.5981	$[M+H]^+$	3	PC(16:0/20:2(11Z,14Z))	C44H84NO8P
786.5981	$[M+H]^+$	3	PC(16:1(9Z)/20:1(11Z))	C44H84NO8P
786.5981	$[M+H]^+$	3	PC(18:0/18:2(9Z,12Z))	C44H84NO8P
786.5981	$[M+H]^+$	3	PC(18:1(11Z)/18:1(11Z))	C44H84NO8P
786.5981	$[M+H]^+$	3	PC(18:1(11Z)/18:1(9Z))	C44H84NO8P
786.5981	$[M+H]^+$	3	PC(18:1(9Z)/18:1(11Z))	C44H84NO8P
786.5981	$[M+H]^+$	3	PC(18:2(9Z,12Z)/18:0)	C44H84NO8P
786.5981	$[M+H]^+$	3	PC(20:1(11Z)/16:1(9Z))	C44H84NO8P
786.5981	$[M+H]^+$	3	PC(20:2(11Z,14Z)/16:0)	C44H84NO8P
786.5981	$[M+H]^+$	3	PC(22:1(13Z)/14:1(9Z))	C44H84NO8P
786.5981	$[M+H]^+$	3	PC(22:2(13Z,16Z)/14:0)	C44H84NO8P
786.5981	$[M+H]^+$	3	Dioleoylphosphatidylcholine	C44H84NO8P
806.5639	$[M+H]^+$	1	Galabiosylceramide (d18:1/12:0)	C42H79NO13
806.5639	$[M+H]^+$	1	Lactosylceramide (d18:1/12:0)	C42H79NO13
201.08771	$[M+H]^+$	3	Dihydroclavaminic acid	C8H12N2O4
201.08771	$[M+H]^+$	3	Barbituric acid, 5-ethyl-5-(2-hydroxyethyl)-	C8H12N2O4
767.46937	$[M+H]^+$	4	MGDG(18:5(3Z,6Z,9Z,12Z,15Z)/18:5(3Z,6Z,9Z,12Z,15Z))	C45H66O10
903.74	$[M+H]^+$	3	TG(18:3(9Z,12Z,15Z)/18:3(9Z,12Z,15Z)/20:2(11Z,14Z))[iso3]	C59H98O6
903.74	$[M+H]^+$	3	TG(18:2(9Z,12Z)/18:3(9Z,12Z,15Z)/20:3(8Z,11Z,14Z))[iso6]	C59H98O6
903.74	$[M+H]^+$	3	TG(16:0/20:4(5Z,8Z,11Z,14Z)/20:4(5Z,8Z,11Z,14Z))[iso3]	C59H98O6
903.74	$[M+H]^+$	3	TG(16:1(9Z)/20:3(8Z,11Z,14Z)/20:4(5Z,8Z,11Z,14Z))[iso6]	C59H98O6
903.74	$[M+H]^+$	3	TG(18:1(9Z)/18:3(9Z,12Z,15Z)/20:4(5Z,8Z,11Z,14Z))[iso6]	C59H98O6
903.74	$[M+H]^+$	3	TG(18:2(9Z,12Z)/18:2(9Z,12Z)/20:4(5Z,8Z,11Z,14Z))[iso3]	C59H98O6
903.74	$[M+H]^+$	3	TG(16:0/20:3(8Z,11Z,14Z)/20:5(5Z,8Z,11Z,14Z,17Z))[iso6]	C59H98O6
903.74	$[M+H]^+$	3	TG(16:1(9Z)/20:2(11Z,14Z)/20:5(5Z,8Z,11Z,14Z,17Z))[iso6]	C59H98O6
903.74	$[M+H]^+$	3	TG(18:0/18:3(9Z,12Z,15Z)/20:5(5Z,8Z,11Z,14Z,17Z))[iso6]	C59H98O6
903.74	$[M+H]^+$	3	TG(18:1(9Z)/18:2(9Z,12Z)/20:5(5Z,8Z,11Z,14Z,17Z))[iso6]	C59H98O6
903.74	$[M+H]^+$	3	TG(17:2(9Z,12Z)/17:2(9Z,12Z)/22:4(7Z,10Z,13Z,16Z))[iso3]	C59H98O6
903.74	$[M+H]^+$	3	TG(17:1(9Z)/17:2(9Z,12Z)/22:5(7Z,10Z,13Z,16Z,19Z))[iso6]	C59H98O6
903.74	$[M+H]^+$	3	TG(17:0/17:2(9Z,12Z)/22:6(4Z,7Z,10Z,13Z,16Z,19Z))[iso6]	C59H98O6
903.74	$[M+H]^+$	3	TG(17:1(9Z)/17:1(9Z)/22:6(4Z,7Z,10Z,13Z,16Z,19Z))[iso3]	C59H98O6
903.74	$[M+H]^+$	3	TG(16:1(9Z)/18:3(9Z,12Z,15Z)/22:4(7Z,10Z,13Z,16Z))[iso6]	C59H98O6

903.74	$[M+H]^+$	3	TG(16:0/18:3(9Z,12Z,15Z)/22:5(7Z,10Z,13Z,16Z,19Z))[iso6]	C59H98O6
903.74	$[M+H]^+$	3	TG(16:1(9Z)/18:2(9Z,12Z)/22:5(7Z,10Z,13Z,16Z,19Z))[iso6]	C59H98O6
903.74	$[M+H]^+$	3	TG(16:0/18:2(9Z,12Z)/22:6(4Z,7Z,10Z,13Z,16Z,19Z))[iso6]	C59H98O6
903.74	$[M+H]^+$	3	TG(16:1(9Z)/18:1(9Z)/22:6(4Z,7Z,10Z,13Z,16Z,19Z))[iso6]	C59H98O6
903.74	$[M+H]^+$	4	TG(18:2(9Z,12Z)/16:0/22:6(4Z,7Z,10Z,13Z,16Z,19Z))[iso6]	C59H98O6
903.74	$[M+H]^+$	4	TG(18:2(9Z,12Z)/18:1(9Z)/20:5(5Z,8Z,11Z,14Z,17Z))[iso6]	C59H98O6